Microalgae production in a biofilm photobioreactor

Ward Blanken

Microalgae production in a biofilm photobioreactor

Ward Blanken

Thesis committee

Promotor

Prof. Dr R.H. Wijffels

Professor of Bioprocess Engineering

Wageningen University

Co-promotor

Dr M.G.J. Janssen

Assistant professor, Bioprocess Engineering

Wageningen University

Other members

Dr B. Podola, University of Cologne, Germany

Prof. Dr M.C.M. van Loosdrecht, Delft University of Technology

Prof. Dr J. Hugenholtz, University of Amsterdam

Prof. Dr H.H.M. Rijnaarts, Wageningen University

This research was conducted under the auspices of the Graduate School VLAG (Advanced studies in Food Technology, Agrobiotechnology Nutrition and Health Sciences).

Microalgae production in a biofilm photobioreactor

Ward Blanken

Thesis

submitted in fulfilment of the requirement for the degree of doctor

at Wageningen University

by the authority of the Rector Magnificus

Prof. Dr A.P.J. Mol,

in the presence of the

Thesis Committee appointed by the Academic Board

to be defended in public

on Friday 2 September 2016

at 4 p.m. in the Aula.

W. Blanken
Microalgae production in a biofilm photobioreactor
234 pages.

PhD thesis, Wageningen University, Wageningen, NL (2016)
With references, with summary in English

ISBN 978-94-6257-842-5
DOI: http://dx.doi.org/10.18174/384908

Contents

Chapter 1 Introduction

1.1 Introduction

Microalgae are the single cell ancestors to plants that employ light energy to convert carbon dioxide and water into sugar by photosynthesis. Because many microalgal species contain valuable products, large-scale microalgae cultivation could add to traditional agriculture and horticulture. The advantages of microalgae are that they do not require arable land, that many species can be cultivated in salt water, and that high productivity can be obtained by photobioreactor design and operation (Davis et al. 2011; Wijffels et al. 2010). Currently photobioreactor design is mainly focused on suspension cultivation. In addition to suspended life, most microalgae are able to grow in a biofilm. Within a biofilm microalgae live in densely packed slimy layers of numerous microalgae together with other microorganisms that attach themselves to solid surfaces (e.g. slippery rocks in shorelines). In this thesis the potential of microalgal cultivation in biofilm photobioreactors will be evaluated.

1.2 Current microalgae production

Microalgae have the potential to be employed for the production of high value products (Del Campo et al. 2007) as well as bulk products (Davis et al. 2011; Wijffels et al. 2010). On a commercial scale only high value products such as, pigments, high value fatty acids, and specific food and feed supplements are produced by cultivating microalgae in suspension (Del Campo et al. 2007). While some companies are investigating the production of bulk products such as, biofuels or ethanol with microalgae, the consensus is that current commercial production costs are too high to compete with comparable agricultural products and oil drilling and refining (Acien et al. 2012; Draaisma et al. 2012). However, it is expected that the production costs of microalgae will drop such that they can compete with agriculture specifically when all biomass components are utilized according to a biorefinery concept (Draaisma et al. 2012; Vanthoor-Koopmans et al. 2013; Wijffels et al. 2010). Based on techno-economic analyses published in the scientific literature the main cost reduction should be achieved by scale up of current technology. The main constraints of large scale microalgal production facilities are photosynthetic efficiency of product formation, nutrient costs, energy required for gas transfer and

mixing of large liquid volumes, and energy costs and capital expensed related to downstream processing (Acien et al. 2012; Norsker et al. 2011).

The photosynthetic efficiency of microalgae varies between strains and culture conditions (Breuer et al. 2015). Typical strategies to accumulate high product concentrations in the microalgal cells are nutrient starvation. However, while most microalgae can obtain high photosynthetic efficiencies during growth under nutrient rich conditions and low light the efficiency typically drops during the product accumulation phase (Breuer et al. 2015). Improvement of the photosynthetic efficiency during the product accumulation phase could therefore increase the economic potential of large scale algae cultivation.

The high costs of mixing large liquid volumes and downstream processing are related to the low algae concentration in the photobioreactors. Typically microalgae concentrations are in the range of 0.05% to 0.5% dry solids (Acien et al. 2012; Pahl et al. 2013), and could be further increased to above 1% by choosing a short light path photobioreactor design (Kliphuis et al. 2011b). Because of the low microalgae concentration large liquid volumes have to be handled during microalgae cultivation. This increases the costs of mixing liquid for both cultivation and medium preparation, and additionally it is costly to separate the biomass from the liquid.

1.3 Advantages of microalgal biofilms

Phototropic biofilms can improve microalgae cultivation economics because concentrated microalgal paste can be directly harvested (Berner et al. 2014) and the hydraulic retention time can be uncoupled from the microalgal retention time. The latter allows to decrease the liquid volume or to employ dilute waste streams. Therefore cultivation of microalgae biofilms can be cheaper than microalgae cultivation in suspended culture. To successfully employ biofilms it is required that microalgal biofilms can be cultivated at high photosynthetic efficiency. In literature reported photosynthetic efficiencies of microalgal biofilm cultivations vary greatly between studies, but these include photosynthetic efficiencies normally obtained in suspension cultures (Berner et al. 2014; Gross et al. 2015). However a detailed

comparison of photosynthetic efficiencies between suspension and biofilms is still missing. An additional advantage of a phototropic biofilm based production system is that carbon dioxide and oxygen is directly interchanged over the biofilm-gas interphase, minimizing the pressure drop required for gassing and thus reducing the energy costs. Although it is recognized that concentrated CO_2 streams are required to ascertain maximal productivity (Ji et al. 2013a; Schultze et al. 2015), the limitations in the CO_2 supply are not identified yet.

1.4 Growing a biofilm

Phototrophic biofilms are densely packed layers of microalgae that grow attached to a solid surface (Figure 1.1). The phototropic biofilm should be illuminated and should be frequently exposed to water containing nutrients including nitrogen, phosphate and trace elements. Supply of water to the biofilm can be ascertained by (intermittently) submerging the biofilm (e.g. rotating the biofilm between gas and liquid), or by cultivating the biofilm on a water permeable membrane. The advantage of both design principles is that a large fraction of the biofilm surface is in direct contact with the gas phase, allowing for transfer of CO_2 into the biofilm and O_2 out of the biofilm. Due to the dense packing of the biofilm light is absorbed and attenuated rapidly and nutrients have to be transported by diffusion processes. These gradients of light and nutrients make microalgal biofilm cultivation more complex compared to suspension cultivation.

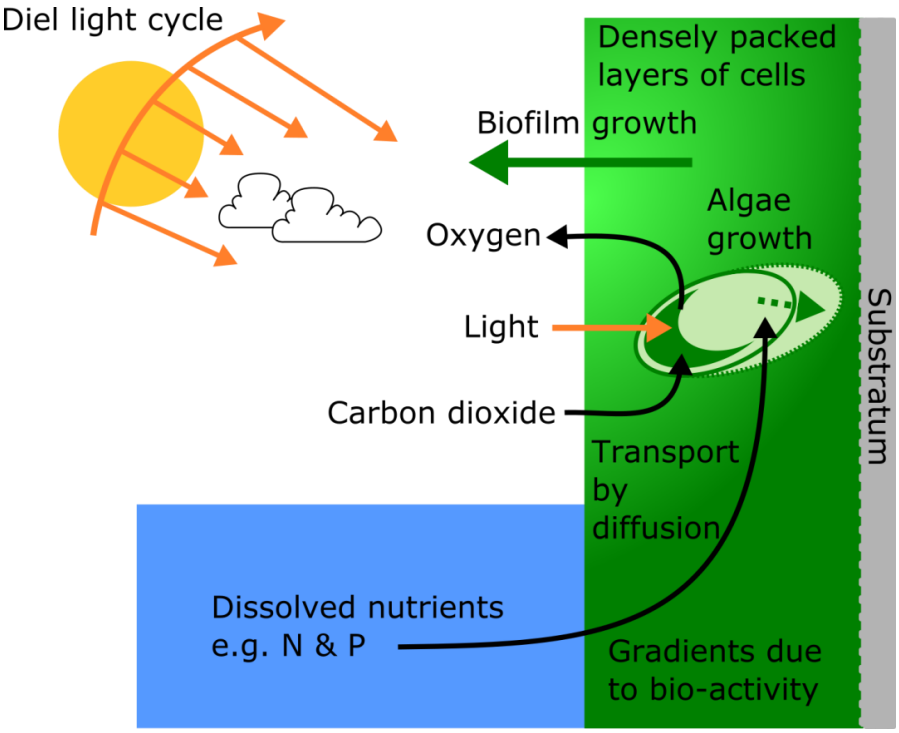

Figure 1.1. Processes influencing biofilm growth**.**

1.5 Thesis outline

To investigate the potential of microalgal biofilm photobioreactors we employed a rotating biofilm contactor based design (Figure 1.2). This photobioreactor design consists of a vertical orientated disk situated in a liquid container. The disk containing the microalgal biofilm rotates such that it alternates between the gas and liquid phase. Because the liquid phase is kept dark we actively selected for biofilm growth on the disk and alternate the biomass on the disk between light and dark to supply the cells both with light and dissolved nutrients. While employing this reactor design the aim of this thesis study was to optimize the productivity of microalgal biomass in phototrophic biofilms.

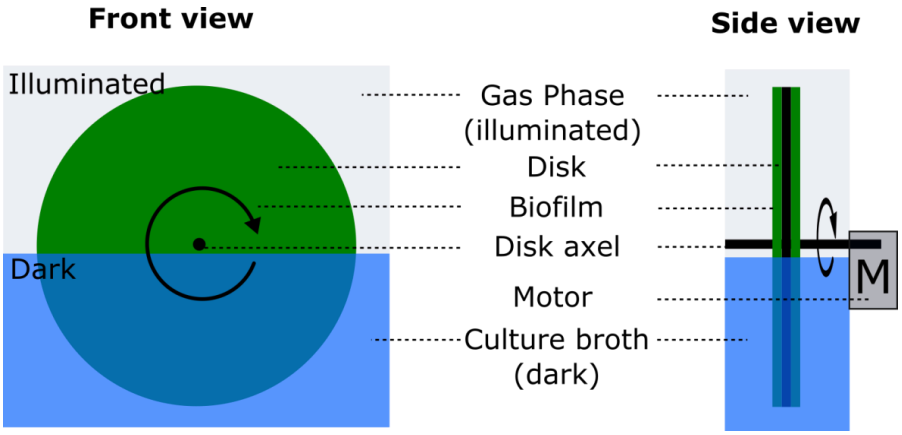

Figure 1.2. The Algadisk reactor. The disk rotates continuously, carbon dioxide is supplied via the gas phase and the other nutrients are dissolved in the water phase, which is kept dark.

In **Chapter 2** illumination of the microalgae culture by artificial light and sunlight is compared. Sunlight is free and abundant but is variable over the day and seasons due to diurnal light cycles, weather conditions, and seasonal changes. These fluctuations in irradiance can be prevented by applying artificial lighting. By means of a techno-economic analysis it was assessed whether the use of artificial light would be an alternative for the utilization of sunlight to drive microalgae production.

In **Chapter 3** the novel biofilm photobioreactor design the Algadisk is introduced (Figure 1.2). The aim of this chapter is to evaluate the potential of the Algadisk photobioreactor with respect to the effects of disk roughness, disk rotation speed and CO_2 supply. These objectives where evaluated in relation to productivity, photosynthetic efficiency, and long-term cultivation stability in a lab-scale Algadisk system by cultivating *Chlorella sorokiniana*. Based on these experiments the window of operation of the Algadisk was identified.

To further understand the conditions inside the biofilm a modelling approach was applied. Due to the lack of models available for *Chlorella sorokiniana*, we first developed a generally applicable kinetic model to predict light limited microalgal growth. This model is presented in **chapter 4** and combines a mathematical

description of photoautotrophic sugar production with a description for aerobic chemoheterotrophic biomass growth. For the calibration and validation of the model both the biological parameters and a large number of calibration and validation experiments were obtained from literature. The model was able to predict the specific growth rate of *Chlorella sorokiniana* and *Chlamydomonas reinhardtii* under a wide range of light limited cultivation conditions.

In **Chapter 5** the influence of diel sunlight variations and prolonged darkness deep inside the biofilm was investigated. This is relevant to understand microalgal biofilm productivity and the microalgal response to conditions inside the biofilm. The microalgal growth model introduced in Chapter 4 was extended with descriptions of day-night driven carbon-partitioning to sugar storage and functional biomass, and the metabolic response to prolonged darkness. This model extension was calibrated and then validated based on experimental results. Model simulations with the validated biofilm growth model were used to compare the photosynthetic efficiency under biofilm growth with that of suspension growth.

In **Chapter 6** a study is described on how to minimize the CO_2 loss of microalgae cultivation to the environment. The loss of CO_2 is undesirable for both environmental and process economics. For this study the phototrophic biofilm growth model from Chapter 5 was incorporated in a reactor model such that CO_2 consumption and productivity of microalgae in biofilm reactors could be maximized. After validation of the extended model, CO_2 utilization and productivity were maximized by changing the gas flow rate, number of biofilm reactors in series, and the gas composition.

In **Chapter 7** current state of the art biofilm photobioreactors are evaluated. Based on this evaluation design elements of the various designs were combined into an improved conceptual biofilm photobioreactor design. In addition, bioprocess control strategies were discussed that allow for optimal harvesting frequencies, efficient temperature control, and maximal nutrient utilization efficiency. By employing these

guidelines the full potential of microalgal biofilm photobioreactors can be exploited in improved and scaled-up systems.

Chapter 2 Cultivation of microalgae on artificial light comes at a cost

This chapter is published as:

Blanken, W.; Cuaresma Franco, M.; Wijffels, R.H.; Janssen, M.G.J.
"Cultivation of microalgae on artificial light comes at a cost"
2013, Algal Research 2 (4). p. 333 - 340

Abstract

Microalgae are potential producers of bulk food and feed compounds, chemicals, and biofuels. To produce these bulk products competitively, it is important to keep costs of raw material low. Light energy can be provided by sun or lamps. Sunlight is free and abundant. Disadvantages of sunlight, however, include day/night cycles, changes in weather conditions, and seasonal changes. These fluctuations in irradiance can be prevented by applying artificial lighting. Artificial lighting will not only increase productivity but will also increase costs associated with microalgae cultivation. This cost increase is recognized, but a detailed quantitative evaluation was still missing. The Costs and energy balance related to microalgae cultivation employing artificial light was evaluated with a literature study.

We calculated that current application of artificial light will increase production costs by 25.3 $ per kilogram of dry-weight biomass. From these calculations, it was determined that 4% to 6% of energy from electric input is fixed as chemical energy in microalgae biomass. Energy loss and increased production cost may be acceptable in the production of high value products, but in general they should be avoided. Microalgae cultivation programs should therefore focus on employing sunlight.

2.1 Introduction

Microalgae are potential production organisms of bulk food and feed compounds, chemicals, or biofuels (Acien et al. 2012; Davis et al. 2011; Draaisma et al. 2012; Norsker et al. 2011; Wijffels et al. 2010). In order to competitively produce these bulk products, it is significant to reduce the raw material costs of production (Norsker et al. 2011). The four major raw materials for microalgae cultivation include phosphorous, nitrogen, carbon dioxide, and light energy.

Light energy can be provided by the sun or with the employment of lamps. This choice is often subject of debate. The exploitation of sunlight as a light source is advantageous in that it is free and abundant. However, it also exhibits certain disadvantages: day/night cycles, changing weather conditions, and seasonal changes. Moreover, all of these factors are location specific. These fluctuations in irradiance levels can be precluded by applying artificial lighting. Continuous and controlled illumination will result in increased productivity as biomass is not dissipated during the night, and artificial lighting can be integrated into the photobioreactor design (Cuaresma et al. 2009; Cuaresma et al. 2011). Volumetric productivity, moreover, can be increased by implementing high density photobioreactors which can be designed with a short light path and high incident light intensity (Gordon and Polle 2007; Lee and Palsson 1994). These advantages have led to numerous initiatives where artificial lighting is employed for the production of microalgae biomass (Chen et al. 2011; Gordon and Polle 2007; Lee and Palsson 1994). The extensive exploitation of artificial light, however, results in investment and electricity costs which will subsequently increase the final production costs (Chen et al. 2011). Although the economical disadvantages of artificial light are customarily referenced, the actual costs and the energy balance are disregarded. However, without this information, an assessment of the process economics and sustainability is impossible. Ignoring the energy balance in life cycle analysis over biofuel production can therefore result in flawed discussions (Amer et al. 2011; Chen et al. 2011). The objective was to evaluate the costs and energy balance related to the implementation of artificial light in microalgae cultivation.

2.2 Input parameters

The final price of microalgal biomass comprises the sum of the costs involved in microalgae cultivation and downstream processing. In this study, the cultivation costs are divided into the costs related to artificial illumination and the estimated normal operating and investment costs of a full-scale photobioreactor plant.

The initial focus will center on the electricity cost required to produce one kilogram of dry microalgae biomass (in dollars per kilogram of dry weight biomass, $ kg-DW^{-1})[1]. In order to calculate this, three values are required; (1) electricity costs; (2) light source efficiency (i.e., the amount of light energy generated for one unit of electrical energy); and (3) microalgae biomass yield from light energy (i.e., the amount of biomass produced per unit of light supplied).

2.2.1 Electricity price

Industrial electricity prices in the European Union (EU) range between 0.07 $ kWh^{-1} in Bulgaria to as much as 0.20 $ kWh^{-1} on Cyprus with an average of 0.12 $ kWh^{-1} over all EU countries (EU 2012). Industries are subject to these prices when consumption reaches between 10 to 40 GWh per year^{-1}. This corresponds to an algae production facility with an approximate annual production of 70 to 280 tonnes of dry microalgae biomass, which is significant considering that the world total microalgae production in 2010 was approximately 5000 tonnes (Wijffels and Barbosa 2010).

Light source efficiency

Numerous types of lamps are commercially available such as fluorescent tubes, high intensity discharge lamps (HID), and light emitting diodes (LED). Ideally, light sources exhibit an extensive wall plug efficiency (WPE) and minimal investment costs. The WPE is the ratio between the radiant flux in watts and the electrical input power in watts. According to Planck's relation, blue light yields less photons per watt when compared to red light (Appendix 2.A). As microalgae can employ all

[1] prices are recalculated from euro to US dollar with the current exchange rate of 1.34 $ €$^{-1}$ (13 June 2013)

photons in the PAR range (wavelength between 400 and 700 nm) regardless of the energy content of the photon, the WPE does not accurately depict the amount of algae that can be grown per unit of electrical energy. Therefore, in this study, the parameter PAR efficiency is introduced with units in µmol PAR photons per second per watt of energy (µmol-ph s^{-1} W^{-1}).

Based on broad experience in horticulture, three types of lamps are identified as the most promising light sources for microalgae cultivation. The first type, fluorescent tubes, exhibits a PAR efficiency of 1.25 µmol-ph s^{-1} W^{-1} and are mostly exploited in laboratories and plant growth chambers. The second type is HID from which the high pressure sodium lamp with a PAR efficiency of 1.87 µmol-ph s^{-1} W^{-1} is the most commonly employed in horticulture. The third type is LED, which are continuously being improved. Currently, commercially available LEDs exhibit a PAR efficiency of 1.91 µmol-ph s^{-1} W^{-1} (Philips 2012a).

As demonstrated in Table 2.1, the different lamps are compared according to their PAR efficiency. The results indicate that HID and LED would be the most suitable lamps for microalgae cultivation. Although they exhibit a comparable PAR efficiency, HID remains the preference in horticulture due to the lower investment costs. PAR efficiency of HID, however, has already almost attained its technical maximum while, on the contrary, the PAR efficiency of LED has rapidly increased over the last decade and is continuously improving. Moreover, the price of LEDs continues to decrease (Liu et al. 2009; Philips 2012b; Pimputkar et al. 2009).

Table 2.1. Overview of various light sources

	WPE	Luminous efficiency	PAR efficiency	Operating current	References
		Lumens W^{-1}	µmol-ph s^{-1} W^{-1}	mA	
Commercial available light sources					
GreenPower LED interlighting module deep red/blue			2.00		(Philips 2012a)
Royal blue LED Philips LUXEON rebel colour	48%		2.00	350	(Lumileds 2012)
Deep red LED Philips LUXEON rebel colour	46%		2.55	350	(Lumileds 2012)
HID lamps			1.65-1.87		(Philips 2012a; Ruijter de et al. 2007)
Fluorescent tubes			1.25		(Philips 2012a)
Optimal lab results					
SHE-blue LED	86%			8	(Narukawa et al. 2010)
Maximum luminous efficiency achieved for cool white LED		203	2.68	350	(Narukawa et al. 2010)
Theoretical maximum cool white LED		260-300	3.40-3.92	Low*	(Narukawa et al. 2010; Pimputkar et al. 2009)

*most likely to be obtained at low operating currents as is discussed above.

Heat production for both, HID and LED light is in the same order of magnitude as their WPE are similar. LED, however, possess a narrow emission band, and in contrast to HID, there is no emission in the infrared range. The lack of infrared radiation makes cooling of the photobioreactor more convenient as only the light source has to be actively cooled. In regards of HID lighting, infrared light heats the radiated surfaces, which, depending on the working temperature and the ambient temperature, could introduce extra costs in order to cool the systems down.

Three major factors continue to limit the efficiency of LEDs: (1) The refractive indices of the materials employed in the LED differ significantly from air, resulting in total internal reflection of photons and, therefore, light loss. This can be reduced by roughening the LED surface; (2) The WPE is high at low currents but decreases with increasing currents subsequently limiting the light output from an LED; (3)

High currents are associated with high temperatures, which can result in degradation of the LED materials, decreasing their lifetime when overheated. The final WPE is determined with the combination of these three main factors (Liu et al. 2009; Narukawa et al. 2010; Pimputkar et al. 2009).

Despite these limitations, improvements to the WPE of LEDs remain available. In literature, blue LEDs are reported with a WPE of above 80%, which corresponds to a PAR efficiency of 3.3 µmol-ph s^{-1} W^{-1} (for calculation, see Appendix 2.A). This WPE is achieved with a very low current (8 mA), resulting in a very low output power (Narukawa et al. 2010). This indicates that a significant number of LEDs should be used in order to supply the high output power required to grow microalgae, which subsequently increases the final price of a luminary. In this aspect, LED research is focused on the development of LEDs that produce greater power output in combination with a high WPE. For example, the current PAR efficiency of high power blue and red LEDs are 2.0 and 2.6 µmol-ph s^{-1} W^{-1}, respectively (Table 2.1) (Lumileds 2012). However, it is anticipated that the PAR efficiency of commercial high power LED lighting systems will eventually increase to 3 µmol-ph s^{-1} W^{-1} in the coming years (Philips 2012b).

Most LED research is focused on developing efficient white LEDs as a replacement for conventional lighting, which consists of incandescent bulbs and fluorescent tubes. A significant number of white LEDs comprise a blue LED with yellow phosphor, which converts a portion of the blue light to yellow light and resulting in white light. In the conversion from blue to yellow light, a loss of energy occurs, decreasing the WPE (Liu et al. 2009; Pimputkar et al. 2009). However, microalgae can exploit all wavelengths within the PAR range (light with a wavelength between 400 to 700 nm), hence, this conversion is not necessary for microalgae growth. Consequently, white LED light is not ideal for microalgae cultivation as energy is unnecessarily lost in the conversion from blue to yellow light, but remains beneficial as an indicator of the WPE of LEDs.

The electrical efficiency of white LEDs is denoted as luminous efficiency in lumens per watt. Lumens are measured relative to the sensitivity of the human eye which is more sensitive to green light. In order to assess their capability for microalgae cultivation, the luminous efficiency should be recalculated to PAR efficiency based on its emission spectrum. The recalculation can be executed with the CIE standard photopic observer curve (see Appendix 2.B). The theoretical maximum luminous efficiency for cool white LED has been estimated at approximately 260-300 lumens per Watt (3.40-3.92 µmol-ph s^{-1} W^{-1}) (Narukawa et al. 2010; Pimputkar et al. 2009). The most extensive luminous efficiency reported in literature is 203 lumens per Watt (2.65 µmol-ph s^{-1} W^{-1}) (Table 2.1) (Narukawa et al. 2010; Pimputkar et al. 2009).

2.2.2 Biomass yield on light energy

In photosynthesis light, energy is harvested and exploited to create new functional biomass, i.e. microalgae cells. During the light reactions of photosynthesis, light energy is employed to transfer electrons from water (H_2O) to oxidized nicotinamide adenine dinucleotide phosphate ($NADP^+$) to yield NADPH and oxygen (O_2). Concurrently, adenosine triphosphate (ATP) is produced. The NADPH and ATP generated by the light reactions are subsequently utilized during the Calvin-Benson Cycle to fix carbon dioxide (CO_2), reduce the carbon, and form triose sugars ($C_3H_6O_3$) (Equation 2.1). The oxygen liberated from water in the light reactions can be employed to calculate the requirement of light energy. Consistent with the accepted Z-scheme of photosynthesis, 8 PAR photons are required to liberate 1 O_2.

In practice, under ideal conditions (low light), a minimal quantum requirement of 10 photons has been ascertained. This value is the average of a number of independent studies, which measured the quantum requirement with various techniques (Bjorkman and Demmig 1987; Dubinsky et al. 1986; Emerson and Lewis 1943; Evans 1987; Ley and Mauzerall 1982; Malkin and Fork 1996; Tanada 1951). Apparently, the light reactions do not perform at 100% efficiency even under ideal low-light conditions. In addition, it can be hypothesized that the ATP/NADPH ratio originating from the light reactions is less than what is required for carbon dioxide reduction in the Calvin-Benson Cycle. This would indicate that additional cyclic

photosynthetic electron transport is required in order to generate additional ATP, which subsequently results in a photon requirement greater than 8 (Allen 2003). The reciprocal of the quantum requirement will be indicated as the yield of oxygen (O_2) on photons $Y_{O2/ph}$ and will be utilized in the analysis below. Its maximal value is 0.10 ($Y_{O2/ph,m}$).

Light reactions plus Calvin-Benson Cycle:

Equation 2.1 $$CO_2 + H_2O + \left(\frac{1}{Y_{O2/ph}}\right) * photons \rightarrow \frac{1}{3} * C_3H_6O_3 + O_2$$

Part of the triose creates building blocks for microalgae growth, and the other part is entirely broken down and oxidized into carbon dioxide and water in order to generate additional ATP. The breakdown of sugars is the combined action of glycolysis, Krebs Cycle, and oxidative phosphorylation; we will refer to this process as mitochondrial respiration.

It is significant to realize that the ATP solely generated by the light reactions is only sufficient to support the production of triose in the Calvin-Benson Cycle. The additional ATP produced by mitochondrial respiration is required to drive the growth reactions in order to create functional biomass (i.e., new microalgae cells) from triose sugars. In addition to growth, ATP is also necessary for maintenance of all energy demanding reactions not strictly related to growth For this analysis the growth independent maintenance requirement is not addressed because its relative impact depends on the actual specific growth rate inside a photobioreactor. By neglecting the growth independent maintenance requirement the most positive biomass yield on light will be calculated. Equation 2.2 exhibits the growth reactions, excluding respiration, for *Chlamydomonas reindhardtii (Kliphuis et al. 2011a)*:

Equation 2.2 $$1.095 \cdot \tfrac{1}{3} \cdot C_3H_6O_3 + 0.14 \cdot NH_3 \rightarrow CH_{1.62}O_{0.41}N_{0.14} + 0.095 \cdot CO_2 + 0.495 \cdot H_2O$$

However, with mitochondrial respiration included, the complete growth reaction is obtained as in Equation 2.3.

Equation 2.3

$$\left(\frac{1}{Y_{x/S}}\right)\cdot \tfrac{1}{3}\cdot C_3H_6O_3+\left(\frac{1}{Y_{x/S}}-1.095\right)\cdot O_2+0.14\cdot NH_3\rightarrow CH_{1.62}O_{0.41}N_{0.14}+\left(\frac{1}{Y_{x/S}}-1\right)\cdot CO_2+\left(\frac{1}{Y_{x/S}}-0.6\right)\cdot H_2O$$

The parameter $Y_{x/S}$ represents the yield of biomass (in C-mol) on 1 C-mol of triose sugar (represented by symbol 'S' of substrate). The value ($1/Y_{x/S}$)- 1.095 depicts the amount of triose that is required to be respired in order to support (i.e., drive) the growth reactions. Its value is not readily available for microalgae growth. It was estimated based on the work of Vejrazja et al. (2013) (Vejrazka et al. 2013) who mensurated a growth-associated respiration rate recalculated to 0.2 mol triose respired per C-mol of biomass produced. This results in a $Y_{x/S}$ for photoautotrophic growth on ammonia of 0.77 C-mol biomass per C-mol triose. Based on the work of Kliphuis (2011) (Kliphuis et al. 2011a), a growth-associated respiration rate of 0.5 mol triose consumed per C-mol of produced biomass was calculated resulting in a $Y_{x/S}$ of 0.63 C-mol biomass per C-mol triose. When growing microalgae on nitrate, the biomass yield will be less in consideration of the decreased degree of reduction. For the analysis in this study, we will use the more favorable nitrogen source of ammonia. Based on these fundamentals, the maximum biomass yield on PAR photons can be calculated with Equation 2.4.

Equation 2.4 $$Y_{x/ph,m}=Y_{x/S}\cdot Y_{S/O2}\cdot Y_{O2/ph,m}$$

Where $Y_{S/O2}$ equals the yield of C-mol triose on 1 mol of oxygen.

Based on the high and low estimates of $Y_{x/S}$, we can calculate a maximum biomass yield ($Y_{x/ph,m}$) between 0.063 and 0.077 C-mol of biomass per mol of PAR photons. We hypothesize that the lower yield is the most realistic because a $Y_{x/S}$ of 0.63 is closer to the maximum values obtained for aerobic chemoheterotrophic growth (von Stockar and Liu 1999). Finally, considering that 1 C-mol of biomass corresponds to

a dry weight of 24 grams (Kliphuis et al. 2011a), the maximum biomass yield on light can also be expressed as 1.5 gram of microalgae biomass per mol of PAR photons.

The biomass yield on light calculation above is based on current understanding of stoichiometry of microalgae growth which is based on the underlying biophysical and biochemical reactions. This analysis is further supported by an thermodynamic analysis (von Stockar and Liu 1999; von Stockar et al. 2011). In our calculation the maintenance respiration, photoinhibition and photorespiration are not taken into account because these can be minimized by selecting appropriate cultivation conditions

2.3 Results

2.3.1 Electricity costs resulting from artificial lighting

Employing the values discussed above, the electricity requirement in order to produce one kilogram of dry microalgae biomass can be calculated. The electricity price utilized in the calculations is 0.12 \$ kWh^{-1}, which is indicative of the average price for significant industries (EU 2012). Regarding the biomass yield on light ($Y_{x/ph}$), two values are depicted: 1.5 g-DW $mol\text{-}ph^{-1}$ and a lesser value of 1.0 g-DW $mol\text{-}ph^{-1}$ the first is the maximum biomass yield derived from our current comprehension of photosynthesis and the second is based on a range of dedicated studies. We believe 1.0 g-DW $mol\text{-}ph^{-1}$ is a realistic aim for a large-scale microalgae production plant as this value is in the higher end of commonly measured biomass yields on light (Kliphuis et al. 2010; Takache et al. 2010; Vejrazka et al. 2011; Zijffers et al. 2010; Zittelli et al. 2006). Figure 2.1 depicts the calculated electricity cost as a function of PAR efficiency. The theoretical maximum PAR efficiency with red light (with 100% WPE) of 5.8 $\mu mol\text{-}ph\ s^{-1}\ W^{-1}$ (see calculations Appendix 2.A) is selected as the maximum value in this graph.

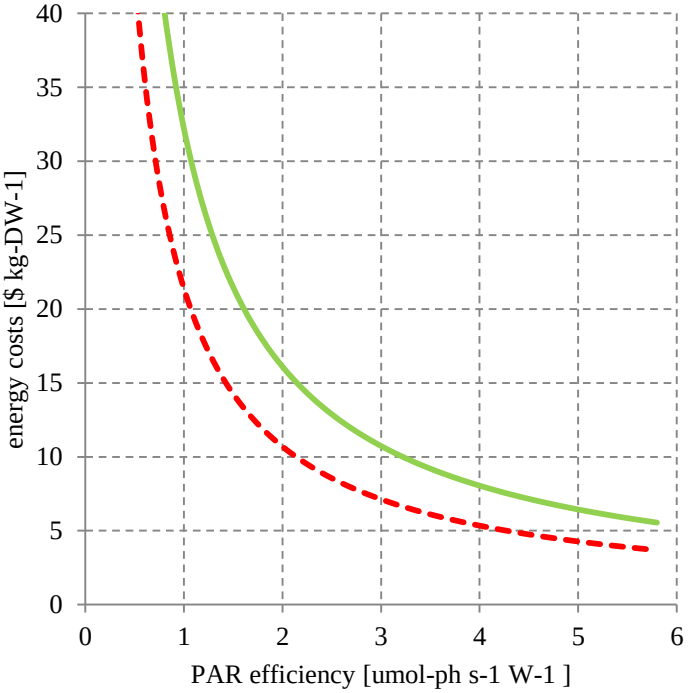

Figure 2.1. Energy cost per kg of biomass produced, as a function of PAR efficiency. Two different biomass yields on light are shown: the maximal yield based on a theoretical analysis (1.5 g-DW mol-ph^{-1}, - - - -) and the estimated maximal yield to be reached in large-scale plants (1.0 g-DW mol-ph^{-1}, ——).

Based on a commercial available light source with a WPE of 2.0 µmol-ph s^{-1} W^{-1} and a $Y_{x/ph}$ of 1.0 g-DW mol-ph^{-1}, the electricity costs are calculated at 16.1 $ kg-DW^{-1}. This could decrease to 10.7 $ kg-DW^{-1} in the future when LED lighting achieves efficiencies of 3 µmol-ph s^{-1} W^{-1} (Philips 2012b).These electricity costs, however, are still optimistic due to the difficulty in maintaining a high $Y_{x/ph}$ over an extended period of time (Tredici 2010) and the WPE of the light source will subsequently decline over time (Philips 2012a). In this respect, electricity costs could possibly be underestimated in the above calculation.

Calculated electricity costs are more than one order of magnitude too high for the production of bulk products and biofuels which both require biomass production costs under 1.3 $ kg-DW^{-1} (Draaisma et al. 2012; Wijffels et al. 2010). In regard to other specific products, the exploitation of artificial light to grow microalgae might still be feasible. Currently, microalgal biomass is mainly produced for high-value food and feed additives or pigments (Del Campo et al. 2007; Milledge 2010; Spolaore et al. 2006). These products possess a higher economic value in comparison to bulk products. Carotenoids, for example, are valued between 300 to 3000 $ kg^{-1} depending on the specification and demand (Ben-Amotz 2004). Carotenoid production, however, is currently mainly produced with sunlight (Del Campo et al. 2007), saving production costs and increasing the profit margin.

2.3.2 Investment costs for artificial light

Investment costs associated with luminaires and power supplies for lamps should also be taken into consideration. Current market prices for installation of high power LED lighting on a large scale will constitute approximately 1.3 $ (µmol-ph s^{-1})$^{-1}$ (Philips 2012b), but that price is expected to decrease in the future in accordance with another source (Ruijter de et al. 2007). The WPE of luminaries decreases over time as light output decreases and dirt accumulates. The WPE of Philips LED luminaires, however, diminishes from the initial WPE to 90% after 25,000 hours and subsequently to 70% after the next 25,000 hours (Philips 2012a). In the case of HID lamps, the installation cost is 0.27 $ (µmol-ph s^{-1})$^{-1}$ (Philips 2012b), and the initial WPE decreases to 90% following 12,000 hours of use (Philips 2012a). Typically, in horticulture, the lamps are replaced after 10,000 hours of use (Philips 2012b). In our calculations, a linear decrease in WPE in time is assumed.

Investment costs per kg-DW of produced microalgal biomass can be calculated according to Equation 2.5, and they are collated to electricity costs calculated according to Equation 2.6. In Table 2.2, the current investment and electricity costs are depicted for LED and HID. The anticipated future costs of LED are based on a 50% cost reduction and a PAR efficiency increase to 3 µmol-ph s^{-1} W^{-1} (Philips 2012b).

Table 2.2. Investment and electricity costs of LED and HID lamps. Current and expected values are listed under results, which are calculated with the values listed under Input.

Calculated Costs				
		LED	**HID**	**LED future**
Investment costs	\$ kg-DW^{-1}	7.4	6.2	3.7
Electricity costs	\$ kg-DW^{-1}	19.3	19.1	12.3
Total costs artificial lighting	\$ kg-DW^{-1}	26.7	25.3	16.0
Input parameters				
Investment costs	\$ (µmol s^{-1})$^{-1}$	1.34	0.27	0.67
PAR efficiency initial	µmol-ph s^{-1} W^{-1}	1.91	1.87	3.00
PAR efficiency average	µmol-ph s^{-1} W^{-1}	1.67	1.68	2.63
$Y_{x/ph}$	g mol^{-1}	1	1	1
Lifetime	Hours	50000	12000	50000
Output loss over lifetime	%	70	90	70
Electricity price	\$ kWh^{-1}	0.116	0.116	0.116

Equation 2.5 $$Investment\ \cos ts = \left(\frac{Cost\ light\ source}{lifetime * Y_{x/ph}} \right)$$ in \$-investment kg-DW^{-1}

Equation 2.6 $$Electricity\ \cos ts = \left(\frac{electricity\ price}{PAR\ efficiency * Y_{x/ph}} \right)$$ in \$-electricity kg-DW^{-1}

Where the light source cost is in \$ (µmol s^{-1})$^{-1}$, and the electricity price is in \$ J^{-1}.

Calculations depict that LED lighting is currently more expensive compared to HID lighting. If the PAR efficiency of LED lighting is ameliorated, and the investment costs reduced, total costs will favour the exploitation of LEDs. During a time frame of five to ten years, LED prices are, indeed, expected to further decrease with introduction of mass production (Liu et al. 2009). Furthermore, LEDs are advantageous in other ways as well when compared to HID lighting. LED

luminaries can be designed to produce more homogeneous light distribution, simplifying the reactor design. Furthermore, LEDs radiate no infrared light depending on the ambient temperature and working temperature decreasing costs in order to cool the systems down.

Another advantage of the narrow emission band of LED is that the optimum wavelength for algae growth can be supplied. Research has demonstrated that the quantum requirement (QR) of photosynthesis of microalgae is less for blue light and most optimal (10 photons per O_2 produced) in the red segment of the spectrum (600 to 680 nm) (Emerson and Lewis 1943; Tanada 1951). Similar results are achieved in more recent studies for a broad range of higher plants (Evans 1987; Hogewoning et al. 2012; Paradiso et al. 2011). Based on the measurement of the QR, red light (660 nm) would be most efficient for photosynthetic growth. Microalgae cultivation in red light, indeed, appears effective in lab scale cultivations (Chen et al. 2010; Cuaresma et al. 2011). Notice that, in the biomass yield on light energy calculations, the maximum QR in red light is considered.

2.3.3 Operation and investment costs of a microalgae plant

In addition to electricity and investment costs for artificial lighting are the costs associated to the operation of a full scale photobioreactor plant. Most of the large scale plants employ open ponds to cultivate microalgae. These systems are inexpensive, but they achieve low productivity and are sensitive to contamination, being most efficient for microalgae growing in extreme conditions (Carvalho et al. 2006). Closed photobioreactors, on the other hand, are more promising since they afford a greater degree of control regarding process parameters. Consequently, higher productivity is achieved and closed systems protect against invading species.

Based on cost calculation studies and analyses of pilot scale facilities with closed photobioreactors, the current operation and investment costs are estimated between 5 to 23 \$ kg-DW^{-1} depending on the plant size (Acien et al. 2012; Davis et al. 2011; Norsker et al. 2011; Wijffels et al. 2010). With anticipated improvements in cultivation and technical design of photobioreactors, the cost of microalgae is

expected to diminish to 0.9-1.1 $ kg-DW^{-1} over the next decade (Davis et al. 2011; Norsker et al. 2011). Considering the current estimations for investment and operation costs, the exploitation of artificial light will double the costs to 31 to 50 $ kg-DW^{-1}. It reinforces the previous statement that microalgae growth in artificial light is only feasible for high value products, and sunlight should be employed when producing bulk products.

2.4 Energy balance

Life cycle analysis is an important tool to evaluate the sustainability of the process. This tool is already used to evaluate outdoor microalgae cultivation systems (Clarens et al. 2010), however, these evaluations are lacking for artificial illuminated systems. Considering the production of biofuels the energy balance should be positive. It is, therefore, significant to consider the energy content of the produced microalgae and the energy input required during the production process.

The energy demand during the process can be compared to the combustion enthalpy of algae biomass (0.477 MJ C-mol^{-1}) (Figure 2.2) (Duboc et al. 1999; Tredici 2010; von Stockar et al. 1993). From Figure 2.2 follows that with a PAR efficiency of 2 µmol-ph s^{-1} W^{-1}, and a biomass yield on light of 1.0 to 1.5 g-DW mol-ph^{-1}, merely 4% to 6 % of the energy from electrical input is conserved in microalgal biomass. The energy conserved actually is half of the one depicted in the Figure 2.2, as the efficiency of electricity generation in power plants is between 40% and 60% (Graus et al. 2008). Based on the large amounts of energy that are lost in the cultivation of microalgae on artificial light, the employment of artificial light should be avoided.

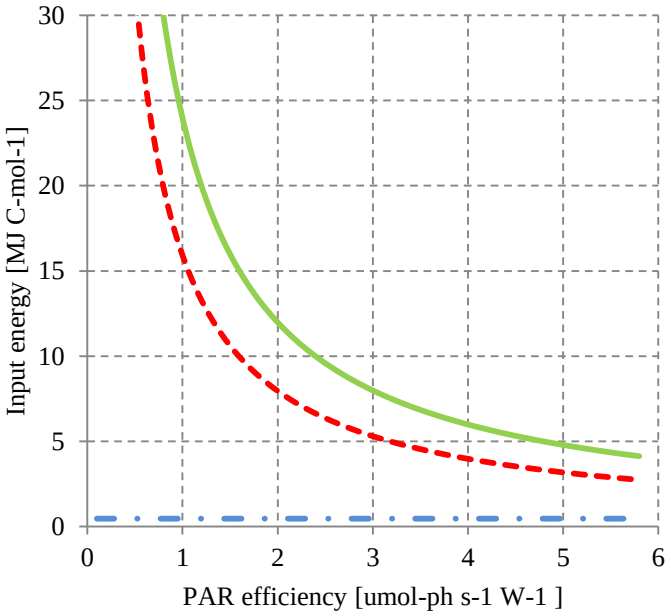

Figure 2.2. Electric energy input of artificial illumination compared to the combustion enthalpy of microalgae, as a function of PAR efficiency. Two different biomass yields on light are shown: the maximal reported in literature (1.5 g-DW mol-ph^{-1}, - - - -) and the averaged value obtained in practice (1.0 g-DW mol-ph^{-1}, ——). These values are compared to the combustion energy of micro algae (0.477 MJ C-mol^{-1}, — · —).

2.4.1 Alternative approaches

Electrical energy required for microalgae cultivation employing artificial light could be generated as 'green' energy instead of that derived exploiting fossil fuels. Three processes are compared regarding their energy balance throughout the entire process (from energy generation to the final creation into biomass). Figure 2.3 depicts three different approaches: (1) coal derived electricity → red LED light → microalgae; (2) photovoltaic (PV) cells derived energy → red LED light → microalgae; and (3) sunlight → microalgae. For a convenient comparison, photosynthetic efficiency (PE) is employed which can be calculated from the biomass yield on light energy (see Appendix 2.C).

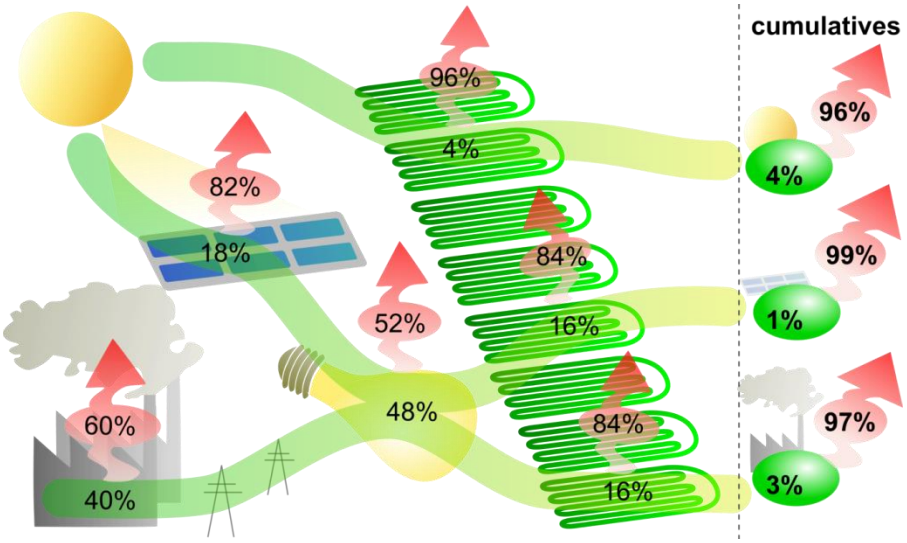

Figure 2.3. Schematic overview of the energy balance on various energy sources. Schematic overview of the energy balance of microalgal biomass production on various energy sources. From top to bottom microalgae production on sunlight, on sunlight via PV-derived electricity, and on fossil fuels via coal-derived electricity. Energy lost is depicted by red arrows pointing upwards. Energy conserved is depicted inside the green flow lines each representing a separate process. The column on the right shows the cumulative energy lost and conserved for each energy source: sunlight, sunlight + PV, coal.

The schematic overview in Figure 2.3 is based on the following assumptions. The PE of microalgae growing in closed photobioreactors on sunlight is calculated as 4% and the PE on red light is 17%. This has two explanations: first, sunlight energy consists of 42.5 % of photons in the PAR region while, for red light, the energy consists of 100% PAR. Secondly, microalgae can exploit red light more efficiently compared to sunlight, therefore, a biomass yield of 1.0 g-DW mol-ph^{-1} is assumed with sunlight compared to a maximum biomass yield of 1.5 g-DW mol-ph^{-1} with red light. Our calculated PE on sunlight is slightly lower compared to the PE of the 5.4% reported in literature (Tredici 2010).

Commercially available photovoltaic cells achieve an efficiency of 18 % in sunlight (Energy 2010). Greater efficiencies have been accomplished in laboratories, but the

techniques employed are too expensive for commercial use (Energy 2010). Most of the energy continues to be generated in coal power plants, which achieve an energy efficiency of 40% in the conversion of coal into electric energy (Graus et al. 2008).

From Figure 2.3, it can be inferred that the direct exploitation of sunlight to cultivate microalgae is the most energy efficient approach. Comparing both processes utilizing artificial light, coal based electricity seems more energy efficient. The energy efficiency of a power plant is higher compared to photovoltaic cells, therefore, the overall energy conservation of fuel obtained from a power plant is greater. However, in practice, it will be more sustainable to employ photovoltaic cells since sunlight cannot be exhausted in contrast to coal.

There are additional alternative energy sources that can provide electric power to lamps in order to produce microalgae. These sources can include green energy ranging from wind, sun, water, or even excess energy from power plants. These sources might incite certain cost savings or create a green profile but, because of the low energy conservation in microalgae, they should only be employed when high value products demand precisely controlled cultivation conditions. Sunlight, however, should be the preferred energy source as it saves energy and costs.

2.5 Conclusions

Microalgae cultivation solely exploiting LEDs or HID lamps and neglecting output decline with light source aging will incite electricity costs of 16.1 \$ kg-DW^{-1} and capture only 4 % of the energy input as chemical energy in microalgae. This could improve to 10.7 \$ kg-DW^{-1} and 6 % energy conservation with the achievement of a LED with a PAR efficiency of 3.0 µmol-ph s^{-1} W^{-1}. Current investment costs for LED are calculated at 7.5 \$ kg-DW^{-1} and 6.2 \$ kg-DW^{-1} for HID. If LED manufacturing costs decrease, and the PAR efficiencies of LED increases, LED is more economical compared to HID.

The two major disadvantages of utilizing artificial light are the increase of the overall costs and the negative energy balance. Overall cost increases as electricity cost and investment cost related to the use of artificial light are introduced. The

investment and electricity costs might decrease from 26.7 $ kg-DW^{-1} to 16.0 $ kg-DW^{-1} as LED WPE improves and manufacturing costs reduces. With cost reduction, however, LED lighting still doubles the operational costs of microalgae production.

The negative energy balance is caused by energy losses in luminaries and energy losses during energy fixation into microalgae biomass. The energy conserved in microalgae biomass is 4% to 6% of the energy from electric input. These disadvantages might be acceptable in the production of high value products but should in general be avoided. Therefore large-scale microalgae cultivation should focus on employing sunlight as the sole energy source.

2.6 Appendices

Appendix 2.A. Theoretical maximum WPE

With Planck's relation (Equation 2.A.1), the amount of energy of one photon can be calculated at the wavelength of interest.

Equation 2.A.1 $$E_{ph} = \frac{h * c}{\lambda}$$

With $E_{ph,}$ the energy of one photon in J, h Planck's constant in J s^{-1}, c the speed of light in m s^{-1} and λ the wavelength in m.

By multiplying the energy of one photon with the Avogadro number, the amount of joules per mol photons can be calculated. From these calculations, it has been ascertained that blue photons contain more energy compared to red photons. Because red light contains less energy per photon, the theoretical maximum PAR efficiency of red light (680 nm) is 5.8 µmol-ph s^{-1} W^{-1} while blue light (488 nm) possesses only 4.1 µmol-ph s^{-1} W^{-1}. The theoretical maximum PAR efficiency at the specific wavelength can be employed to recalculate the WPE to PAR efficiency.

Appendix 2.B. From luminous efficiency to wall plug efficiency

To recalculate a luminous efficiency in lumens s^{-1} to a PAR efficiency in µmol-ph s^{-1} W^{-1}, the amount of photons per lumen should be defined. As lumens and the amount of mol-photons is different for every wavelength, a spectral measurement of the light source and the CIE standard photopic observer curve (CIE 1931) can be used (CIE 2013). The CIE 1931 provides the amount of lumens per Watt light energy for every wavelength (Figure 2.B.1). In our case, we measured the spectrum of a cool white LED with the Avaspec 2048 spectrophotometer (Avantes, Apeldoorn, The Netherlands). This gives the spectrum in µmol $(m^2\ s)^{-1}$ nm^{-1} and in Watt m^{-2} nm^{-1}. The measured spectrum in Watt m^{-2} can be converted to lumens m^{-2} using the CIE 1931 (Figure 2.B.2). From Figure 2.B.2, it is clear that the intensities described in lumens value green light more compared to blue or red.

Because microalgae only employ PAR (light between 400 to 700 nm), the amount of lumens in the PAR range must be converted to the amount of photons in the PAR range. A conversion factor ($Y_{ph/lm,}$ unit photons per lumen) can be calculated by adding the lumens $(m^2\ nm)^{-1}$ ($I_{lm,nm}$) and the µmol-photons $(m^2\ s\ nm)^{-1}$ ($I_{ph,nm}$), from 400 to 700 nm. The conversion factor $Y_{ph/lm}$ is subsequently calculated by dividing the cumulatives (see Equation 2.B.1).

Equation 2.B.1 $$\sum_{\lambda=400}^{\lambda=700} I_{ph,nm} \Big/ \sum_{\lambda=400}^{\lambda=700} I_{lm,nm} = Y_{ph/lm}$$

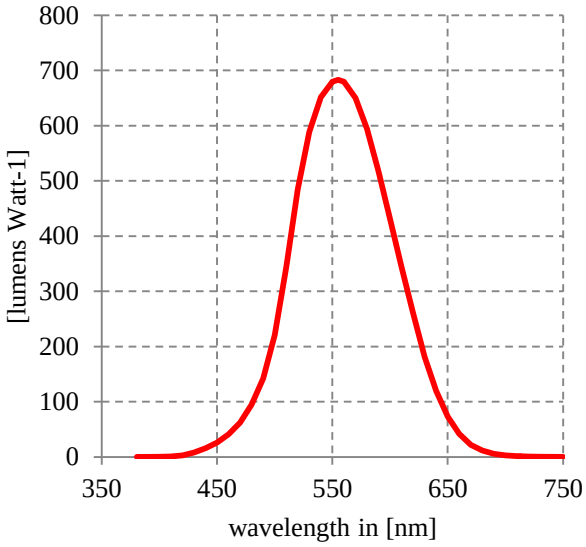

Figure 2.B.1. The CIE standard photopic observer curve.

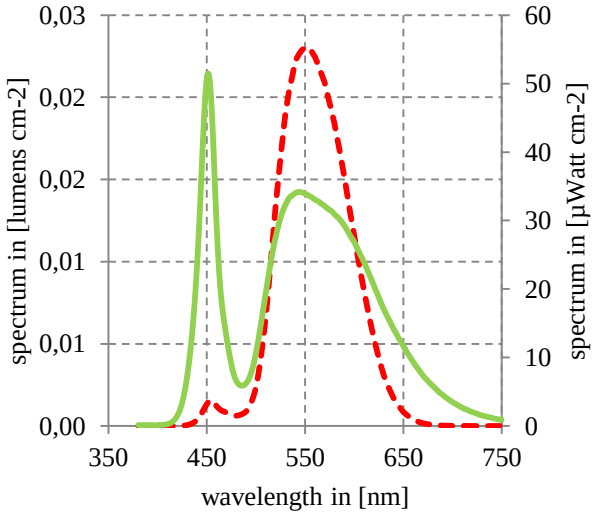

Figure 2.B.2. Spectrum of a cool white LED, luminous efficiency (- - - -) and absolute irradiance (——).

Appendix 2.C. Calculation of photosynthetic efficiency.

Photosynthetic efficiency (PE) is the equivalent of the biomass yield on PAR-photons and provides the percentage of fixed energy as chemical energy inside the microalgae biomass over the supplied sunlight energy. The PE can be calculated according to Equation 2.C.1.

Equation 2.C.1 $$PE = \frac{Y_{x/ph} * \Delta_r H^{\circ}}{E_{ph} * M_x} * 0.425$$

In Equation 2.C.1, $Y_{x/ph}$ is the biomass yield on light in g-DW mol-ph^{-1}. $\Delta_c H^0$ is the combustion energy of microalgae in kJ c-mol^{-1} which is 477 kJ c-mol^{-1} (Duboc et al. 1999; Tredici 2010; von Stockar et al. 1993). E_{ph} is the energy of a PAR photon in kJ mol-ph^{-1} which can be calculated from Planck's relation. M_x is the molecular weight of the microalgae in g-DW c-mol^{-1}.

When calculating photon energy for PAR sunlight, the E_{ph} of 550 nm can be employed because the sunlight spectrum is relatively flat in the PAR range. Because PAR is only 42.5% of the sun irradiance, a factor of 0.425 is added to Equation 2.C.1.

Chapter 3 Biofilm growth of *Chlorella sorokiniana* in a rotating biological contactor based photobioreactor

This chapter is published as:

Blanken, W.M.; Janssen, M.G.J.; Cuaresma, M.; Libor, Z.; Bhaiji, T.; Wijffels, R.H. "Biofilm growth of Chlorella sorokiniana in a rotating biological contactor based photobioreactor"
2014, Biotechnology and Bioengineering, 111 (12), p. 2436 - 2445

Abstract

Microalgae biofilms could be used as a production platform for microalgae biomass. In this study, a photobioreactor design based on a rotating biological contactor (RBC) was used as a production platform for microalgae biomass cultivated in biofilm. In the photobioreactor, referred to as Algadisk, microalgae grow in biofilm on vertical rotating disks partially submerged in a growth medium. The objective is to evaluate the potential of the Algadisk photobioreactor with respect to the effects of disk roughness, disk rotation speed and CO_2 concentration. These objectives where evaluated in relation to productivity, photosynthetic efficiency, and long-term cultivation stability in a lab-scale Algadisk system. Although the lab-scale Algadisk system is used, operation parameters evaluated are relevant for scale-up.

Chlorella Sorokiniana was used as model microalgae. In the lab-scale Algadisk reactor, productivity of 20.1 ±0.7 gram per m^2 disk surface per day and a biomass yield on light of 0.9 ±0.04 grams dry weight biomass per mol photons were obtained. Different disk rotation speeds did demonstrate minimal effects on biofilm growth and on the diffusion of substrate into the biofilm. CO_2 limitation, however, drastically reduced productivity to 2-4 gram per m^2 disk surface per day. Productivity could be maintained over a period of 21 weeks without re-inoculation of the Algadisk. Productivity decreased under extreme conditions such as pH 9-10, temperature above 40ºC, and with low CO_2 concentrations. Maximal productivity, however, was promptly recovered when optimal cultivation conditions were reinstated. These results exhibit an apparent opportunity to employ the Algadisk photobioreactor at large scale for microalgae biomass production if diffusion does not limit the CO_2 supply.

3.1 Introduction

Biofilm-photobioreactors can turn the problem of biofilm formation on the walls of suspended photobioreactors (Jacobsen et al. 2010) into an opportunity. Biofilm-photobioreactors pose several advantages over suspended cultivation of microalgae including the harvest of high dry solid content, a decreased energy requirement (Ozkan et al. 2012), and the possibility of operating at short hydraulic retention times without wash out of the microalgae (Patwardhan 2003). Disadvantages are the formation of gradients over the biofilm for pH, nutrients, and light (Wolf et al. 2007).

Biofilm-photobioreactors are increasingly attracting attention as a cultivation platform because of the advantages discussed above. Because of the possibility to operate at short hydraulic retention times biofilm-photobioreactors are widely studied as part of wastewater treatment. Wastewater treatment plants often operate to clean diluted waste streams at short hydraulic retention times (Patwardhan 2003). Biofilm photobioreactor designs that have been proposed for waste water treatment include rotating spools (Christenson and Sims 2012), rotating brushes (Wei et al. 2008), vertical sheets (Boelee et al. 2012), tubular flow cells (de Godos et al. 2009) and horizontal flow cells (Wilkie and Mulbry 2002). The main disadvantage most of the above systems share are limited control of microalgae species and low productivities. In recent years, a range of biofilm-photobioreactors were developed that intend to employ the biofilm growth as a controllable production platform of dedicated microalgal species. Examples include the twin layer system (Naumann et al. 2012; Nowack et al. 2005; Shi et al. 2007), a similar design referred to as an attached photobioreactor (Ji et al. 2013a; Ji et al. 2013b), the rotating spool system (Christenson and Sims 2012), and the rotating algal biofilm cultivation system (Gross et al. 2013).

In this study a biofilm photobioreactor based on the rotating biological contactor (RBC) design, the Algadisk system, was tested. RBC were exploited for aerobic wastewater treatment (Patwardhan 2003), however a recent study evaluated the performance of a phototropic RBC to remove heavy metal from waste streams

(Orandi et al. 2012). The four major advantages of the RBC design are (1) the lower ratio between footprint and cultivation surface compared to horizontal systems (Wijffels and Barbosa 2010); (2) the opportunity to regulate the average light intensity per disk by varying the disk size and distances between disks (Orandi et al. 2012); (3) that rotation ensures a simple but repetitive contact with the growth medium; and (4) efficient gas-biofilm mass transfer as a result of a large biofilm area exposed to the gas phase and short diffusion paths from gas to the biofilm. The enhanced gas-biofilm mass transfer saves energy since the energy intensive sparging of the culture broth might not be needed (Patwardhan 2003). However, two disadvantages of the RBC design include: (1) the influence of rotation speeds on biofilm performance, high rotation speeds will increase mass transfer and shear while slow rotation speeds will decrease mass transfer and might result in drying (Gross et al. 2013); (2) spatial separation of light and CO_2 from the dissolved nutrients, which could result in nutrient limitations. To test the Algadisk design, a lab-scale version was constructed.

The objective is to evaluate the potential of the Algadisk photobioreactor with respect to the effects of disk roughness, disk rotation speed and CO_2 concentration. These objectives where evaluated in relation to productivity, photosynthetic efficiency, and long-term cultivation stability in a lab-scale Algadisk system. Although the lab-scale Algadisk system is used, operation parameters evaluated are relevant for scale-up.

3.2 Materials and methods

3.2.1 Pre cultivation

The microalgae *Chlorella sorokiniana* (Sorokin and Myers 1953) was pre-cultivated in shake flasks with M8-a medium (Kliphuis et al. 2010). The algae suspension was used to inoculate the disks, as will be explained later. The M8-a media was supplemented with 30 mM Urea as nitrogen source, and pH was set to 6.7. In the reactor medium, an additional 8 mM $NaHCO_3$ was included after setting the pH to increase the dissolved CO_2 concentration. Anti-foam B (J.T.Baker, The Netherlands)

was directly added to the culture broth in the event of foam formation. The M8-a medium contains all dissolved species in excess, therefore microalgae grow under nutrient-replete and light-limited conditions in our experiments.

3.2.2 Experimental set-up

The experimental setup consisted of a water tight container, four disks and eight lamps, (Figure 3.1). The container measured 1220*70*130 mm (L*W*H) and contained 11 L of the M8-a medium. The disks were located inside the water tight container with 42% of the disk surface submerged. The liquid volume in the container was kept constant via an overflow connected to a 10 L buffer tank (polycarbonate). The total volume of the system was 21 L. The temperature was measured and kept at 38 ±1 °C via a heat exchanger inside the buffer tank. The medium was circulated between the buffer tank and the container at a rate of 6 L min^{-1} (MD-6Z, Iwaki, Japan). The pH in the buffer tank was maintained between 6.7 and 6.8 by pulse-wise addition of CO_2 gas or HCl (see section 2.4). Liquid lost by evaporation was detected with a level sensor in the buffer tank and was automatically replaced by filtered tap water.

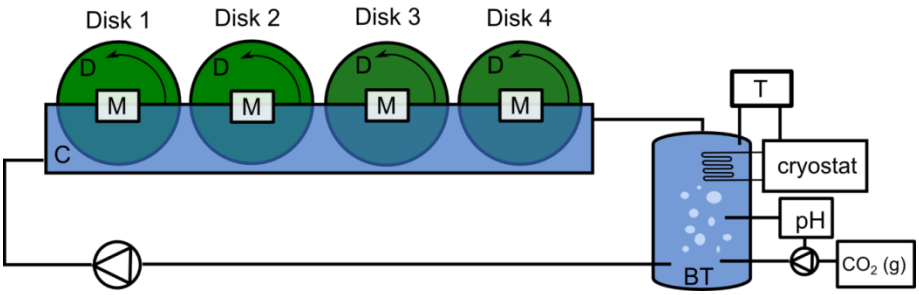

Figure 3.1. Schematic overview of Algadisk lab scale reactor. D = disk, M = motor driving the disk, C = container , T = temperature control system, BT = buffer tank. Both the top of the container and buffer tank are open. Liquid in the reactor vessel flows from left to right, and the direction of disk rotation is depicted in the figure.

Both sides of the disks were illuminated by a warm-white directional LED light source (warm white 45mil chip, Bridgelux, USA). Since the open water container was not transparent, only the upper portion of the disks was illuminated. This

strategy allowed for a selective pressure to stimulate biofilm growth while it minimized microalgae growth in the suspension. Inoculation was performed by adding a microalgae suspension pre-cultivated in a shake flask to the container with the culture media. The selective pressure for biofilm growth was used to initiate biofilm development. After the initial biofilm developed, the biofilm was harvested by scraping. After harvesting, the biofilm could re-grow from the biomass that remained on the disk surface. After the initial harvest (discussed in section 2.7), the biofilm was harvested every seventh day; this cycle is referred to as a 7 day growth-harvest cycle. An example of a typical 7 day growth-harvest cycle is illustrated in Figure 3.2. After every growth-harvest cycle the reactor was cleaned and filled with fresh medium.

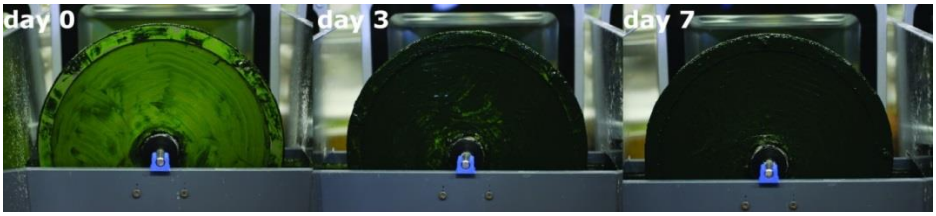

Figure 3.2. Photographs taken during a typical 7 day growth-harvest cycle on the rough metal mesh. The day within the growth-harvest cycle is indicated in white. On day 7, biofilm is harvested and a new cycle begins.

3.2.3 Disk rotation speeds

The rotation speed of the disks could be modified and is depicted in revolutions per minute (rpm). The actual rotation speed is provided for each experiment. However, only the rotation speeds 3, 6, 11, and 20 rpm were evaluated in this study. These speeds correlate to velocities over the disk radius ranging from 0.01 to 0.25 m s^{-1} (section 3.3). All disks were spun in the same direction as the liquid flow (0.01 m s^{-1}), assuming constant flow over the entire cross section. All rotation speeds were tested at all disk positions to exclude possible effects of positioning within the container.

3.2.4 CO_2 supply

Three CO_2 supply conditions were evaluated. The first condition is at nutrient-replete conditions. In all experiments at nutrient-replete conditions 8 mM of $NaHCO_3$ was added to increase the dissolved CO_2 concentration. During the cultivation the CO_2 concentration was controlled based on pH. When microalgae consumed CO_2 the pH increased. This pH increase is countered by CO_2 addition resulting in a constant total carbon concentration of 15 mol m^{-3}. The total carbon concentration is the sum of dissolved CO_2 and HCO_3. The second condition was obtained by using a continuous airflow via sparging the water, containing 0.5%$_{v/v}$ CO_2 corresponding to a total carbon concentration of 0.7 mol m^{-3} if in equilibrium with water. The pH was controlled by the addition of hydrochloric acid (1.5 M HCl in water). The third conditions was obtained by not sparging the liquid and, therefore, only atmospheric CO_2 from the surrounding air was available. The 0.04%$_{v/v}$ CO_2 present in the atmosphere corresponds to a total carbon concentration of 0.06 mol m^{-3} at equilibrium with water. The pH was controlled by HCL addition. For both CO_2 limiting conditions no additional $NaHCO_3$ was added.

3.2.5 Disk materials

Three different disk materials were used during this study: two stainless steel woven meshes and one sanded polycarbonate disk. The first mesh is a Twilled Dutch Weave type 80/700 (GKD SolidWeave, Gemany) with a tread thickness of 0.10/0.076 mm and a particle pass size of 47 μm, referred to as rough mesh. The second mesh is a Twilled Dutch Weave type 200/1400 (GKD SolidWeave, Germany) with tread thickness of 0.071/0.041 mm and a particle pass size of 15 μm, referred to as smooth mesh. The metal meshes were clamped onto a solid stainless steel disk with a 268 mm diameter with a stainless steel ring. The stainless steel ring (i.e., the clamp) was 14 mm wide and 2 mm thick resulting in a biofilm growth area with a 240 mm diameter. In the centre of the disk, a plastic cylinder with a diameter of 50 mm attached the axel to the disk.

The polycarbonate (PC) disk was coated with a polyelectrolyte multilayer coating. Polyvinylpyrrolidone (PVP, 55 000 Mw) and Polyacrylic acid (PAA , Mw 1800)

(Sigma Aldrich, USA) were used for this coating. PVP is a neutral polymer that becomes positively charged when dissolved in phosphate buffer (PBS), and PAA is polyanionic and is negatively charged when dissolved. Polyelectrolytes solutions for dip coating were prepared at a concentration of 1 mg/ml of the polymer dissolved in PBS buffer. The polycarbonate disk was first cleaned with 70% ethanol and deionised water. The PC disk was subsequently submerged into the polyelectrolyte solution (PVP) to ensure that its surface was entirely covered for 15 minutes. The disk was then rinsed twice with deionised water and dried with nitrogen gas at room temperature and submerged into the oppositely charged polyelectrolyte (PAA) for 15 minutes followed by the same washing and drying procedure described above. This was repeated until the desired number of layers (PVP/PAA/PVP/PAA/PVP) was achieved. The PC disk was then placed under UV light for approximately 4 hours. The PC disk has the same growth area as the metal meshes.

The pore depth of the two metal meshes and the polycarbonate disk were compared. For the two steel meshes, the pore depth could be estimated based on CSLM analysis. From the CSLM analysis, it was determined that the rough mesh exhibited a maximal pore depth of 140 µm, and the fine mesh featured a maximal pore depth of 80 µm. To determine the structure on the hand sanded polycarbonate disk, a Dektak stylus profiler (Veeco, USA) was utilized. From the Dektak analysis over 2 mm, it was ascertained that the groves were, on average, 1 µm deep with a maximal depth of 10 µm.

3.2.6 Light measurement

The average light intensity over the illuminated disk surface was individually measured for every side of the disks. The light intensity was measured with a LI-COR 190-SA 2π quantum sensor (PAR range 400-700 nm) employing a template with 11 evenly spaced measure positions diffused over the disk surface as displayed in Appendix 3.A. The average light intensity over all disk surfaces was 422 µmol $(m^2 s)^{-1}$.

3.2.7 Harvest

Harvesting was performed by scraping as much biomass as possible from the disk surface with a metal scraper. The total weight of the collected wet biomass was measured, i.e. the wet biofilm weight. Afterwards, the biomass was dried overnight in an oven at 105 °C and weighed again, i.e. the dry biomass weight. By dividing the dry biomass weight with the wet biofilm weight, the mass fraction of biomass to water in the wet biofilm ($f_{x/w}$) was obtained (unit g/g).

3.2.8 Calculations

The surface productivity (P_x) in units g $(m^2\ d)^{-1}$ was calculated according to Equation 3.1 with the total harvested dry weight (M_d) in g, the growth-harvest cycle time (t) in days, and disk surface (A_d) in m^2.

Equation 3.1, $$P_X = \frac{M_d}{t \cdot A_d}$$

The biomass yield on light ($Y_{X/ph}$) in g mol^{-1} was calculated according to Equation 3.2 with incident light intensity (I_{in}) in mol $(m^2\ d)^{-1}$. The incident light is specific for every disk side and is compensated for the illuminated fraction above the water phase. The illuminated fraction of the disk is 58% [see Appendix 3.A].

Equation 3.2, $$Y_{X/e} = \frac{P_x}{I_{in}}$$

The biofilm thickness (z) in m was calculated based on an estimated biofilm density (ρ_b) in kg m^{-3} (Equation 3.3 and 3.4). The ρ_b is based on the assumption that water has a density (ρ_w) of 1000 kg m^{-3} and that the biomass has a density (ρ_X) of 1029 kg m^{-3} (Salim et al. 2013). The calculation of the mass fraction of biomass to water ($f_{x/w}$) was explained in section 2.7.

Equation 3.3, $$\rho_b = \left(f_{x/w} \cdot \rho_X\right) + \left(\left(1 - f_{x/w}\right) \cdot \rho_w\right)$$

Equation 3.4, $$z = \frac{M_d}{\rho_b \cdot A_d}$$

Standard deviations were calculated according to Equation 3.5, with the individual measurements (x) (one 7 day growth-harvest cycle for one side of a disk)), the mean of all measurements ($\bar{x}$), and the number of measurements (n). The standard deviation of the areal productivity was calculated based on the variance in the measured areal productivities. All other Standard deviations were based on the rules of error propagation.

Equation 3.5, $$\sqrt{\frac{\sum(x-\bar{x})}{(n-1)}}$$

All p-values were calculated using an unpaired t-test.

3.3 Results

3.3.1 Evaluation of different disk materials

This experiment was performed to assess the influence of disk material on the biofilm growth rate. To compare the two metal meshes and the polycarbonate disk, we performed an experiment at 422 µmol $(m^2 s)^{-1}$, constant rotation speed of 11 rpm, and nutrient- and CO_2 replete conditions. A biofilm formed on the disks within 10 days following the inoculation of the medium with a microalgae suspension (optical density of 0.03 at 750 nm after inoculation).

The productivity in the experiment's start-up phase was much less compared to the productivity of the subsequent growth-harvest cycles. Therefore, the start-up phase was not included in the presented data. Following the first harvest, four growth-harvest cycles were performed (n=8 as both sides are measured individually). The rough mesh productivity of 20.7 ±1.3 g $(m^2 d)^{-1}$ was greater compared to both the productivity of 18.0 ±1.6 g $(m^2 d)^{-1}$ of the fine mesh (p=0.002) and the 14.8±4.9 g $(m^2 d)^{-1}$ of the polycarbonate (p=0.012) in an unpaired t-test (Figure 3.3). Between the polycarbonate and the fine mesh no difference was observed (p=0.12). Therefore, the rough mesh was selected for the remaining experiments in this study.

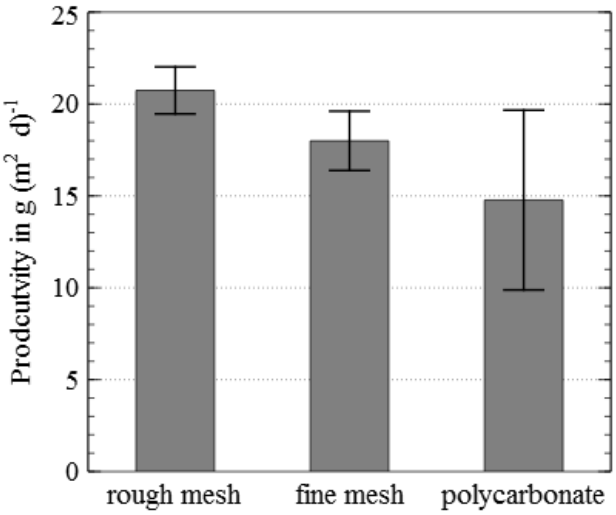

Figure 3.3. Average productivity over 4 growth-harvest cycles with 8 measurements per disk (4 weeks times 2 disk sides) for three types of disk materials. The experiment was performed under light limited conditions at a constant rotation speed of 11 rpm. Error bars indicate the standard deviation.

3.3.2 Reproducibility of the Algadisk reactor

The reproducibility of the lab-scale Algadisk reactor was evaluated by comparing the productivity of the disks at four different positions within the container (Figure 3.1). Productivity was monitored during four growth-harvest cycles for the same material (rough steel mesh) at a constant rotation speed of 11 rpm and 422 µmol $(m^2 s)^{-1}$ light. Nutrients and CO_2 were supplied in excess. From Table 3.1, it can be ascertained that disk 1 had significantly less productivity, less biomass thickness, and a higher mass fraction biomass to water when compared to disks 2, 3 and 4. That decrease was less pronounced for the biomass yield on light. Disks 2, 3 and 4 showed similar results. Neglecting the results of Disk 1, the average biomass productivity over the disks was 20.1 ±0.7 g $(m^2 d)^{-1}$, and the average biomass yield in light was 0.88 ±0.04 g mol^{-1}.

Table 3.1. The surface productivity (P_x), mass fraction biomass to water ($f_{x/w}$), biomass yield to light ($Y_{x/ph}$) and biofilm thickness (z) results of the reproducibility experiment. The reproducibility experiment is performed at nutrient replete conditions with a light intensity of 422 µmol $(m^2\ s)^{-1}$ on a rough metal mesh at a constant rotation speed of 11 rpm. Parameter 'n' represents the number of experiments. Each experiment represents data of one side of the disk during a 7 day growth-harvest cycle. Standard deviation is shown.

	P_x	$f_{x/w}$	$Y_{x/ph}$	z	n
	$g\ (m^2\ d)^{-1}$	$g\ kg^{-1}$	$g\ mol^{-1}$	µm	
disk 1	17.5 ±2.1	192 ±6	0,77 ±0,10	634 ±76	8
disk 2	19.9 ±0,8*	174 ±9**	0,89 ±0,06*	800 ±41**	8
disk 3	19,8 ±0,2*	173 ±4**	0,85 ±0,06	797 ±24**	6
disk 4	20,1 ±0,7**	172 ±9**	0,91 ±0,09*	847 ±67**	8

* $p<0.05$ with unpaired t-test compared to disk 1

** $p<0.01$ with unpaired t-test compared to disk 1

3.3.3 Influence of disk rotation on productivity

The effect of various disk rotation speeds on productivity was evaluated by comparing rotation speeds of 3, 6, 11, and 20 rpm. This experiment was performed with disks of rough steel mesh at 422 µmol $(m^2\ s)^{-1}$ and under nutrient- and CO_2-replete conditions. The difference in productivity between the different rotation speeds was minimal (Table 3.2). The disk operated at 11 rpm, however, achieved significantly greater productivity than it did at 3 rpm (p 0.006) and at 20 rpm (p 0.002). The mass fraction of biomass to water and the biofilm thickness data did not exhibit a particular trend.

Table 3.2. The surface productivity (P_x), mass fraction biomass to water ($f_{x/w}$), biomass yield to light ($Y_{x/ph}$), biofilm thickness (z) results and disk velocity for different rotation speeds. The disk velocity provides the lowest and highest liquid velocity corresponding to that revolution per minute. Experiments are performed in nutrient replete conditions with a light intensity of 422 µmol $(m^2\ s)^{-1}$ on a rough steel mesh. Parameter 'n' represents the number of experiments. Each experiment represents data for one disk side during a 7 day growth-harvest cycle.

	P_x	$f_{x/w}$	z	n	disk velocity	
					low	high
	$g\ (m^2\ d)^{-1}$	$g\ kg^{-1}$	μm	#	$m\ s^{-1}$	$m\ s^{-1}$
3 rpm	18.7 ±1.1	166 ±9	783 ±60	8	0.008	0.038
6 rpm	19.5 ±1.3	152 ±13	900 ±138	6	0.016	0.075
11 rpm	20.1 ±0.7	168 ±15	842 ±101	24	0.029	0.138
20 rpm	18.5 ±1.0	143 ±11	910 ±113	8	0.052	0.251

3.3.4 Substrate limitation

The influence of CO_2 limitation was evaluated for rotation speeds: 3, 11 and 20 rpm. This experiment was performed with disks of rough steel mesh at 422 µmol $(m^2\ s)^{-1}$. The CO_2 replete conditions (discussed in section 3.3) were compared to two CO_2-limiting conditions, resulting in 3 experimental conditions per rotation speed: (1) 15 mol m^{-3} CO_2 ($n \geq 8$ see section 3.3); (2) 0.7 mol m^{-3} CO_2 (n=8); and (3) 0.06 mol m^{-3} CO_2 (n=4).

Comparing CO_2 replete conditions to CO_2 limiting conditions, we observed a significant decrease in productivity from 20 g $(m^2\ d)^{-1}$ to below 4 g $(m^2\ d)^{-1}$ (Figure 3.4A). The difference between 0.7 mol m^{-3} CO_2 and 0.06 mol m^{-3} CO_2 was more moderate, but still significant. For 0.06 mol m^{-3} CO_2, the different tested rotation speeds did not result in changed productivity (Figure 3.4A). In contrast, for 0.7 mol m^{-3} CO_2 the productivity of 3 rpm significantly differs from both 11 rpm (p=0.018) and 20 rpm (p=0.010). These results indicate that rotation speed influences the amount of substrate diffusing from the liquid phase into the biofilm. Between 11 rpm and 20 rpm, no significant difference was ascertained.

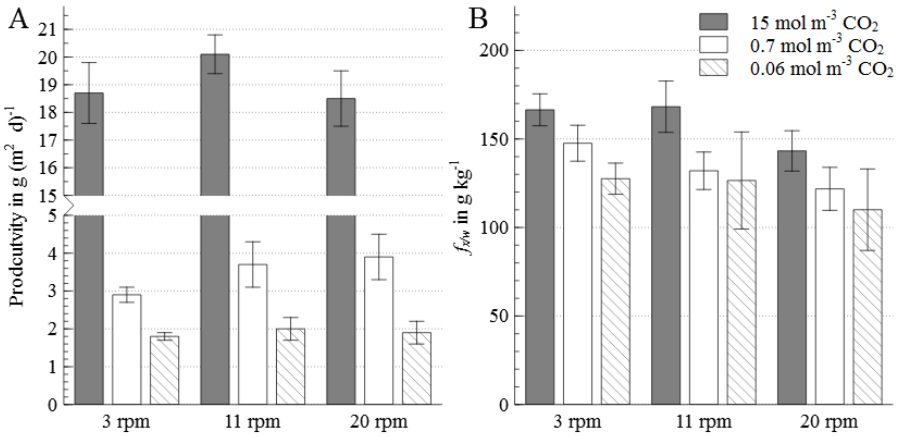

Figure 3.4. Average productivity (A) and Mass fraction of biomass to water in wet biofilm (B) for different CO2 concentrations at three rotation speeds. The experiment with 15 mol m-3 CO2 was at light limiting and nutrient replete conditions. For 0.7 mol m-3 CO2, the bulk liquid in the buffer tank was continuously gassed with 0.5 %v/v CO2 enriched air. For 0.06 mol m-3 CO2, the bulk liquid was not gassed and thus there was only atmospheric CO2 available via direct gas biofilm contact. The error bars indicate the standard deviation.

The mass fraction of biomass to water in the wet biofilm decreased with diminishing CO_2 concentrations (Figure 3.4B). Replete conditions led to a significantly greater mass fraction of biomass to water compared to 0.7 mol m^{-3} CO_2 ($p<0.001$) for all three tested rotation speeds. The data at 0.06 mol m^{-3} CO_2 exhibited a greater standard deviation and were not significantly different. From Figure 3.4B, however, a trend toward decreasing mass fraction of biomass to water in the wet biofilm could be detected with increasing CO_2 limitation.

3.3.5 Long-term stability

To perform the experiments, the Algadisk reactor was operated for 21 consecutive weeks. Due to technical problems, only the results corresponding to 13 weeks were incorporated into the experiments already discussed. The technical problems included: overnight pH rise to pH 10, 24 hours of darkness, and temperatures above 40 °C. These stressful conditions negatively influenced the productivity in the corresponding 7 day growth-harvest cycle. Productivities, however, recovered to

maximal within one week after the conditions were reverted back to optimal. Furthermore, reproducibility was tested at weeks 5, 6, 7 and 19 to ensure no long-term changes occurred during the experiment (section 3.2). Although the experimental set-up was open no contaminations with grazers, other microalgae species or large increases in bacteria population where observed with microscope analysis. Figure 3.5 shows in chronological order the average productivity over all four disks per growth-harvest cycle.

3.4 Discussion

This study demonstrates that it is feasible to achieve consistent high disk surface productivities of 20 g $(m^2\ d)^{-1}$ over a period of 21 weeks (approximately 150 days) in the Algadisk system. Considering that, in the Algadisk system, only 58% of the disk surface was illuminated, the productivity based on illuminated surface is 34.7±1.3 g $(m^2\ d)^{-1}$. The productivity achieved in this study is in accordance to, or improved over, biofilm productivities described in literature (Table 3.3).

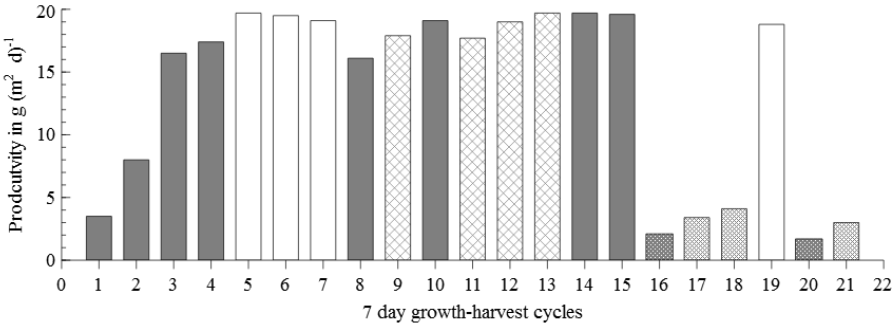

Figure 3.5. Average productivity, calculated as the average of the 4 disks productivity per growth-harvest cycle, in chronological order. The grey bars represent the growth-harvest cycles that were not employed due to technical problems. The white bars represent the data from reproducibility experiment. The cross lined bars represent the experiments on rotation speed and the dark dotted and light dotted represent the experiments on CO_2 limitation (dark dotted without sparging of the bulk liquid and light dotted with sparging of the bulk liquid).

Table 3.3. Comparison between biofilm reactors reported in literature and this study for biomass productivity (P_X), biomass yield on light ($Y_{X/e}$) and light conditions. If a day/night cycle is applied the light intensities depicted are averaged over 24 hours (thus include the dark). For some studies to a biomass yield on light could not be calculated.

P_X	$Y_{X/e}$	Light intensity	L/D	Species	Literature
g $(m^2\ d)^{-1}$	g mol^{-1}	µmol $(m^2\ s)^{-1}$	h/h		
20	0.9	422	24/0	*C. Sorokinana*	This study
6	1.0	96	24/0	*Pseudochlorococcum*	Ji et al. 2013a
9	1.1	100	24/0	*A. obliquus*	Ji et al. 2013b
14	-	642	15/9*	*C. vulgaris*	Gross et al. 2013
20-31	-	208	12/12*	Mixed culture	Christenson and Sims 2012
2	-	18-320	15/9*	*Phaeodactylum*	Naumann et al. 2012

* Actual day-length varies due to seasonal changes

Biomass yield on light and biomass productivities per ground surface are, collectively, an effective manner to evaluate systems' performances (Wijffels and Barbosa 2010). In lab-scale experiments, light is often manipulated, and possibly ground surface is not known or not representative for a potential large scale reactor. Biomass yield on light therefore is a more suitable manner to evaluate reactor performance. In our experiments, a biomass yield on light of 0.88 g mol^{-1} was achieved (Table 3.2). This biomass yield on light is calculated based on the illuminated disk surface and productivity (Equation 3.2) and compared to values reported for other biofilm-photobioreactors (Table 3.3). The two systems that exploited light of 100 µmol $(m^2\ s)^{-1}$ in their experiments, obtained lower productivities but achieved similar biomass yields on light as we did. Compared to lab-scale suspended systems our obtained biomass yield on light are in the higher range (Kliphuis et al. 2010; Takache et al. 2010), and approximately 2/3 of the theoretical maximum biomass yield on light of 1.5 g mol^{-1} (Blanken et al. 2013). As the biofilm in the Algadisk reactor is operated as a sequential batch, light is wasted after harvesting at the beginning of a new batch (Figure 3.2). By minimizing this loss of light, our biomass yield on light could be further improved. Furthermore future experiments have to validate that the obtained productivity and biomass yield

on light can be maintained under outdoor light regimes. Although the obtained results are a good starting point for further scale-up.

During the experiments, biomass concentration in the suspension remained rather low (optical density measured at 750 nm remained below 1.0) although some biomass appeared to sediment at the bottom of the container. It was assumed that re-attachment of microalgae from the liquid to the disks did not occur. Due to the directional light source and the opaque container walls, the light intensity in the liquid was less than the light compensation point of photosynthesis (10 µmol $(m^2 s)^{-1}$) (Takache et al. 2010; Vejrazka et al. 2013). Light intensities lower than the light compensation point are too low to sustain growth. Therefore, it is most likely that most of the settled biomass came from the disks and that suspended growth of microalgae did not occur. The actual amount of settled biomass could not be measured. However, by preventing sedimentation of this biomass or by regularly harvesting the sediment, the productivity of the Algadisk could be further increased.

The harvested biomass from the lab-scale Algadisk reactor exhibited a high mass fraction biomass to water. The mass fraction biomass to water under CO_2 replete conditions was approximately 170 g kg^{-1} while it decreased to 120 g kg^{-1} under CO_2 limiting conditions. Mass fraction biomass to water in suspended systems is typically around 1 to 10 g kg^{-1} (Norsker et al. 2011). To concentrate the microalgae broth to a 150-250 g kg^{-1} mass fraction biomass to water, a broad spectrum of processes is proposed including: flocculation, flotation, filtration, and/or centrifugation (Pahl et al. 2013). The primary disadvantages of these processes are that they are energy consuming, species specific, and often difficult to scale (Pahl et al. 2013). Cultivation of microalgae in the Algadisk system would prevent the concentration issue and result in a cost and space reduction for downstream processing.

3.4.1 Evaluation of different disk materials

Previous studies comparing substratum for phototrophic biofilm growth are limited. One study indicated that *Chlorella* has an elevated attachment to polystyrene foam

(Johnson and Wen 2010). Two other studies ascertained that cotton duct (Gross et al. 2013) and cotton rope (Christenson and Sims 2012) were the most favourable substratum for biofilm growth. These studies share the conclusion that structured surfaces promotes stable re-growth. This conclusion is in accordance with our findings that the more structured rough mesh exhibited greater and more consistent biofilm productivities. In our case, however, we could not determine the optimal pore depth since the rough mesh had the deepest pores.

The polycarbonate disk did not perform effectively, and productivity varied from one growth-harvest cycle to the other resulting in a greater standard deviation of the average productivity (Figure 3.3). The substantial standard deviation could be the result of lack of structure resulting in the formation of empty spots following harvesting which were required to be re-colonized by microalgae. Although re-growth was not stable, the initial attachment was the fastest for the polycarbonate disk (data not shown). This demonstrates the potential of the positively charged polyelectrolyte multilayer coating to improve initial attachment. However, Most important remains stable re-growth and robustness of the system.

3.4.2 Influence of disk rotation on productivity

During the experiment evaluating the influence of disk rotation on productivity, the differences were only minimal, although 11 rpm had a significantly greater productivity compared to 3 and 20 rpm. Based on traditional RBC literature, this could be due to the build-up of toxic compounds inside the biofilm at low rotation speeds and shear stress at high rotation speeds (Lu et al. 1997). However, the low effect of rotation speed on productivity shows a clear possibility to use larger disks in scaled up systems, e.g., based on the range of tested velocities (0.01 to 0.25 m/s) a disk with a diameter of 1.5 m could be used at 3 rpm.

Regarding the mass fraction of biomass to water and the biofilm thickness, no trend was observed during the various conditions assayed. This was contrary to other studies where biofilm surfaces exposed to increased hydrodynamic forces resulted in thinner and denser biofilms (Kugaprasatham et al. 1992; Picioreanu et al. 2000).

This denser biofilm was observed in the reproducibility experiment for disk 1 which was exposed to liquid velocities of 2 m s^{-1} from the recycle inlet (Figure 3.1). The liquid velocity at the recycle inlet is much higher compared to the 0.01 to 0.25 m s^{-1} velocities that were applied when studying the influence of disk rotation on productivity (Table 3.2). Although the biofilm on disk 1 grew more compact it still featured a lower productivity, which is most likely caused by hydrodynamic wash-off of microalgae. Another factor that might have influenced the mass fraction of biomass to water at lower rotation speeds could be that low rotation speeds resulted in a dryer biofilm. With low rotation speeds, the air/water frequency is also lower. To our knowledge there is no dedicated research performed on this topic, however, other researchers have noticed drying of the biofilm at low air/water frequencies (Gross et al. 2013).

3.4.3 Substrate limitation

For phototropic growth, CO_2 is the primary carbon source. If the CO_2 supply is less than CO_2 consumption, the productivity of the microalgae will decrease due to carbon limitation. During our experiments, a decrease in the CO_2 concentration resulted in a 5 to10 times reduction in productivity compared to CO_2 replete conditions. The actual CO_2 concentrations in the bulk liquid were not measured, hence they remain unknown. From the operating conditions and assuming equilibrium between gas and liquid phases, we could estimate the maximal CO_2 concentration in the liquid as is described in the results section. In reality, however, equilibrium will not be achieved due to consumption of CO_2 by the microalgae and, therefore, the actual CO_2 concentrations will be lower.

The CO_2 dissolved in the bulk liquid is transported by diffusion into the biofilm. The rate of diffusion primarily depends on: concentration difference between bulk liquid and biofilm, distance over which diffusion occurs, and the diffusion coefficient. In the lab-scale Algadisk system, three factors play a role when cultivating microalgae under CO_2 limitation: (1) thickness of the stagnant layer between the biofilm and the bulk liquid or gas; (2) diffusion of dissolved CO_2 from the bulk liquid into the

biofilm when it is submerged; and (3) diffusion of atmospheric CO_2 gas into the biofilm when it is above the water.

At 0.06 mol m^{-3} CO_2 no difference between the various rotation speeds was detected. This could indicate that the thickness of the stagnant film layer in the gas phase has only minimal influence on the diffusion of CO_2 to the biofilm, or it could indicate that the film layer covering the biofilm in the gas phase is not influenced by the rotation speed. The latter, however, is unlikely as a previous study has demonstrated a correlation between rotation speed and attached film thickness (Kubsad et al. 2004). At 0.7 mol m^{-3} CO_2, it seems that higher productivities are obtained with increasing rotation speeds. This could be due to improved mass transfer by a decreased stagnant film layer thickness in the liquid. More likely, however, is that the higher frequency between substrate absorption (biofilm submerged and dark) and substrate consumption (biofilm in air and illuminated) resulted in increased CO_2 uptake by the biofilm. During substrate limiting growth, the driving force for CO_2 diffusion into the biofilm is greatest upon re-entering the liquid as CO_2 concentration in the biofilm is at its lowest.

The above discussion illustrates that the absorption and consumption cycles introduced by growing a biofilm on a rotating disk are difficult to evaluate and that there is still opportunity for improvement upon better comprehension of these processes. Finally, it is noteworthy that the supply of sufficient nutrients is important to maintain optimal productivity. Therefore, nutrient supply should be carefully considered in the design of a scaled up Algadisk system.

3.5 Conclusions

In this study, *Chlorella sorokiniana* was cultivated in the Algadisk system. In the lab-scale RBC based photobioreactor, a productivity of 20.1 ±0.7 gram per m^2 disk surface per day and a biomass yield on light of 0.88 ±0.04 grams dry biomass per mol photons were achieved. The results obtained were stable over 21 weeks and showed that disk diameters up to 1.5 meter were possible. Together, the obtained

results demonstrate a clear opportunity for larger scale Algadisk photobioreactors to produce microalgae biomass, although, adequate CO_2 supply should be ensured.

3.6 Appendices

Appendix 3.A light distribution over the disk

Figure 3.A.1. Different measure positions on the disk surface, with hole 3 as the centre of the disk.

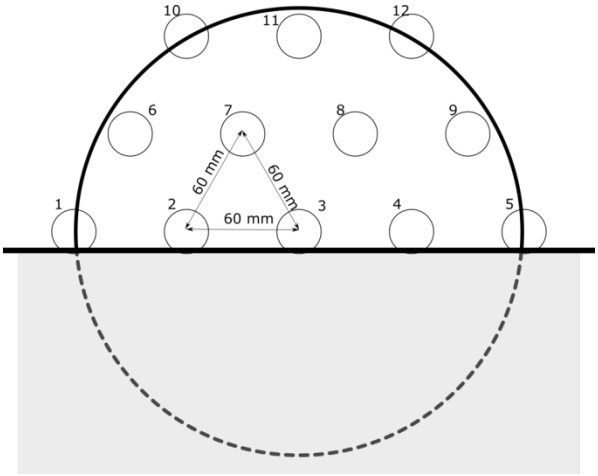

Table 3.A.1. Light distribution over the different disk positions with F for front and B for Back. Light is measured in μmol $(m^2\ s)^{-1}$.

	disk 1 F	disk 1 B	disk 2 F	disk 2 B	disk 3 F	disk 3 B	disk 4 F	disk 4 B
1	324 ± 18	309 ± 16	322 ± 32	329 ± 12	335 ± 10	330 ± 15	331 ± 40	304 ± 28
2	447 ± 26	420 ± 27	453 ± 36	443 ± 16	470 ± 20	442 ± 12	462 ± 22	393 ± 23
3	498 ± 22	447 ± 43	508 ± 20	463 ± 20	531 ± 36	465 ± 10	511 ± 14	433 ± 22
4	437 ± 8	416 ± 31	421 ± 18	441 ± 25	452 ± 32	417 ± 19	459 ± 19	395 ± 19
5	318 ± 15	305 ± 13	312 ± 14	331 ± 16	329 ± 28	307 ± 37	316 ± 5	302 ± 33
6	448 ± 38	409 ± 41	448 ± 37	405 ± 20	471 ± 19	425 ± 12	448 ± 36	388 ± 24
7	602 ± 49	548 ± 47	599 ± 54	541 ± 37	637 ± 48	567 ± 9	631 ± 25	502 ± 13
8	589 ± 33	543 ± 56	519 ± 68	542 ± 35	618 ± 54	551 ± 23	632 ± 26	506 ± 24
9	433 ± 11	424 ± 38	449 ± 27	420 ± 18	453 ± 49	410 ± 36	450 ± 12	397 ± 39
10	474 ± 42	430 ± 33	455 ± 44	423 ± 26	458 ± 57	449 ± 6	472 ± 31	400 ± 10
11	518 ± 25	497 ± 49	527 ± 47	491 ± 36	582 ± 58	508 ± 19	560 ± 31	460 ± 16
12	458 ± 8	438 ± 41	446 ± 38	437 ± 23	483 ± 46	443 ± 27	480 ± 26	408 ± 26
ave	462 ± 17	432 ± 33	455 ± 22	439 ± 21	485 ± 35	443 ± 11	479 ± 16	407 ± 18

Chapter 4 Predicting microalgae growth

This chapter is published as:

Blanken, W.; Postma, P.R.; de Winter, L; Wijffels, R.H.; Janssen, M.

"Predicting microalgae growth "

March 2016, Algal Research, Volume 14, Pages 28-38

Abstract

A generally applicable kinetic model is presented to predict light limited microalgal growth. This model combines a mathematical description for photoautotrophic sugar production with a description for aerobic chemoheterotrophic biomass growth. The model is based on five parameters which are directly measurable but were obtained from literature for the purpose of this study. The model was validated for *Chlorella sorokiniana* with 52 experiments derived from eight publications and for *Chlamydomonas reinhardtii* with 32 experiments derived from seven publications. The specific growth rate was initially predicted with a mean absolute percent error (MAPE) of 34-36%. The low accuracy is most likely caused by simplifications in the light model and inaccurate parameter estimations. When optimizing the light model per experimental dataset, a 1-2% MAPE was obtained. When optimizing input parameters separately from the light model, a 2-18% MAPE was realized. After validating this model on batch data, we conclude that this model is a reliable engineering tool to predict growth in photobioreactors provided the light field is accurately measured or calculated.

4.1 Introduction

Microalgae exploit photosynthesis to convert water and carbon dioxide into sugars by means of light energy. These sugars are subsequently used to support biomass growth. Microalgae growth in a photobioreactor can thus be calculated based on a model describing light-dependent sugar production by photosynthesis in combination with a model describing aerobic chemoheterotrophic growth on sugar. Ideally, the model parameters are all independently measurable in dedicated small-scale experiments in addition to the actual process to be predicted. In order to be suitable as a tool for photobioreactor engineers, the model should be as uncomplicated as possible while still including the most important reactions and providing sufficient accuracy.

Models that predict the light gradient include the Lambert-Beer Law, the radiative transfer equation (RTE), and a simplification of the two-flux model (Cornet et al. 1995; Pilon et al. 2011). The Lambert-Beer Law is the simplest as it accounts only for light absorption but can be extended and improved by including light scattering (Klok et al. 2013). The most dominant effect of light scattering is the increase in the light path travelled through the microalgae suspension increasing the probability of light absorption. This effect can be accounted for by modifying the attenuation coefficient. As such, it is possible to describe the light gradient with sufficient accuracy with the Lambert-Beer Law (Luo and Al-Dahhan 2012).

To describe photosynthesis, a model is required that describes the photosynthetic activity in response to light exposure. Photosynthetic activity increases linearly with light intensity under low light levels and then begins to stabilize towards a maximum photosynthetic rate at high light intensities. This trend is confirmed by the mechanistic description of photon absorption and utilization using a cumulative one-hit Poission function (Dubinsky et al. 1986) which results in the exponential model of Webb (Webb et al. 1974). According to literature, the photosynthetic response, however, is best described by yet another hyperbolic function based on the hyperbolic tangent function (Jassby and Platt 1976). As a result, the photosynthetic

efficiency is maximal at low photon absorption rates and decreases slowly when approaching the maximal photosynthetic rate.

Sugar produced by photosynthesis in the chloroplast of the microalgae is used to support biomass growth. This growth metabolism is complex and can be described as aerobic chemoheterotrophic growth. Two general processes can be distinguished, i.e., the formation of new biomass and cellular maintenance (anabolism), which are both supported by aerobic respiration of sugars in the mitochondria (catabolism). The partitioning of sugar between anabolism and catabolism is described according to Pirt (Pirt 1965). Pirt states that per biomass unit produced a fixed amount of sugar has to be respired, which is described by the biomass yield on sugar. Additionally a small amount of sugar is continuously respired providing energy for cellular maintenance

Current light-limited microalgae growth models can be divided in photosynthesis-irradiance (PI) curve based models (Bechet et al. 2014a; Geider et al. 1997; Klok et al. 2013; Quinn et al. 2011; Slegers et al. 2011) and empirical models that are fitted to measured relations between specific growth rate and irradiance (Cornet and Dussap 2009; Lee et al. 2014; Takache et al. 2012). Although these models often include a respiratory term, Geider et al. (Geider et al. 1997) included a growth-related respiratory term. In reality, however, sugar is respired for energy to support cellular maintenance and anabolic reactions. Consequently, when neglecting this partitioning, respiration is often identified as energy loss.

What is lacking in the current models used for engineering studies is a simple microalgae growth model which takes into account compartmentalization between chloroplast and mitochondria. The proposed model, therefore, differentiates between photosynthesis and respiration by combining the Lambert-Beer Law, Jassby and Platt (Jassby and Platt 1976), and Pirt (Pirt 1965). With this strategy, differentiation is made between photosynthethically derived sugars used for: (1) cellular maintenance, (2) growth-related respiration, and (3) cell growth. The advantage of this differentiation is that the microalgae metabolism is more accurately represented

while maintaining simplicity with the model formulation as much as possible and minimizing the number of parameters required.

In this study, an engineering model for microalgae growth in photobioreactors is introduced and validated with *Chlorella sorokiniana* and *Chlamydomonas reinhardtii*. The model input parameters can be measured with dedicated experiments. For the purpose of this study, the model input parameters are acquired from literature and include: molar mass of the microalgae (M_x); specific light absorption coefficient ($a_{x,\lambda}$); sugar yield on photons ($Y_{s/ph}$); biomass yield on sugar ($Y_{x/s}$); maintenance specific sugar consumption rate (m_s); maximal specific sugar production rate ($q_{s,m}$); and maximal specific growth rate (μ_m). In this manner, a robust evaluation of the model accuracy could be constructed. This is one of the few studies where one single microalgae growth model is employed to predict growth experiments of various studies under completely different conditions.

4.2 Theory

4.2.1 Growth model

4.2.1.1 Photoautotrophic sugar production

All of the sugar that is used for aerobic chemoheterotrophic biomass growth is produced by photoautotrophic sugar production. In our model, the photoautotrophic sugar production is represented by coupling photosynthesis and the Calvin-Benson cycle. Hereby, it is assumed that all energy generated in the form of ATP and NADPH during photosynthesis is used in the Calvin-Benson cycle to incorporate CO_2 into triose sugars.

The rate of photoautotrophic sugar production is dependent on light intensity (Equation 4.1). This equation is equivalent to the model of Jassby and Platt which is based on a hyperbolic tangent function (Jassby and Platt 1976). The original equation proposed by Jassby and Platt has been rewritten to make sugar the end product of photosynthesis (Equation 4.4). In Equation 4.1, the parameter alpha (α) describes the initial slope of the curve which levels off to the maximal specific sugar

production ($q_{s,m}$). Please note that α can also be expressed as the product of the sugar yield on photons and the specific light absorption coefficient (Equation 4.2) which is in accordance to the approach of Geider (Geider et al. 1996). Equation 4.3 depicts the relation to calculate the specific photon absorption rate based on the light intensity and the specific light absorption coefficient. By incorporating Equations 4.2 and 4.3 into Equation 4.1, the sugar production rate (Equation 4.4) becomes a function of the maximal specific sugar production ($q_{s,m}$), the specific photon absorption rate (q_{ph}), and the sugar yield on photons ($Y_{s/ph}$) which are process parameters or measurable characteristics of the microalgae. Variable q_{ph} thus replaces I_{ph} in the Jassby & Platt model, and this is practical for the integration of the light model within the growth model, which will be discussed later.

Equation 4.1 $$q_s = q_{s,m} \cdot tanh\left(\frac{\alpha \cdot I_{ph}}{q_{s,m}}\right)$$

Equation 4.2 $$\alpha = Y_{s/ph} \cdot a_x$$

Equation 4.3 $$q_{ph} = I_{ph} \cdot a_x$$

Equation 4.4 $$q_s = q_{s,m} \cdot tanh\left(\frac{q_{ph} \cdot Y_{s/ph}}{q_{s,m}}\right)$$

4.2.1.2 Aerobic chemoheterotrophic growth model

The sugar produced in the light reaction is exploited as as a fundament for new biomass and is oxidized in the mitochondra to obtain extra energy that is necessary to support growth related processes and cell maintenance. This partitioning of sugar between anabolic and catabolic reactions can be described using Pirt's Law (Equation 4.5) (Pirt 1965) which states that a small amount of substrate (sugar) is continuously consumed for maintenance (m_s). The remaining sugar is available for growth (μ) resulting in new biomass according to a constant biomass yield on sugar ($Y_{x/s}$), which indirectly implies that a fixed amount of sugar is respired per carbon mol-x (cmol-x) produced. The validity of adopting Pirt's description for partitioning of photosynthetically derived energy has been established for several microalgae species (Kliphuis et al. 2011a; Zijffers et al. 2010). Please note that the specific

sugar production rate (q_s) in Equation 4.5 is predicted employing Equation 4.4. To summarize, a typical photosynthesis model is combined with the classical aerobic chemoheterotrophic growth model of Pirt to predict the specific growth rate of microalgae (Equation 4.5).

Equation 4.5 $$\mu_{pre} = (q_s - m_s) \cdot Y_{x/s}$$

4.2.2 The light attenuation model

Light attenuation within a microalgae suspension in flat plate photobioreactors is described based on the Lambert-Beer Law which states that the attenuation of light over distance is proportional to the light intensity itself with the proportionality constant being the volumetric absorption coefficient. The latter is the product of the specific light absorption coefficient (a_x) and the biomass concentration (C_x).

Equation 4.6 $$\frac{dI_{ph}}{dz} = -a_x \cdot C_x \cdot I_{ph}$$

The Lambert-Beer Law (Equation 4.6) can be rewritten to extract the specific photon absorption rate (q_{ph}) of microalgae:

Equation 4.7 $$\frac{\frac{dI_{ph}}{dz}}{C_x} = q_{ph} = -a_x \cdot I_{ph}$$

Taking the integral of the Lambert-Beer from 0 to z results in:

Equation 4.8 $$I_{ph}(z) = I_{ph}(0) \cdot \ e^{(-a_x \cdot C_x \cdot z)}$$

and taking into account wavelength dependency the following expression is obtained:

Equation 4.9 $$I_{ph}(z) = \sum_{\lambda=700}^{\lambda=400} I_{ph,\lambda}(0) \cdot \ e^{(-a_{x,\lambda} \cdot C_x \cdot z)} \cdot \Delta\lambda$$

By employing Equation 4.9 we calculate the light decrease per wavelength, and as such we take into account that green light penetrates deeper compared to red and blue light. The calculation of wavelength dependent incident light intensity ($I_{ph,\lambda}(0)$) is explained in Appendix 4.A and Supplementary Excell file 2 which also provides

additional detailed information on the wavelength dependency of the specific absorption coefficient. As discussed, we propose the use of the specific photon absorption rate (q_{ph}) within the photosynthesis model. Based on a microbalance of light, we can calculate a local specific photon absorption rate $q_{ph}(z)$ as follows:

Equation 4.10 $$q_{ph}(z) = \frac{I_{ph}(z) - I_{ph}(z+dz)}{C_x \cdot dz}$$

The variable $I_{ph}(z)$ is then calculated based on Equation 4.9.

4.2.3 Model input parameters

The parameters required as input for the above described model to predict the specific growth rate can be divided into two categories: (1) measurable characteristics of microalgae and (2) process parameters. The measurable parameters are obtained from literature (Table 4.1) and include: molar mass of the microalgae (M_x); specific light absorption coefficient per wavelength ($a_{x,\lambda}$); sugar yield on photons ($Y_{s/ph}$); biomass yield on sugar ($Y_{x/s}$); maintenance-related specific sugar consumption rate (m_s); and maximal specific sugar production rate ($q_{s,m}$). Parameter $q_{s,m}$ can be calculated by substituting the maximal specific growth rate (μ_m) in Equation 4.5 because μ_m values are often available in literature (Table 4.1). The biomass yield on sugar is divided into one value for ammonium and one value for nitrate. Cultures growing on urea are assumed to have the same biomass yield on sugar as that for ammonium. The process parameters depend on culture conditions and include: biomass concentration (C_x), wavelength specific incident light intensity ($I_{ph,\lambda}$), and reactor depth (L).

In this study, the microalgae characteristics that were required as model input were acquired or deduced from a wide range of literature studies as discussed in Appendix 4.B. With this strategy, we obtained ranges for all of the parameters without performing any experiments ourselves. It should be noted that in some cases validation data was also used as input for the input parameter estimation. For other microalgae strains, the model parameters can either be obtained from literature or

can be determined by performing dedicated experiments as discussed in Appendix 4.B.

Table 4.1. Overview of model input parameters for *Chlorella sorokiniana* and *Chlamydomonas reinhardtii*. The specific absorption coefficient (a_x) is depicted as the spectral average over 400-700 nm. For the sugar yield on photons ($Y_{s/ph}$), an average value for microalgae and plants leafs is depicted. Parameters were obtained from literature where 'n' represents the number of experiments used to estimate their values (Appendix 4.B). The values reported for the maximal specific sugar production rate ($q_{s,m}$) where calculated according to Equation 4.5, therefore, 'n' represents the amount of calculated values.

	μ_m	M_x	m_s	a_x	$Y_{x/s}$		$q_{s,m}$		$Y_{s/ph}$
					NH_4	NO_3	NH_4	NO_3	
	h^{-1}	g cmol-x^{-1}	cmol-s (cmol-x s)$^{-1}$	m^2 cmol-x^{-1}	cmol-x cmol-s^{-1}		cmol-x (cmol-s s)$^{-1}$		cmol-s mol-ph^{-1}
	Chlorella sorokiniana								Microalgae
used	**0.27**	**24.0**	**2.5E-06**	**7.1**	**0.59**	**0.54**	**1.3E-04**	**1.4E-04**	**0.10**
average	0.26	24.5	2.5E-06	5.8	0.59	0.54	1.3E-04	1.4E-04	0.10
high	0.27	25.0	3.7E-06	7.1	0.70	0.63	1.7E-04	1.9E-04	0.11
low	0.25	23.7	1.2E-06	4.1	0.44	0.40	1.0E-04	1.1E-04	0.08
n	3	4	18	27	5	13	270	702	8
	Chlamydomonas reinhardtii								Plants
used	**0.14**	**24.0**	**2.0E-06**	**6.2**	**0.69**	**0.58**	**6.0E-05**	**7.1E-05**	-
average	0.14	24.0	2.0E-06	4.6	0.69	0.58	6.1E-05	7.2E-05	0.10
high	0.16	24.0	3.6E-06	6.2	0.78	0.64	7.7E-05	8.9E-05	0.11
low	0.13	24.0	1.6E-07	3.0	0.61	0.52	4.9E-05	5.9E-05	0.09
n	4	2	6	15	3	2	216	144	5

4.3 Computational Methods

4.3.1 Computational Methods

This model employs five equations to calculate the average specific growth rate within a microalgae culture inside a photobioreactor (Figure 4.1). Light intensity changes along the culture depth. The specific photon absorption rate and the specific

sugar production rate both depend on the light intensity and, therefore, change with the culture depth. In Figure 4.1, the Equations already introduced are rewritten such that they depend on culture depth. In accordance with Figure 4.1, the local light intensity ($I_{ph}(z)$) is used to calculate the local specific photon absorption rate ($q_{ph}(z)$) which is subsequently coupled to the sugar production and integrated over the reactor to acquire the average specific sugar production rate (Equation 4.11). The partitioning of the produced sugar between functional biomass (anabolism), growth-related respiration (catabolism), and maintenance-related respiration is described by Equation 4.5.

With the equations listed in Figure 4.1 , the only parameters not specified are: biomass concentration, incoming light intensity, specific growth rate, and the reactor thickness. The specific growth rate of the microalgae chemostat culture can be calculated with this model provided the biomass concentration is known. The above equations were discretised by subdividing the photobioreactors into 199 layers along the light path and then solved with MATLAB R2012a. In case of the predictions for batch cultures Equation 4.12 is solved with the MATLAB R2012a ode15s solver.

Equation 4.11 $$q_s = \int_0^L q_s(z) \cdot dz$$

Equation 4.12 $$\frac{dC_x}{dt} = \mu_{pre} \cdot C_x$$

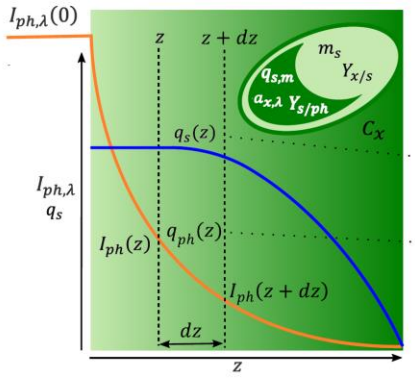

$$\mu_{pre} = (q_s - m_s) \cdot Y_{x/s} \quad \text{Eq. 5}$$

$$q_s = \int_0^L q_s(z) \cdot dz \quad \text{Eq. 11}$$

$$q_s(z) = q_{s,m} \cdot tanh\left(\frac{-q_{ph}(z) \cdot Y_{s/ph}}{q_{s,m}}\right) \quad \text{Eq. 4}$$

$$q_{ph}(z) = \frac{I_{ph}(z) - I_{ph}(z + dz)}{C_x \cdot dz} \quad \text{Eq. 10}$$

$$I_{ph}(z) = \sum_{\lambda=700}^{\lambda=400} I_{ph,\lambda}(0) \cdot e^{(-a_{x,\lambda} \cdot C_x \cdot z)} \cdot \Delta\lambda \quad \text{Eq. 9}$$

Figure 4.1. Model calculation scheme, containing all equations necessary to predict the microalgae specific growth rate.

The light limited microalgae growth model was validated for *Chlorella sorokiniana* based on 17 chemostat experiments performed over a wide range of dilution ranges (Cuaresma Franco et al. 2012; Cuaresma et al. 2009; Tuantet et al. 2014), 2 D-stat experiments including 32 data points (Zijffers et al. 2010) and three batch experiments (Kliphuis et al. 2011b; Kliphuis et al. 2010; Van Wagenen et al. 2015). The model was also validated for *Chlamydomonas reinhardtii* based on seven chemostat experiments (Kliphuis et al. 2011a), 22 turbidostat experiments (de Mooij et al. 2014; Kliphuis et al. 2011c; Takache et al. 2012; Vejrazka et al. 2011; Vejrazka et al. 2012) and three Batch experiments (Jacobi 2013; Takache et al. 2012). All experiments utilized for validation were performed in flat plate photobioreactors or a similar design. The design details are listed in Table 4.2, and the chemostat and batch observations are listed in Supplementary Excell file 3. The results from the D-stat experiment were assumed to be representative of steady state cultures according to the analysis of Hoekema et al. (Hoekema et al. 2014).

Table 4.2. Summary of the Materials and Methods per dataset used to validate the model. FWHM stands for Full width at half maximum and gives an indication of the light beam angle from a light source.

z_r	$I_{ph,in}$	N source	Light source	FWHM	Reactor type	Reactor back	Operating mode	Strain number	Reference
mm	µmol $(m^2\ s)^{-1}$			°					
					Chlorella sorokiniana				
10	1530*2	Urea	High pres Na	45	Flat panel	Both sides illuminated	Chemostat	CCAP211/8K	(Tuantet et al. 2014)
14	800	Urea	Red LED	68	Flat panel	Stainless steel (reflective)	Chemostat	CCAP211/8K	(Cuaresma Franco et al. 2012)
14	2100	Urea	Red LED	68	Flat panel	Stainless steel (reflective)	Chemostat	CCAP211/8K	(Cuaresma et al. 2009)
12.5	871	Urea	Fluorescent tube	diffuse	Flat panel	Open	d-stat	CCAP211/8K	(Zijffers et al. 2010)
20.5	940	Urea	Fluorescent tube	diffuse	Flat panel	Open	d-stat	CCAP211/8K	(Zijffers et al. 2010)
12	200-1500	NO_3	Halogen tungsten	27	Tube in tube	Tube (reflective)	Batch	CCAP211/8K	(Kliphuis et al. 2010)
12	200-1500	NO_3	Halogen tungsten	27	Tube in tube	Tube (reflective)	Batch	CCAP211/8K	(Kliphuis et al. 2011b)
250	2000	Urea	White LED*	8	ePBR	Open (opaque)	Batch	CCAP211/8K	(Van Wagenen et al. 2015)

Table 4.2. continued

z_r	$I_{ph,in}$	N source	Light source	FWHM	Reactor type	Reactor back	Operating mode	Strain number	Reference
mm	µmol $(m^2\ s)^{-1}$			°					
					Chlamydomonas reinhardtii				
25	80	NO_3	Red LED	6	Flat panel	Open	Chemostat	CC1690	(Kliphuis et al. 2011a)
12	620	NO_3	Halogen tungsten	27	Tube in tube	Tube (reflective)	Turbidostat	CC1690	(Kliphuis et al. 2011c)
25	100-500	NH_4	Red-blue LED	68-55	Flat panel	Black metal	Turbidostat	CC-124	(Vejrazka et al. 2011)
25	110-220	NH_4	Red-blue LED	68-55	Flat panel	Black metal	Turbidostat	CC-124	(Vejrazka et al. 2012)
14	800-1500	Urea	Warm white LED	25	Flat panel	Open	Turbidostat	CC1690	(de Mooij et al. 2014)
40	110-1000	NH_4	Cold white LED	8	Flat panel	Stainless steel (reflective)	Turbidostat	137 AH	(Takache et al. 2012)
40	110-700	NH_4	Cold white LED	8	Flat panel	Stainless steel (reflective)	Batch	137 AH	(Takache et al. 2012)
20	500	NH_4	White LED	6	Flat panel	Open	Batch	WT13	(Jacobi 2013)

* The LED spectrum of the ePBR is confidential, therefore the White LED from Jacobi was used instead.

4.3.2 Monte Carlo simulations

The accuracy of the model predictions of the specific growth rate was studied with Monte Carlo simulations. The parameters $Y_{x/s}$, m_s, $a_{x,\lambda}$ and $Y_{s/ph}$ were randomly varied within the range presented in Table 4.1 by the MATLAB random generator. The parameter $Y_{x/s}$ makes an exception to this rule and a lower value of 0.4 cmol-x cmol-s^{-1} was selected for both microalgae and nitrogen sources. This value corresponds to the lowest reported $Y_{x/s}$ based on a stoichiometry analysis (von Stockar and Liu 1999). The best fit was selected based on the smallest sum of squared errors of 100,000 simulations. The Monte Carlo simulations were performed separately for *C. sorokiniana* and *C. reinhardtii* on the combined data and per set of data as presented in Table 4.2 (each line represents one dataset).

4.3.3 Light gradient fit

The light gradient might be predicted incorrectly by Lambert-Beer Law as discussed in the Introduction. To correct for this, a light correction factor (c_I) is added to the Lambert-Beer equation (Equation 4.13). With Equation 4.13, the predicted specific growth rate is fitted by changing a light correction factor with the fminsearch function of MATLAB to minimize the squared error per experimental condition. During the fminsearch, all other input parameters were as depicted in Table 4.1.

Equation 4.13 $$I_{ph}(z) = \sum_{\lambda=700}^{\lambda=400} I_{ph,\lambda}(0) \cdot e^{(-a_{x,\lambda} \cdot c_x \cdot z \cdot c_I)} \cdot \Delta\lambda$$

4.3.4 Calculations

The squared sum of errors (SSE) is calculated with Equation 4.14.

Equation 4.14. $$\text{SSE} = \sum \left(\frac{\mu_{obs} - \mu_{pre}}{\mu_{obs}}\right)^2$$

The model accuracy is measured as the mean absolute percent error (MAPE) and was used to evaluate the prediction accuracy. The MAPE is calculated according to Equation 4.15 (Mayer and Butler 1993).

Equation 4.15. $$\text{MAPE} = \frac{100}{n} \sum \left(\frac{|\mu_{obs} - \mu_{pre}|}{|\mu_{obs}|}\right)$$

4.4 Results and discussion

4.4.1 Model predictions chemostat cultivation

The light-limited growth model introduced in this study was validated for *Chlorella sorokiniana* with literature based input parameters. The datasets used for the validation data were derived from four independent studies which adopted three different photobioreactor designs (Table 4.2). In Figure 4.2A, the predicted specific growth rate is plotted against the observed specific growth rate (MAPE of 36%). It can be determined that the predicted specific growth rate deviates from the observed specific growth rate (Figure 4.2A). In Figure 4.2C, the relative error between the predicted and the observed specific growth rate is depicted. From Figure 4.2C, it is evident that the relative divergence is most substantial for the lower specific growth rates compared to the higher growth rates. Overall, for *C. sorokiniana*, there is a trend that low specific growth rates were overestimated while high specific growth rates were underestimated.

The light to growth model introduced in this study is validated for *Chlamydomonas reinhardtii* based on six independent studies (Table 4.2). In Figure 4.2B, the predicted specific growth rate is plotted against the observed specific growth rate (MAPE 34%) and, in Figure 4.2D, the relative error between the predicted and the observed specific growth rate is depicted. From Figure 4.2B, it can be deduced that the predicted specific growth rate for *C. reinhardtii* tends to overestimate the measured growth rate.

For both, the microalgae accuracy of the prediction based on the literature based parameters was low. Most likely, the low accuracy originates from: (1) inaccuracy in the light gradient prediction as Lambert-Beer Law neglects photoacclimation, light scattering, and incident light angle; and (2) inaccuracy in the literature based estimation of the model input parameters. In order to illustrate that our proposed simple engineering model is able to accurately predict the microalgae specific growth rate, both possibilities were more extensively evaluated by computational experiments.

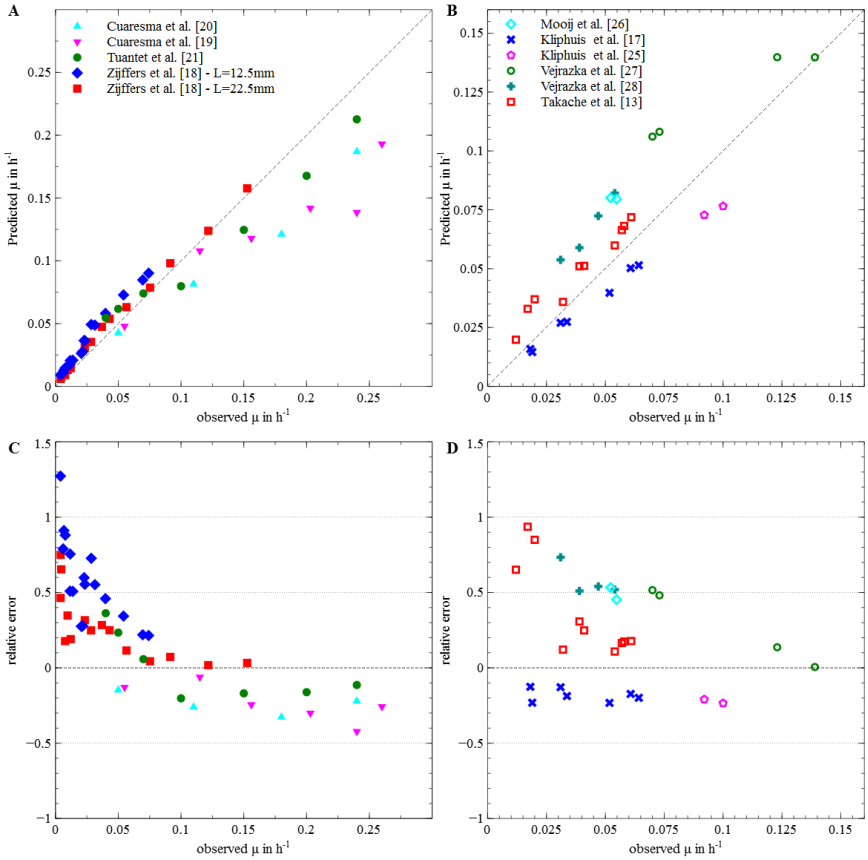

Figure 4.2. Predicted specific growth rate plotted against the measured specific growth rate (A & B) and the relative error of the prediction (C & D). The dashed line represents a relative error of zero. A and C. Data for *C. sorokiniana*. B and D. Data for *C. reinhardtii*.

4.4.2 Light gradient description and model prediction

The Lambert-Beer Law was used to predict the light gradient through the culture suspension. The accuracy of the Lambert-Beer Law can be increased by introducing a light correction factor in the exponent of Equation 4.9. Included in such a light correction factor are: (1) differences in the incident light angle on the photobioreactor surface in the different studies included (Table 4.2); (2) scattering of

light by microalgae leading to a change in light direction within the reactor; and (3) changes in specific light absorption due to photoacclimation (Figure 4.3). Changes in the light direction can result in a longer light path through the reactor. In literature, similar strategies to improve the Lambert-Beer Law were reported and include: introducing a scattering correction factor for microalgae (Klok et al. 2013), including scattering by gas bubbles (Zhang et al. 2015), including a backscattering coefficient (Fachet et al. 2014), or including an extinction coefficient determined for the actual photobioreactor and microalgae suspension that is used which thus includes both light absorption and scattering (Bechet et al. 2014a). In all three examples, the light gradient correction factor is included in the exponent of the Lambert-Beer Law equation.

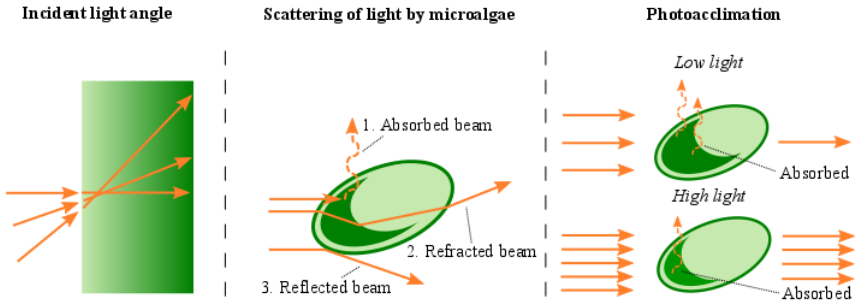

Figure 4.3. Illustration of the effect of incident light angle, scattering of light by microalgae, and photoacclimation on the light path travelled within a microalgae culture.

In our model, the specific absorption coefficient is assumed to be constant, however, it varies because of photoacclimation. Based on the data reported in Table 4.2, the minimal specific absorption coefficient is approximately half of the maximal value which clearly indicates the impact of photoacclimation. The actual value, however, was often not reported for the studies used for the model validation. For the initial model predictions the measured higher values were utilized which represent low light acclimated microalgae. In some situations the actual absorption coefficients would be closer to high light acclimated microalgae. This would imply that they will employ a reduced absorption coefficient which will be reflected by a light correction

factor between 1 and 0.5. As previously discussed, both scattering and a decreasing angle of the incident light will increase the light path which will be reflected in a correction factor greater than 1. In literature, the highest measured light correction factor correlated to scattering is 2.5 (Klok et al. 2013). Therefore, realistic values for the light correction factor should fall within the range of 0.5 to 2.5.

The overall accuracy of the model was maximized with the light gradient fit, with a MAPE of only 1% for *C. sorokiniana,* and a MAPE of 2% for *C. reinhardtii*. In Figures 4.4A and 4.4B, it can be observed that the fit reached 100% accuracy for most experimental points, however, a few predictions still deviate. In this simulation experiment, we fitted the predicted specific growth rate to the measured specific growth rate by changing the light gradient. Due to the design of the simulation experiment, a high prediction accuracy was logically obtained. The value of the correction factor for the different experiments, however, then provides information on the extent errors in the light gradient estimation and can explain the deviation between model predictions and experimental results.

The light gradient correction factor is plotted against the observed specific growth rate (μ) in Figures 4.4C and 4.4D. For *C. sorokiniana,* it can be observed that the correction factor is larger at low μ, which was expected. This correlation appears to be similar for the light correction factor of *C. reinhardtii* plotted against observed specific growth rates. The light gradient correction factors predicted for *C. sorokiniana* were close to, or within, the realistic range of 0.5 to 2.5, although there were a number of outliers.

The light gradient correction factors for *C. reinhardtii* included many outliers beyond the maximal value of 2.5 and almost no correction factors under the minimal value of 0.5. The primary outlier is from the dataset of Vejrazka et al. (Vejrazka et al. 2011) with experiments performed at low biomass concentrations and 500 μmol $(m^2\ s)^{-1}$ incident light. Under these light saturating conditions, the influence of the correction factor on the predicted growth rate is very low and result in a substantial correction factor. Most likely, the discrepancy between measured and predicted

specific growth rates is then related to other factors such as the different strains and nitrogen sources used for *C. reinhardtii* (Table 4.2) or differences in reactor operation related to pH, temperature, and mixing intensity (i.e. shear stress).

The light gradient correction factor includes the change in specific absorption coefficient due to photoacclimation and, therefore, the results can be compared to the measured specific absorption coefficient in the studies that were used. Only Zijffers et al. (Zijffers et al. 2010), Mooij et al. (de Mooij et al. 2014), Takache et al. (Takache et al. 2012), and Vejrazka (Vejrazka et al. 2011; Vejrazka et al. 2012) measured the real specific absorption coefficients (Appendix 4.B). When evaluating the datasets separately, they all indicate photo acclimation, however, when combined, no trend was observed. Furthermore, comparing the predicted light gradient correction factors to the measured specific absorption coefficient did not reveal a trend (data not shown). This would indicate that differences in the incident light angle and scattering of light within the microalgae suspension are also important factors in the light gradient prediction.

The light source will determine the incident light angle. An indication of the incident light angle can be obtained by looking at the full width at half maximum (FWHM) (Table 4.2). Where, the larger FWHM indicate that a large part of the incident light is falling on the reactor surface at an angle and the smaller the FWHM indicate that incident light is collimated into a beam. Although a trend can be observed that increasing FWHM results in increased light correction factors, it is evident that the incident light angle is not the only factor influencing the light correction factor.

For the majority of datasets, only the average incident light intensity is reported, however, light intensities often vary over the illuminated surface (Bechet et al. 2014a; de Mooij et al. 2014; Vejrazka et al. 2011). In the case of Vejrazka et al. (Vejrazka et al. 2011; Vejrazka et al. 2012), the light intensity ranges from 30% of the average in the corners to 140% of the average in the center of the reactor (FMT150, PSI, Czech Republic). All other datasets do not report the light distribution over the illuminated surface. The light distribution over the reactor

surface will influence the growth rate as high light will result in increased photosaturation as reflected in the hyperbolic trend of photosynthesis versus irradiance (Equation 4.4). This effect will also be included in the light correction factors fitted. To eliminate this effect, a reactor surface should be subdivided into sufficiently small zones with their corresponding incoming light intensity which should all be measured (Bechet et al. 2014a; Slegers et al. 2011). Alternatively, indoor research reactors should be designed such that illumination is actually homogenous across the surface.

Apart from light absorption characteristics of the microalgae and the angular distribution of the incoming light, light scattering within the microalgae suspension also influences the light gradient in a photobioreactor. When light hits a microalga but is not absorbed, the direction of light propagation will change due to reflection or refraction events. The scattering of light, therefore, will change the light path through the reactor. The effect of scattering can be accommodated for by using the two-flux model which includes scattering but neglects the angle of incident light (Cornet et al. 1995; Pilon et al. 2011). As an alternative approach the radiation field can be simulated based on a Monte Carlo approach (Heinrich et al. 2012) which includes scattering as well as the angular distribution of incident light. However, with increasing accuracy, the complexity and number of parameters of the model also increases.

To summarize, in order to model microalgae light limited growth, an accurate predictive light model is essential in combination with sufficient measurements of light distribution across the reactor surface and the angular distribution of incident light. Nevertheless, this analysis demonstrates that a more significant part of the deviation between predicted and measured growth can be accounted for by a better light description. This conclusion is based on the observation that the light gradient correction factor falls within the realistic rage of 0.5 to 2.5. Our simple model for microalgae growth, therefore, could continue to provide sufficient accuracy for engineering purposes provided the light field is better characterized.

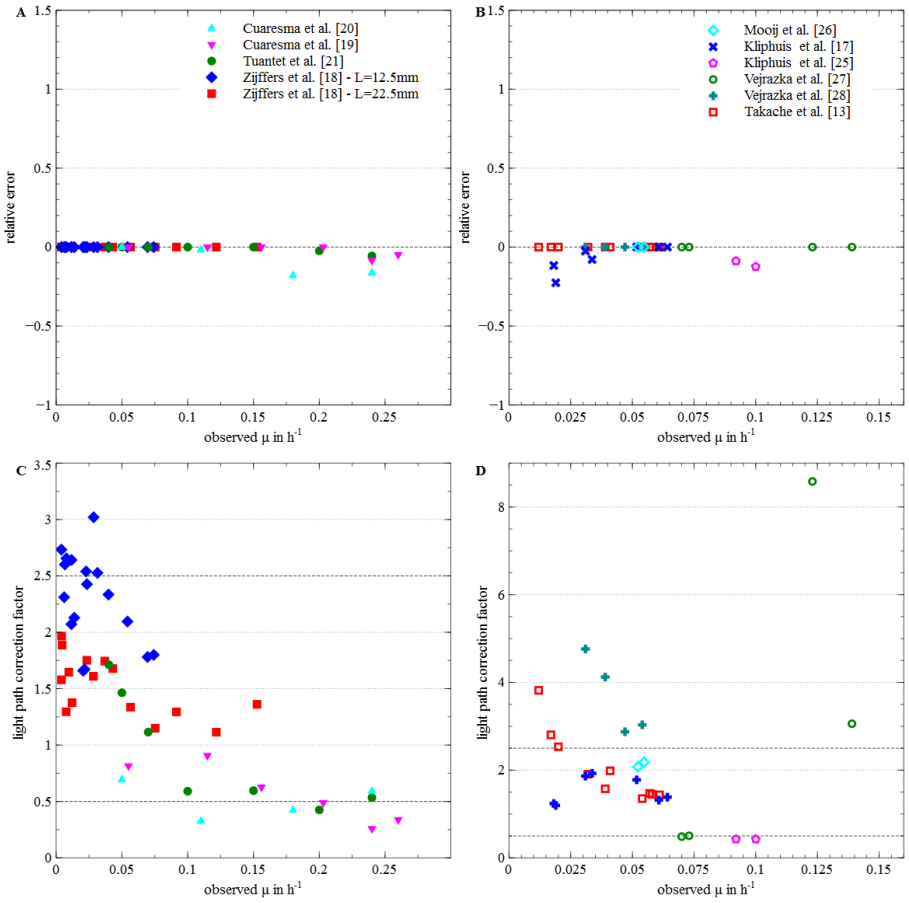

Figure 4.4. Results of the specific growth rate prediction employing light gradient correction factors per data point. On the left, results are depicted for *C. sorokiniana* and on the right for *C. reinhardtii*. A and B show the relative error for the prediction**.** C and D depict the light gradient correction factor plotted against the specific growth rate. The dotted lines in C and D represent the range for realistic light gradient correction factors (0.5 to 2.5).

4.4.3 Improving estimation model parameters

Stepping back from the accuracy of the light field prediction, part of the variation observed in the initial model predictions of the specific growth rate can be related to remaining errors in the estimation of the model parameters. For this reason, Monte Carlo simulations were performed, varying the parameters $Y_{x/s}$, m_s, $a_{x,\lambda}$ and $Y_{s/ph}$

randomly within the range presented in Table 4.1. Please note that, also in this approach, we take into account the possible effect of photoacclimation since parameter $a_{x,\lambda}$ is allowed to vary within the range reported in literature. For $a_{x,\lambda}$, it was assumed that the relative spectral distribution of the specific absorption coefficient remained constant (Supplementary file 1.A). The maximal specific growth rate (μ_m) was fixed and, because of its simple and reliable measurement, the accuracy of this parameter is high.

Monte Carlo simulations were performed on all datasets of either *C. sorokiniana* or *C. reindhardtii* to identify characteristics of microalgae species that were not correctly estimated. Furthermore, simulations per dataset were performed to identify variances between cultivation conditions which can include dissimilarities in: oxygen and carbon dioxide levels, temperature, and shear stress as well as variation between isolates of the *C. reinhardtii* that was employed in the different studies. Datasets were specified as presented in Table 4.2. The combinations of parameters that resulted in the lowest SSE are presented in Table 4.3, and the corresponding predictions are depicted in Figures 4.5A to 4.5E.

The growth predictions for *C. sorokiniana* were clearly improving with the parameter estimation based on the Monte Carlo simulation (Figure 4.5). The predictions range from 36% MAPE to 18% MAPE with the overall fit, and 9-17% MAPE for the fit per dataset. The new parameters presented in Table 4.3 demonstrate an obvious deviation between the datasets of Zijffers et al. (Zijffers et al. 2010) and the other datasets. It appears that the datasets from Zijffers et al. (Zijffers et al. 2010) are characterized by less efficiency of photosynthesis and growth on sugar compared to the other datasets. This is visible from the low $Y_{x/s}$ and $Y_{s/ph}$ fitted for Zijffers et al. (Zijffers et al. 2010) in combination with a high $a_{x,\lambda}$. Due to the substantial number of points derived from Zijffers et al. (Zijffers et al. 2010), the overall fit is also close to the values of Zijffers et al. (Zijffers et al. 2010). This could be an indication that the experiments from Zijffers et al. (Zijffers et al. 2010) were performed under suboptimal conditions compared to the studies of Tuantet et al. (Tuantet et al. 2014) and Cuaresma et al. (Cuaresma Franco et al. 2012;

Cuaresma et al. 2009). The medium recipe, pH, and gas flow rate were similar for all studies. Hydrodynamic forces were plausibly different within the various reactors resulting in variable shear stress between the studies (Walls et al. 2014). It should be noted that, although trends can be observed from the results, errors in the light gradient prediction (see previous section) will also affect the outcome of the Monte Carlo simulations.

The growth predictions for *C. reinhardtii* also improved by adjusting the model parameter based on Monte Carlo Simulations. Compared to *C. sorokiniana*, the increase in accuracy is similar; from a 34% MAPE, the MAPE decreased to 15% with the overall fit and 2-18% with the fit per dataset. For *C. reinhardtii*, all datasets were predicted accurately except for the dataset from Takache et al. (Takache et al. 2012). The dataset of Takache et al. (Takache et al. 2012) might be difficult to predict due to the significant variation in the observed specific absorption coefficient. A clear photoacclimation response was thus observed by Takache et al. (Takache et al. 2012), and this effect cannot be described with our approach based on a constant specific absorption coefficient (Takache et al. 2012). Compared to *C. sorokiniana*, there is much more variation in the m_s parameter which fluctuates between the low and high boundary (Table 4.1). For *C. reinhardtii*, the $Y_{x/s}$ varies over the complete range and, against expectations, the $Y_{x/s}$ for nitrate is predicted to be higher than the $Y_{x/s}$ for ammonium.

From the experimental data and model predictions for *C. reinhardtii*, it appears that it employs light more efficiently cultivated on nitrate compared to urea or ammonium. This was an unexpected result as the reduction of nitrate to ammonium expends energy (Kliphuis et al. 2011a) which is in accordance with the lower $Y_{x/s}$ for nitrate obtained from literature compared to the $Y_{x/s}$ for ammonium (Table 4.1). Based on the experimental design, the only clear difference between the experiments performed with nitrate and ammonium is this nitrogen source (Table 4.2). This observation is strengthened by the fact that the high $Y_{x/s}$ for nitrate is predicted for two different reactors and light sources. The significant divergence between nitrate and ammonium cultivated *C. reinhardtii* is also observed in the overall fit where the

$Y_{x/s}$ for nitrate remains at its maximum while the ammonium $Y_{x/s}$ decreases to its minimum. The decrease in $Y_{x/s}$ for ammonium is to counteract the increase in $Y_{s/ph}$ which is necessary for accurate prediction of the data of Kliphuis et al. (Kliphuis et al. 2011a; Kliphuis et al. 2011c).

The datasets of *C. reinhardtii* are likely more difficult to predict as the various studies employed different species of *C. reinhardtii*. It is possible that these species exhibit different growth characteristics. The strain used by Vejrazka et al. (Vejrazka et al. 2011; Vejrazka et al. 2012), for example, is a wild type which carries mutations in the nitrate reducing genes and can only grow on ammonium. Furthermore, there is a more extensive variation in incident light intensities between the datasets used for *C. reinhardtii* compared to *C. sorokiniana*. *C. reinhardtii* cultures grown at high incident light intensities are expected to grow at reduced efficiency due to negative effects of high light, e.g. photoinhibition. Photoinhibition is not included in this model because of its complexity and time dependence.

Table 4.3. Estimated model parameters based on Monte Carlo simulations (Figure 4.5). Results are shown for the overall fit and for every dataset separately which are both compared to the literature based estimates.

	m_s	$a_{x,\lambda}$	$Y_{x/s}$		$Y_{s/ph}$	**MAPE**
			NH_4	NO_3		
	cmol-s (cmol-x s)$^{-1}$	m^2 cmol-x^{-1}	cmol-x cmol-s^{-1}		cmol-s mol-ph^{-1}	%
	Chlorella sorokiniana					
Literature based estimates Results Monte Carlo simulations	**2.5E-06**	**7.1**	**0.59**	**0.54**	**0.10**	**36**
Overall fit	3.7E-06	4.5	0.50	-	0.08	18
(Tuantet et al. 2014)	3.7E-06	6.9	0.69	-	0.08	17
(Cuaresma Franco et al. 2012)	3.6E-06	5.1	0.70	-	0.11	8
(Cuaresma et al. 2009)	3.7E-06	5.6	0.70	-	0.11	14
(Zijffers et al. 2010)	3.6E-06	6.9	0.46	-	0.08	10
(Zijffers et al. 2010)	3.7E-06	7.1	0.50	-	0.10	9
	Chlamydomonas reinhardtii					
Literature based estimates Results Monte Carlo simulations	**2.0E-06**	**6.2**	**0.69**	**0.58**	**0.10**	**34**
Overall fit	1.8E-06	6.1	0.41	0.64	0.10	15
(Kliphuis et al. 2011a)	1.6E-06	6.1	-	0.64	0.11	5
(Kliphuis et al. 2011c)	2.1E-07	3.2	-	0.64	0.11	2
(Vejrazka et al. 2011)	4.0E-07	6.2	0.43	-	0.08	4
(Vejrazka et al. 2012)	4.0E-07	6.2	0.40	-	0.08	5
(de Mooij et al. 2014)	3.0E-06	6.1	0.40	-	0.08	6
(Takache et al. 2012)	3.6E-06	6.2	0.66	-	0.08	17

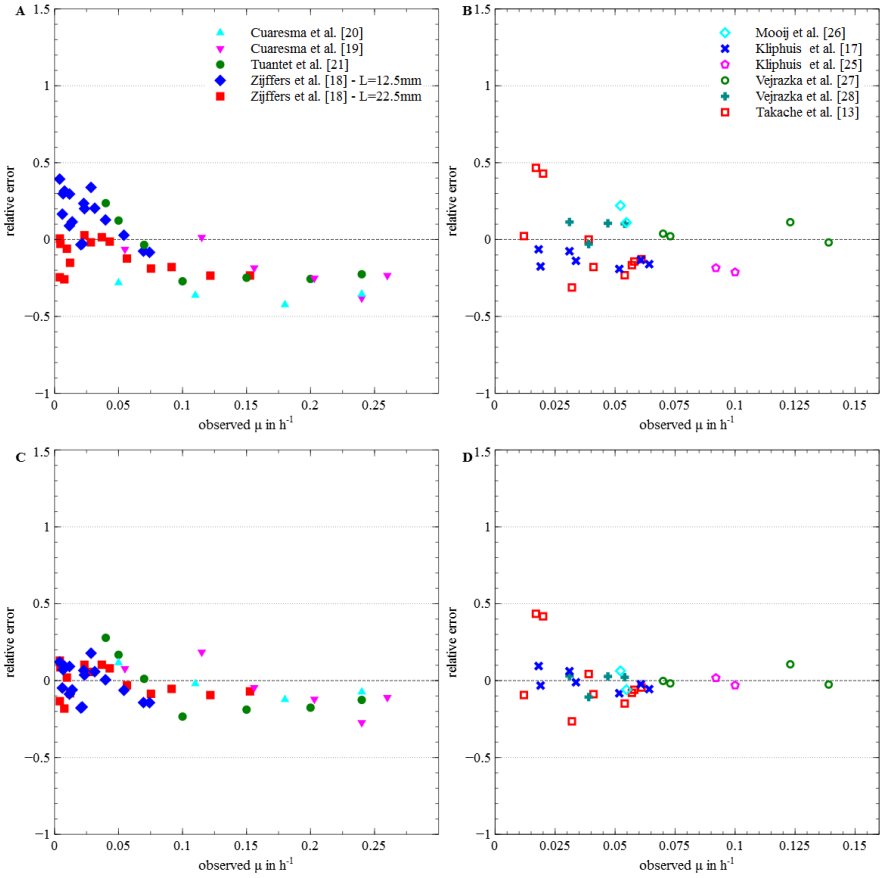

Figure 4.5. Results of Monte Carlo simulations to improve estimation of model parameters. The results are plotted as the relative error for predicted specific growth rate against the measured specific growth rate. For the Monte Carlo simulations, the model input parameters were varied (Table 4.3). On the left, *C. sorokiniana* is depicted and, on the right, *C. reinhardtii*. A and B show the results with the smallest SSE of the Monte Carlo simulation per microalgae species. C and D depict the results with the smallest SSE of the Monte Carlo simulation per dataset (every line in Table 4.2 represents one dataset). The initial literature based prediction are depicted in Figure 4.2C and 4.2D.

4.4.4 Model Predictions batch cultivation

The light limited growth model was validated on published studies on microalgal batch cultivation. The light limited growth model is able to describe the exponential

growth phase at low biomass concentrations and the transition to slower growth with increasing biomass concentrations. The light limited growth model is, however, unable to predict the lag phase in some cases observed at the start of a batch. For this reason, the start of the prediction is in some cases not equivalent to the start of the batch. All data used is presented in Supplementary file 3, where also the start of the simulation is indicated.

For *C. sorokiniana* the model was validated with batch data from three studies (Kliphuis et al. 2011b; Kliphuis et al. 2010; Van Wagenen et al. 2015). The study of Kliphuis et al. (Kliphuis et al. 2011b) was also used to obtain a value for the maintenance sugar consumption. The biomass increase of *C. sorokiniana* was slightly over estimated for two studies (Kliphuis et al. 2011b; Van Wagenen et al. 2015) when employing the literature based estimated parameters (Figure 4.6). For both of these studies the prediction accuracy increases with the parameters obtained with the overall fit for *C. sorokiniana*. In case of Kliphuis et al (Kliphuis et al. 2010), however, the data is actually predicted accurately with the literature based parameters and is underestimated with the parameters obtained with the overall fit. The predictions starting at low biomass concentration, however, are sensitive to the starting concentration and will in reality feature a lower specific absorption coefficient resulting in less over-saturation and a more rapid increase in biomass concentration. This in combination with the observation that dry weight measurement on dilute cultures often feature a lower accuracy we believe that the model predicts all cases accurately. Furthermore, the experiment of Kliphuis et al (Kliphuis et al. 2011b) is predicted accurately and those experiments are the continuation of the experiments in Kliphuis et al. (Kliphuis et al. 2010). Finally it should be noted that Kliphuis et al. (Kliphuis et al. 2011b) observed biofilm formation and that therefore the observed biomass concentrations are underestimations.

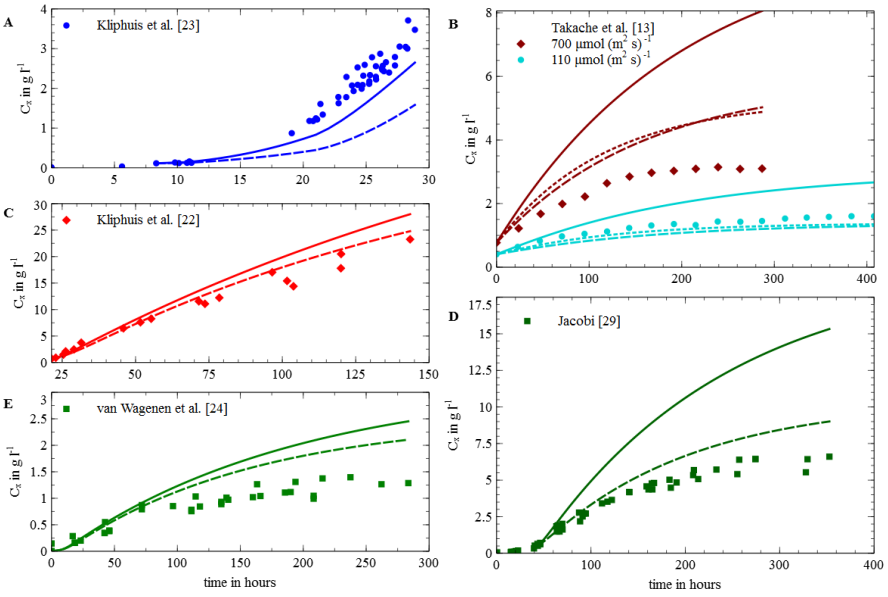

Figure 4.6. Light to growth model validation on batch data For *C. sorokiniana* (A,C,E) and *C. reinhardtii* (B,D). The data represented by symbols is observed data from the corresponding study in the legend. The solid line represents the model prediction with the literature based estimations. The dashed line represents the model prediction with for *C. sorokiniana* the overall fit parameters and for *C. reinhardtii* the averaged parameters from the monte carlo fit for *C. reinhardtii* cultivated with NH4.

For *C. reinhardtii* the model was validated with batch data from two studies (Jacobi 2013; Takache et al. 2012), from which Takache et al. (Takache et al. 2012) also was used to identify the specific absorption coefficient and the molar mass for *C. reinhardtii*. The observed biomass increase during batch growth of *C. reinhardtii* is overestimated when using the literature based parameter estimation (Figure 4.6). Because of the big difference in the parameter fit between *C. reinhardtii* cultivated on ammonia or nitrate (Table 4.3) the fit parameters for the four studies cultivated on ammonia where averaged instead of including the nitrate-derived data as well. In all cases this approach improved the prediction although still a discrepancy between observed and predicted values remains for *C. reinhardtii*. Additionally the batch data of Takache et al (Takache et al. 2012) is also predicted by employing the parameters

obtained with the fit performed on the chemostat data reported in Takache et al (Takache et al. 2012) (Table 4.3), which obtained very similar results to the averaged parameters. The batch validation validates the lower values obtained with the parameter fit compared to the literature based estimates in case of *C. reinhardtii*.

In summary the light limited growth model is able to predict batch cultivations for *C. sorokiniana* accurately. For *C. reinhardtii* it seems that at high light intensities the growth model seems to overestimate the productivity while at lower light intensities the model is accurate. These results are an indication that *C. reinhardtii* features reduced photosynthetic capacity or higher maintenance at high light intensities, which could imply photo damage. Furthermore, the light limited growth model is able to predict the exponential, linear and stationary growth phase.

4.4.5 General Discussion

This model was able to predict the specific growth rate for a wide range of chemostat conditions with a MAPE of 36% for *C. sorokiniana* and 34% for *C. reinhardtii*. This is lower compared to light limited growth models reported in literature (Bechet et al. 2014a; Cornet and Dussap 2009). With *Chlorella vulgaris*, Bechet obtained an overall accuracy of 15% in one lab scale system (Bechet et al. 2014a) and a 8% overall accuracy for one outdoor system (Bechet et al. 2014b). Cornet et al. (Cornet and Dussap 2009) obtained a 15% overall accuracy for eight different reactor configurations with *Arthrospira platensis*. The model proposed, however, increased the accuracy to similar accuracies reported in literature after fitting per dataset, however, a perfect prediction was not obtained. The advantage of the proposed model over previously reported models is that this model introduces a simple but clear mathematical distinction between processes related to photosynthesis and processes related to growth.

Another advantage of this model is that the parameters necessary for the model predictions are measurable characteristics of the microalgae. By using parameters that are measurable characteristics, it is possible to modify this model for other microalgae utilizing the enormous amount of information already present in

literature and/or performing a limited number of dedicated experiments to derive those parameters. The most convenient experiments to determine the model parameters include: (1) The maximal specific growth rate being measured by performing a light limited turbidostat where the average light intensity is close to the light saturation point; (2) The specific absorption coefficient being measured with a dedicated spectrophotometer featuring an integrated sphere and a wavelength scan; (3) The molecular weight being derived from the ash weight and an elemental analysis of the microalgae biomass; (4) The biomass yield on sugar being measured with a dark sugar limited growth experiment or with an experiment at sub-saturating light from which the biomass yield on sugar can be derived based on the linearity of photosynthesis versus light intensity (Kliphuis et al. 2011a); and (5) Measuring the sugar yield on photons is experimentally challenging, therefore, we estimated it based on theoretical considerations. A detailed overview and additional detailed experimental designs can be found in Supplementary file 1.B.

To increase the accuracy of microalgae growth models, experimental work should be further standardized. To properly compare various reactor set ups and validate biological growth models, the dry biomass concentration and biomass specific absorption coefficient should be measured. Furthermore, based on the presented results, an accurate description of the light field is important but difficult to model. Modelling light would be facilitated if the spatial distribution of the incident light, the spectral distribution of the incident light, the incident light angle, and light intensity at the back of the photobioreactor were all measured and reported. For research purposes, flat photobioreactors are preferably used where light is homogeneously distributed over the surface and the incident light angle is well-defined.

4.5 Conclusions

This paper has introduced and validated a model to describe microalgae growth under light-limited conditions. The model is based on only five measurable characteristics of the microalgae, and photosynthetic sugar production is separated from other growth-related processes. With this compartmentalization, the model is

able to distinguish between sugar used for growth related respiration, maintenance related respiration, and precursors for biomass. Validation with different datasets obtained from literature was successful. Furthermore, input parameters where accurately identified from literature and improved with Monte Carlo simulations. This approach can be easily modified for other microalgae species. Due to its simplicity and acceptable accuracy, this model represents a beneficial engineering tool for the design and operation of microalgae based production processes.

4.6 Nomenclature

Parameters	
a	specific (light) absorption coefficient in m^2 $cmol^{-1}$
A	area in m^2
c	correction factor
C	concentration in mol m^{-3}
E	energy of a photon
FWHM	full width at half maximum in degrees
I	light in mol-ph $(m^2\ s)^{-1}$
L	reactor depth in m
M	molar mass in g mol^{-1}
m	cell maintenance in mol $(cmol\text{-}x\ s)^{-1}$
MAPE	mean absolute percent error
N	number of steps
n	number of experimental points
PAR	photosynthetic active region
PI	Photosynthetic irradiance
q	rate in mol $(cmol\text{-}x\ s)^{-1}$
r	rate in g $(m^3\ s)^{-1}$
SSE	squared sum of errors
z	distance in m
Y	yield in (mol/mol)
α	Initial slope of PI curve
Subscripts	
in	incident light
m	maximal
n	normalized
obs	observed
ph	photons in mol-ph
pre	predicted
s	sugar in cmol-s
x	dry biomass in cmol-x
λ	wavelength in nm^{-1}
I	light

Parameters	
a	specific (light) absorption coefficient in m^2 $cmol^{-1}$
A	area in m^2
c	correction factor
C	concentration in mol m^{-3}
E	energy of a photon
FWHM	full width at half maximum in degrees

4.7 Appendices

Appendix 4.A. Spectral distribution of the light source and specific absorption coefficient

The incoming light ($I_{ph}(0)$) and microalgae specific absorption coefficient ($a_{x,\lambda}$) were both expressed for the whole PAR wavelength range from 400 to 700 nm with a resolution of 1 nm. Expressing $a_{x,\lambda}$ and $I_{ph}(0)$ as a function of wavelength increases the accuracy of the model as the spectral distribution of the light source used and the specific absorption coefficient of the microalgae both vary over the PAR spectrum. The spectral distribution of the light source $I_{ph,\lambda}(0)$ (unit µmol $(m^2\ s)^{-1}\ nm^{-1}$) is obtained by multiplying the incoming photon flux density in the complete PAR range $I_{ph}(0)$ (unit µmol $(m^2\ s)^{-1}$) with the normalized spectrum $E_{n,\lambda}$ (unit nm^{-1}) (Equation 4.A.1). An overview of all PAR normalized light spectra $E_{n,\lambda}$ used in this study is depicted in Figure 4.A.1 and in the Supplementary Excell file 2.

Equation 4.A.1 $$I_{ph,\lambda}(0) = I_{ph}(0) \cdot E_{n,\lambda}$$

The $a_{x,\lambda}$ used for *C. sorokiniana* and *C. reinhardtii* are both depicted in Figure 4.A.2 (de Mooij et al. 2014; Zijffers et al. 2010) and supplied in the Supplementary Excel file 2. The relative spectral distribution of the absorption coefficient is assumed to remain constant in the Monte Carlo simulations. Therefore, $a_{x,\lambda}$ can be calculated according Equation 4.A.2 with the specific absorption coefficient per wavelength ($a_{x,\lambda}$), the average specific absorption coefficient from 400 to 700 nm (a_x), the average maximal specific absorption coefficient from 400 to 700 nm ($\bar{a}_{x,\lambda,m}$), and the maximal specific absorption coefficient per wavelength ($a_{x,\lambda,m}$).

Equation 4.A.2 $$a_{x,\lambda} = \frac{a_x}{\bar{a}_{x,\lambda,m}} \cdot a_{x,\lambda,m}$$

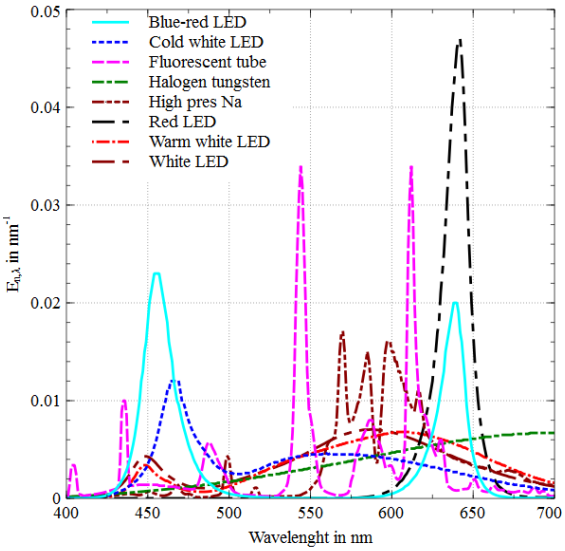

Figure 4.A.1 Overview of all PAR normalized emission spectra of the light sources used in this study.

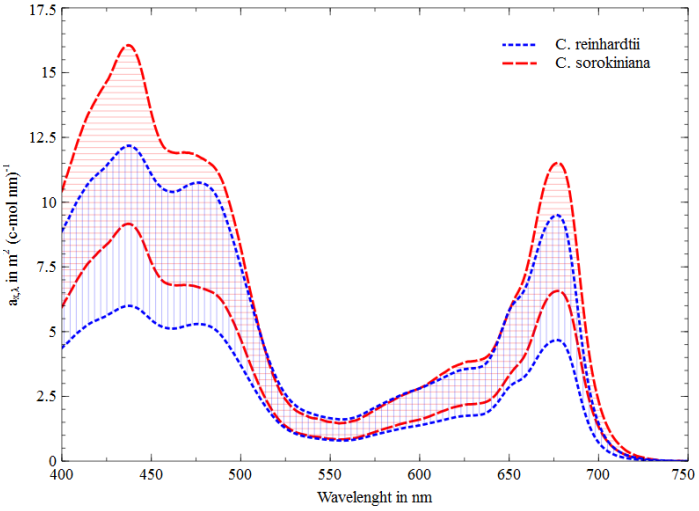

Figure 4.A.2 The spectral distribution of the maximal and minimal specific absorption coefficient used in this study. The range used in the Monte Carlo simulations is depicted for *C. sorokiniana* with horizontal stripes and with vertical stripes for *C. reinhardtii*.

Appendix 4.B. Background behind the model parameters

This Appendix contains the detailed background behind all five model parameters. For every model parameter, the important references are listed with a detailed discussion on how the most likely value was determined from the literature data. Furthermore, for every model parameter, there is a table that contains all data used to estimate the model parameter value.

4.B.1 Molar mass

The molar mass in g dry weight biomass per cmol biomass of microalgae (M_x) is used to translate measurements based on dry weight to cmol biomass. This is important as most yields that are used are derived from the molar stoichiometry. The Molecular weight of microalgae is measurable by elemental analysis. Two studies reported the M_x of *C. sorokiniana* (Kliphuis et al. 2010; Samejima and Myers 1958), and two for *C. reinhardtii* (Kliphuis et al. 2011a; Takache et al. 2012); values can be found in Table 4.B.1 and a summary in Table 4.1. In the predictions, it was decided to use an average M_x for microalgae of 24 g-x cmol-x^{-1}, which is based on the M_x of multiple microalgae species (Cornet and Dussap 2009). Under nutrient replete nutrient conditions, M_x is stable. When cultivation conditions change, however, the molar mass can change. For example, microalgae that have a high amount of accumulated lipids will contain lower nitrogen content. This M_x change is not relevant for this study as this model aims to predict light limited growth and not nitrogen limited growth.

The elemental composition of the microalgal biomass is used to obtain the stoichiometry of microalgae growth (Table 4.B.1). From the stoichiometry, it is possible to derive the biomass yield on oxygen and carbon dioxide that is necessary for the recalculation of input parameters obtained from other studies. The presented stoichiometry of growth presented in equations B.1 and B.2 is the average of all data used to calculate M_x. Note that the stoichiometry changes depending on the nitrogen source.

Equation 4.B.1

CO_2+0.14 NH_4+0.59 H_2O+0.014 PO_3+0.005 SO_4→ $CH_{1.74}O_{0.45}N_{0.14}P_{0.014}S_{0.005}$ + 1.10 O_2

Equation 4.B.2

CO_2+0.14 NO_3+0.87 H_2O+0.014 PO_3+0.005 SO_4→ $CH_{1.74}O_{0.45}N_{0.14}P_{0.014}S_{0.005}$ + 1.45 O_2

Table 4.B.1. Molecular weight of a cmol of biomass M_x derived from published data. The M_x calculated is not corrected for ash minerals.

Reference	N source	M_x g cmol-x^{-1}	C	H	O	N	P	S	M_x calculated g cmol-x^{-1}
			mol-i cmol-C						
Chlorella sorokiniana									
(Kliphuis et al. 2010)	NO3	23.7	1	1.71	0.4	0.15			22.2
(Samejima and Myers 1958)	NO3	25.0	1	1.75	0.50	0.15			23.8
	NH4	24.4	1	1.74	0.49	0.11			23.2
	urea	25.0	1	1.81	0.48	0.13			23.4
Chlamydomonas reinhardtii									
(Kliphuis et al. 2011a)	NO3	24.0	1	1.62	0.41	0.14	0.01	0.003	22.5
(Takache et al. 2012)	NH4	24.0	1	1.78	0.44	0.18	0.018	0.007	24.0
overall average									
overall average	-	24.4	1	1.74	0.45	0.14	0.01	0.01	23.20

4.B.2 Specific light absorption coefficient

The spectral dependence of the specific light absorption coefficient was already discussed in Appendix 4.A. This specific absorption coefficient is measurable in multiple ways. Most accurate is to use a spectrophotometer with an integrated sphere that is able to correct for the effect of light scattering in order to obtain the real specific light absorption coefficient. In contrast, a normal spectrophotometer will measure an extinction or attenuation coefficient which includes both light scattering

and absorption by the microalgae cells. A second option to measure the extension or attenuation coefficient is measuring the light attenuation through the culture broth. In this study, specific absorption coefficient data originates from various sources measured with different techniques which are, for the sake of simplicity. all categorized under the term specific absorption coefficient.

The specific absorption coefficient ($a_{x,\lambda}$) is not a fixed value but is subjected to change in response to environmental changes. A few studies predicted the specific absorption coefficient in response to, e.g., incident light (Takache et al. 2012), nitrogen availability (Fachet et al. 2014), biomass concentration (Bechet et al. 2014a), biomass yield on light (Klok et al. 2013), or by the ratio of realized to potential photosynthetic electron flow (Geider et al. 1996). However, the current models did not provide an appropriate correlation to describe the dependency of $a_{x,\lambda}$ in our case. Therefore, in this model, we decided to use the maximal specific absorption coefficient ($a_{x,\lambda,m}$) for both microalgae. The $a_{x,\lambda,m}$ resulted in the best predictions and should be valid for dense light-limited cultures with a steep gradient.

The a_x for *C. sorokiniana* is based on one study (Zijffers et al. 2010). The reported a_x were weighted to the light source used for cultivation by Zijffers et al. and, therefore, were recalculated to the non-weighted a_x. The a_x for *C. reinhardtii is* based on five studies (de Mooij et al. 2014; Fouchard et al. 2009; Takache et al. 2012; Vejrazka et al. 2011; Vejrazka et al. 2012). An overview of the a_x found in literature is depicted in Table 4.B.2. The a_x values in the table are averaged values over the PAR range, however, in the model, specific light absorption coefficient per nm is used ($a_{x,\lambda}$) (see Appendix 4.A and Supplementary Excell file 2). The $a_{x,\lambda}$ for *C. sorokiniana* is based on unpublished results and is measured during a turbidostat cultivation using an Avaspec 2048 spectrophotometer. The $a_{x,\lambda}$ for C. reinhardtii is measured by de Mooij et al. (de Mooij et al. 2014).

Table 4.B.2. Specific light absorption coefficient a_x derived from published data. For several references, the specific absorption coefficient was given as a weighted average for the light spectrum of the light source used according to the methodology used by Dubinsky and coworkers (Dubinsky et al. 1986). In the case of weighted specific absorption coefficients, they are recalculated to an unweighted value based on the normalized light spectrum of the light source used in those studies.

	C_x	μ_{obs}	$I_{ph}(0)$	a_x	
				weighted	unweighted
	kg m^{-3}	h^{-1}	µmol-ph $(m^2\ s)^{-1}$	m^2 cmol-x^{-1}	
			Chlorella sorokiniana		
(Zijffers et al. 2010) [1]	0.7	0.15	940	2.9	4.1
	1.1	0.12	940	4.1	5.7
	1.4	0.09	940	5.1	7.1
	1.8	0.08	940	5.1	7.1
	2.2	0.06	940	4.7	6.5
	2.6	0.04	940	4.7	6.5
	2.9	0.04	940	4.9	6.9
	3.8	0.03	940	3.8	5.3
	4.3	0.02	940	3.6	5.1
	7.9	0.01	940	3.2	4.5
	8.5	0.01	940	3.4	4.7
	10.9	0.01	940	3.9	5.4
	12.1	0.00	940	4.1	5.8
	12.4	0.00	940	4.2	5.9
	13.8	0.00	940	3.8	5.3
	2.5	0.07	871	5.0	7.1
	3.2	0.05	871	4.8	6.7
	4.0	0.04	871	5.1	7.1
	4.6	0.03	871	5.0	7.0
	6.1	0.02	871	4.7	6.6
	7.8	0.02	871	4.2	5.8
	9.8	0.01	871	3.9	5.5
	11.2	0.01	871	3.8	5.3
	12.8	0.01	871	3.9	5.5
	14.1	0.01	871	3.8	5.3
	15.7	0.01	871	3.6	5.0
	17.7	0.00	871	3.4	4.8

Table 4.B.2 continued.

	C_x	μ_{obs}	$I_{ph}(0)$	a_x	
				weighted	unweighted
	kg m^{-3}	h^{-1}	µmol-ph $(m^2\ s)^{-1}$	m^2 cmol-x^{-1}	
Chlamydomonas reinhardtii					
(Takache et al. 2012) [2]	0.4	0.03	110		4.8
	0.4	0.04	200		4.5
	0.5	0.05	300		4.2
	0.5	0.06	400		4.1
	0.6	0.06	500		3.8
	0.6	0.06	600		3.6
	1.1	0.04	1000		3.1
(de Mooij et al. 2014) [3]	2.6	0.05	1469	5.2	5.1
(Fouchard et al. 2009) [4]	-				4.1
(Vejrazka et al. 2011) [3]	0.1	0.07	100		5.6
	0.1	0.13	500		3.0
(Vejrazka et al. 2012) [3]	0.3	0.05	220		6.2
	0.4	0.05	220		5.7
	0.3	0.03	110		5.4
	0.3	0.04	110		5.7

[1] recalculated to unweighted a_x

[2] a_x derived from pigment measurement and algae analysis

[3] a_x measured with integrated sphere

[4] model parameter

4.B.3 Sugar yield on photons

The sugar yield on photons ($Y_{s/ph}$) is derived from the quantum yield of microalgae. The theoretical maximum quantum yield based on analysis of the Z-scheme is eight photons per molecule of oxygen liberated or carbon dioxide fixed. However, four independent studies with five different microalgae species determined, on average, a quantum requirement of ten photons per liberated oxygen (Arnold 1949; Dubinsky et al. 1986; Emerson and Lewis 1943; Ley and Mauzerall 1982; Tanada 1951). The same quantum yield was obtained with several techniques in plant research (Bjorkman and Demmig 1987; Evans 1987; Malkin and Fork 1996). The lower efficiency of photosynthesis compared to the z-scheme could be explained by a less

efficient ATPase that requires 14 protons instead of 12 protons. With this ATPase cyclic photosynthetic electron transport around photosystem, I is necessary to retain the 3:2 ATP:NADPH ratio (Allen 2003). This would require an extra photon compared to the theoretical requirement of eight photons bringing the total requirement to nine photons. In that scenario, still one photon is missing considering a requirement of ten photons was measured. We will assume this last photon represents an intrinsic inefficiency of photosynthesis. The reciprocal of the quantum requirement gives the sugar yield directly on photons ($Y_{s/ph}$, Table 4.B.3) in cmol since the carbon dioxide fixed is all converted into triose sugars by photosynthesis.

Table 4.B.3 Sugar yield on photons $Y_{s/ph}$ derived from published data.

Referenence	**Species**	$Y_{s/ph}$ cmol-s mol-ph^{-1}	**note**
		Microalgae	
(Emerson and Lewis 1943)	*Chlorella pyrenoidosa*	0.082	oxygen measurements (wavelength averaged)
(Arnold 1949)	*Chlorella pyrenoidosa*	0.109	calorimetric analysis (values are from Malkin and Fork 1996)
	Chlorella vulgaris	0.090	
	Scenedesmus sp.	0.097	
(Tanada 1951)	*Navicula minima*	0.102	oxygen measurements (wavelength averaged)
(Ley and Mauzerall 1982)	*Chlorella Vulgaris*	0.099	oxygen measurements (wavelength averaged)
(Dubinsky et al. 1986)	*Thalassiosira weisflogii*	0.091	Calculated
	Isochrysis galbana	0.105	
		Plants	
(Bjorkman and Demmig 1987)	average over 44 plants	0.085	based on oxygen measurements
(Evans 1987)	spinacia	0.106	oxygen measurements (wavelength averaged)
	plants in general	0.086	
(Malkin and Fork 1996)		0.105	calorimetric analysis
(Allen 2003)	plants in general	0.111	Theoretical assessment of photosynthesis

4.B.4 Biomass yield on sugar and maintenance requirement for sugar

In the model proposed in this study, photosynthetically derived sugar is either used as a building block of new biomass or respired in the mitochondria to generate energy in the form of ATP which is necessary to drive the growth reactions and fulfill the maintenance requirements. It can be argued that additional ATP can be generated in the chloroplast by cyclic photosynthetic electron transport around photosystem I. There are indications that ATP and or NADPH produced during photosynthesis can also be used for other purposes than solely CO_2 fixation (Hoefnagel et al. 1998). However based on based on a stoichiometric analysis of *C. reinhardtii* microalgae gain more ATP by using photosynthesis to generate sugar in the chloroplast which is respired again in the mitochondria(Kliphuis et al. 2011a). Increased levels of respiration have indeed been measured in the light (Geider and Osborne 1989; Kliphuis et al. 2011b; Vejrazka et al. 2013). For this reason and for the sake of model simplicity, therefore, it is assumed that the chloroplast only generates sugar and that microalgae growth outside the chloroplast can be described by the same relations used to describe aerobic chemoheterotrophic growth.

Respiration as described by Pirt consists of two parts: sugar consumption related to cell maintenance and growth related sugar consumption (Geider and Osborne 1989; Pirt 1965). Cell maintenance related sugar consumption (m_s) can be measured with various techniques, but measuring the dark oxygen consumption of the microalgae is the most common method (Kliphuis et al. 2011b; Le Borgne and Pruvost 2013; Myers and Graham 1971; Pickett 1975). To convert the oxygen consumption to sugar consumption, we have assumed that every mol of oxygen consumed is used to respire one cmol of sugar; this assumption is based on the stoichiometry of aerobic respiration. However, in case other carbon structures are respired (e.g., lipids or proteins), this value would change (Geider and Osborne 1989; Le Borgne and Pruvost 2013). A similar method is based on the measurement of CO_2 production instead of oxygen consumption (Geider and Osborne 1989; Harris et al. 1983). However, another method to measure the m_s makes use of the linearity of photosynthesis versus light intensity at sub-saturating light. Linearly extrapolating

photosynthesis measurements at low light intensities to a light intensity of zero m_s is obtained. This method was employed with *C. reinhardtii* growing on acetate (Chen and Johns 1996) and light (Harris et al. 1983; Kliphuis et al. 2011a; Vejrazka et al. 2013; Zijffers et al. 2010). Table 4.B.4 shows an overview of the values obtained for m_s for both, *C. sorokiniana* and *C. reinhardtii.* To prevent effect of outliners from literature on the used value m_s value, the average m_s obtained from the literature study was used as the model input.

In accordance with the approach of Pirt (Pirt 1965), growth related sugar consumption depends on the actual specific growth rate and the biomass yield on sugar ($Y_{x/s}$). The $Y_{x/s}$ can be calculated based on heterotrophic growth experiments (Chen and Johns 1991; Chen and Johns 1996; Lee et al. 1996; Li et al. 2014; Shi et al. 1997). Another method again utilizes the linearity of photosynthesis versus light intensity in sub-saturating light. The slope of this linear trend can be used to estimate $Y_{x/s}$ (Kliphuis et al. 2011a; Vejrazka et al. 2013). Because energy is expended and reduces power to convert nitrate into ammonia, the $Y_{x/s}$ depends on the nitrogen source. Cultures grown on ammonia or urea will have a higher $Y_{x/s}$ compared to cultures grown on nitrate. In Table 4.B.5, an overview of the obtained values is presented. The average $Y_{x/s}$ was used as input for the model because this minimizes possible measurement errors, and the average obtained values are closer to the $Y_{x/s}$ obtained for heterotrophic organisms (von Stockar and Liu 1999).

Table 4.B.4. Maintenance related specific sugar consumption rate m_s derived from published data.

reference	m_s	measure time	note
	cmol-s (cmol-x s)$^{-1}$	s	
		Chlorella sorokiniana	
(Kliphuis et al. 2011b)	2.0E-06	210	derived from dark oxygen consumption experiments
(Zijffers et al. 2010)	2.3E-06	-	determined based on the corresponding light use
(Pickett 1975)	1.7E-06	600	derived from dark oxygen consumption experiments
	2.0E-06	600	
	2.1E-06	600	
	3.0E-06	600	
(Myers and Graham 1971)	3.7E-06	180	measured after transfer to dark
	3.2E-06	180	derived from dark oxygen consumption experiments
	3.0E-06	180	
	2.3E-06	180	
	1.6E-06	180	
	1.2E-06	180	
	3.6E-06	210	measured at the end of a PI curve
	3.0E-06	210	
	3.5E-06	210	
	3.1E-06	210	
	2.4E-06	210	
	2.2E-06	210	
		Chlamydomonas reinhardtii	
(Kliphuis et al. 2011a)	3.6E-06	-	Derived from chemostats data
(Vejrazka et al. 2013)	2.6E-06	-	Derived from PI curves data
(Le Borgne and Pruvost 2013)	1.5E-06	24 h	long term dark experiments (24 h)
	1.3E-06	24 h	
(Chen and Johns 1996)	2.5E-06	-	derived from a series of heterotrophic batch experiments
	2.3E-06	-	
(Harris et al. 1983)	1.6E-07		^{14}C measurement

Table 4.B.5. Biomass yield on sugar $Y_{x/s}$ derived from published data.

reference	$Y_{x/s}$		substrate	concentration	note
	NH_4	NO_3			
	cmol-x cmol-s^{-1}			kg m^{-3}	
			Chlorella sorokiniana		
(Chen and Johns 1991)		0.54	glucose	5	
		0.61	glucose	8	
		0.61	glucose	15	
		0.63	glucose	18	
(Shi et al. 1997)		0.60	glucose	9	Basal medium
		0.53	glucose	9	Khul medium
		0.59	glucose	36	Basal medium
(Li et al. 2014)		0.40	glucose	2	
		0.43	glucose	4	
		0.56	glucose	6	
		0.55	glucose	8	
		0.54	glucose	10	
		0.48	glucose	20	
(Lee et al. 1996)	0.44		glucose	18	During the dark
	0.61		glucose	18	average over the day
	0.61		glucose	18	during the day (Cx of 2 kg m^{-3})
	0.70		glucose	18	during the day (Cx of 4 kg m^{-3})
	0.58		glucose	18	during the day (Cx of 7 kg m^{-3})
			Chlamydomonas reinhardtii		
(Kliphuis et al. 2011a)		0.52	light	-	derived from chemostat experiments
	0.61		light	-	recalculated based on stoichiometry
(Vejrazka et al. 2013)	0.78		light	-	Derived from PI curves
		0.64	light	-	recalculated based on stoichiometry
(Chen and Johns 1996)	0.68		acetate	0.4	

4.B.5 Maximal specific sugar production rate

The maximal sugar production rate ($q_{s,m}$) can be obtained by substituting the maximal specific growth (μ_m) rate (Equation 4.B.3). By calculating $q_{s,m}$ according Equation 4.B.3 the value of $q_{s,m}$ will vary depending on the value for biomass yield on light and the maintenance related sugar consumption. Consequently the calculated $q_{s,m}$ is higher for cultures growing on nitrate as these cultures typically have a lower biomass yield on light, and thus need to produce more sugar to still reach the same maximal specific growth rate. This seems odd, and therefore it might as well be that in addition to a lower biomass yield on light also the maximal specific growth rate is lower for cultivations on nitrate. There are no reports, however, on lower maximal specific growth rates on nitrate in comparison to ammonia. For this reason it could also be argued that it is relatively easy for the cells to obtain reducing power to reduce nitrate to ammonia .The reduction of nitrate is performed in the chloroplast at the expense of reduced ferredoxin, which could be available in excess at over saturating light intensities. In our model description all reducing equivalents are assumed to flow through sugar to nitrate so such a mechanism would result in an higher $q_{s,m}$.

To measure the μ_m of a microalgae species, experimental conditions should be light saturating with a high light absorption rate per biomass while preventing inhibiting light intensities. These conditions can be obtained by turbidostat or during the exponential growth phase in a batch culture. In Table 4.B.6, an overview of the μ_m obtained from literature for *C.sorokiniana* (Cuaresma et al. 2009; Van Wagenen et al. 2014) and *C. reinhardtii* (Fouchard et al. 2009; Janssen et al. 2000; Janssen et al. 1999; Vejrazka et al. 2011) are presented. In the case of *C. sorokiniana*, it was chosen to use the highest obtained value. In the case of *C. reinhardtii*, the highest obtained value had a very significant standard deviation, therefore, the second largest was chosen.

Equation 4.B.3 $$q_{s,m} = \frac{\mu_m}{Y_{x/s}} + m_s$$

Table 4.B.6. Maximal specific growth rates μ_m derived from published data.

	μ_{obs}	$I_{ph,in}$	C_x	**note**
	h^{-1}	µmol-ph $(m^2\ s)^{-1}$	kg m^{-3}	
		Chlorella sorokiniana		
(Cuaresma et al. 2009)	0.26	2100	1.5	measured in flat plate reactor
(Van Wagenen et al. 2014)	0.27	700	-	measured in microplates
	0.25	83	0.1	measured in flat plate reactor
(Janssen et al. 1999)	0.27	630	-	measured in airlift loop reactor
		Chlamydomonas reinhardtii		
(Vejrazka et al. 2012)	0.139	500	0.1	measured in flat plate reactor
(Janssen et al. 2000)	0.132	600	-	measured in flat plate reactor
(Janssen et al. 1999)	0.16	240	0.2	measured in airlift loop reactor
(Fouchard et al. 2009)	0.14	300	-	very large standard deviation measured in flat plate reactor

Chapter 5 Microalgal biofilm growth under day-night cycles

This chapter is prepared manuscript for submission as:

Blanken, W.; Magalhães, A.; Sebestyén, P.; Rinzema, A.; Wijffels, R.H.; Janssen, M.

"Microalgal biofilm growth under day-night cycles"

Abstract

Microalgal biofilms of *Chlorella sorokiniana* were cultivated under simulated day-night cycles at high productivity and high photosynthetic efficiency. Comparing day-night to continuous illumination did not demonstrate differences in the light utilization efficiency. This indicates that biomass consumed overnight represents sugar consumption for synthesis of new functional biomass and maintenance related respiration.

Modelling microalgal biofilm growth was employed to calculate maximum productivities and photosynthetic efficiencies. A light limited microalgal biofilm growth model in which both diurnal carbon-partitioning and maintenance under prolonged dark conditions were taken into account was developed, calibrated, and validated experimentally. Extended periods of darkness resulted in reduced maintenance related respiration. Based on simulations with the validated biofilm growth model, it could be determined that the photosynthetic efficiency of biofilm growth can be higher than that of suspension growth. This is related to the fact that the maintenance rate in the dark zones of the biofilm is lower compared to that in the dark zones of suspension cultures which are continuously mixed with the photic zone.

5.1 Introduction

Phototropic biofilms are thin, densely packed layers of microalgae cells attached to a solid surface. Usually, substrate and light enter the biofilm from the same side. The biofilm cells are fixed spatially, and gradients of dissolved substrates and light will develop because of cellular consumption, diffusion, and shading. Nevertheless, high productivities and light utilization efficiencies are obtained with phototrophic biofilms (Blanken et al. 2014; Christenson and Sims 2012; Gross and Wen 2014; Naumann et al. 2012) and are similar to suspended cultures (Cuaresma Franco et al. 2012). The biofilm productivities can be better understood by studying microalgal biofilm dynamics under diel light variations and the metabolic response to prolonged darkness deep inside the biofilm. Such an experimental approach must be combined with mathematical modelling of microalgae biofilm growth to provide an analytical framework of the process.

Monoalgal biofilm growth has been mathematically modelled for light and nutrient limited growth under continuous light by fitting the models to experimental data (Li et al. 2016; Murphy and Berberoglu 2014). These studies focused on nutrient limitations inside the biofilm by including diffusion and convection driven nutrient transport through the biofilm (Li et al. 2015a; Li et al. 2016). Other studies have included phototrophic growth in multispecies biofilm models, studying inter-species interactions in mixed biofilms under continuous light (Cole et al. 2014; Munoz Sierra et al. 2014) and day/night light regimes (Wolf et al. 2007). Lacking are biofilm studies that include diurnal carbon partitioning inside biofilms, even though diurnal carbon-partitioning is widely observed in microalgae (Baroukh et al. 2014; de Winter 2015; Tuantet 2015), cyanobacteria (Post et al. 1986), and plants (Scialdone et al. 2013; Stitt and Zeeman 2012). These observations include the accumulation of storage compounds during the day which are consumed during the night. This partitioning has been mathematically described for suspension cultures [19] but not for biofilm growth.

In addition to darkness during the night, an increasing part of the biofilm interior will be exposed to consecutive days of darkness prior to harvest. This is caused by

continuous biofilm growth and the concomitant increase of self-shading (Li et al. 2015a; Li et al. 2016). Based on the observation that the respiration rate decreases upon prolonged starvation for microalgae (Ruiz-Martinez et al. 2016), plants (Gary et al. 2003) and bacteria (Hoehler and Jorgensen 2013; Riedel et al. 2013); we believe that prolonged darkness will decrease maintenance related respiration as a starvation response.

To fully understand biofilm productivity, diurnal carbon-partitioning and light starvation deep inside the biofilm should be included in a biofilm growth model. Therefore, the goal is to develop and validate a microalgal biofilm growth model that takes both day-night driven carbon-partitioning and the metabolic response to prolonged darkness into account. The model will be calibrated employing suspended batch cultivations with *Chlorella sorokiniana* and validated with experiments in the Algadisk, a rotating biological contactor designed for microalgal biofilm cultivation.

5.2 Theory

Phototropic growth of eukaryotic microalgae can be simplified as a combination of phototrophic sugar production and aerobic chemo-heterotrophic growth on sugar (Blanken et al. 2016). Phototrophic growth can, therefore, be described by coupling the kinetics of phototrophic sugar production in the chloroplast to overall microalgal growth by means of a sugar balance (Blanken et al. 2016). This balance equation for photosynthetically derived sugar then describes the partitioning of sugar between growth and maintenance. The sugar used for growth is partly utilized as a building block for new biomass and partially respired to derive the energy required for this growth process.

Microalgae cultivated under natural sunlight conditions experience a day-night cycle. Observations indicate that microalgae exposed to natural light conditions accumulate storage compounds during the day which are consumed during the night (Tuantet 2015). For *Chlorella sorokiniana*, the main storage compound is starch (Tuantet 2015) which will be referred to as sugar with unit carbon mole in the equations below.

5.2.1 Mass balances Sugar and functional biomass

To describe diurnal carbon-partitioning between storage and biomass growth, the total biomass (C_b) will be divided into functional biomass (C_x) and accumulated sugar biomass (C_s) (Equation 5.1). This results in two mass balances: Equation 5.2 for functional biomass and Equation 5.3 for accumulated sugar. Equation 5.2 describes the biomass accumulation rate where $q_{s,c}$ is the specific sugar consumption rate which is dependent on the internal sugar concentration and where m_x is that part of the maintenance requirement fulfilled by degradation of functional biomass (Beeftink et al. 1990). Equation 5.3 describes the sugar accumulation rate which is a balance between the specific sugar consumption rate ($q_{s,c}$), the maintenance related sugar consumption rate (m_s), and the specific photosynthetic sugar production rate ($q_{s,p}$). The specific sugar production rate ($q_{s,p}$) depends on the light intensity. Consequently, biomass growth is only possible when the internal sugar concentration is sufficient.

Equation 5.1 $$C_b = C_x + C_s$$

Equation 5.2 $$\frac{dC_x}{dt} = \left(Y_{x/s} \cdot q_{s,c}(C_s, t) - m_x\right) \cdot C_X$$

Equation 5.3 $$\frac{dC_s}{dt} = \left(q_{s,p}(C_x, z) - q_{s,c}(C_s, t) - m_s(C_s)\right)c_X$$

5.2.2 Sugar production

All sugar is produced photosynthetically and limited by the amount of light that the microalgae absorb. Consequently, the specific sugar production rate ($q_{s,p}$) can be described by Equation 5.4 (Blanken et al. 2016; Jassby and Platt 1976) in combination with the local specific photon absorption rate (Equation 5.5) and the local light intensity (Equation 5.6). These equations were described in detail by Blanken et al. (Blanken et al. 2016). In the current model description, however, the specific light absorption coefficient ($\alpha_{x,\lambda}$) is normalized to functional biomass (C_x). Cells with a high internal sugar concentration will thus feature a lower specific absorption coefficient per total biomass.

Equation 5.4 $$q_{s,p}(C_x, z) = q_{s,p,m} \cdot tanh\left(\frac{q_{ph}(C_x,z) \cdot Y_{s/ph}}{q_{s,p,m}}\right)$$

Equation 5.5 $$q_{ph}(C_x, z) = \frac{I_{ph}(z) - I_{ph}(z+dz)}{C_x \cdot dz}$$

Equation 5.6 $$I_{ph}(z) = \sum_{\lambda=700}^{\lambda=400} I_{ph,\lambda}(0) \cdot e^{(-a_{x,\lambda} \cdot C_x \cdot z \cdot c_I)} \cdot \Delta\lambda$$

5.2.3 Sugar consumption

The specific sugar consumption rate is dependent on the internal sugar concentration, and the kinetics are different for day time and night time (Equation 5.7 and 5.8) where the time of the day is the time according to the 24-hour time notation with sunrise at 0:00. Equation 5.9 is a Droop Equation (Droop 1968) and describes the sugar consumption during the day. It also includes the maximal sugar consumption rate ($q_{s,m,c}$). Equation 5.10 describes the specific sugar consumption during the night where the consumption is linear such that all available sugar is consumed at sunrise (in accordance with experimentally derived kinetics determined for higher plants (Scialdone et al. 2013; Stitt and Zeeman 2012)). Both equations contain a minimal sugar concentration ($C_{s,min}$) (Equation 5.7). Consequently, the total biomass will always contain a small fraction of sugar that is not consumed for biomass production but only to fuel maintenance related sugar consumption (m_s).

Equation 5.7 $$C_{s,min} = C_b * f_{s/b,min}$$

Equation 5.8

$$q_{s,c}(C_s, t) = \begin{cases} q_{s,c}(C_s, t) = 0, & C_s < C_{s,min} \\ q_{s,c}(C_s, t) = q_{s,c,light}(C_s), & t_d < t_{sunset} \\ q_{s,c}(C_s, t) = q_{s,c,dark}(C_s, t), & t_d > t_{sunset} \end{cases}$$

Equation 5.9 $$q_{s,c,light}(C_s) = q_{s,m,c} \cdot \left(1 - \frac{C_{s,min}}{C_s}\right)$$

Equation 5.10 $$q_{s,c,dark}(C_s, t) = \frac{C_s - C_{s,min}}{(24 - t_d) * C_x} - m_s(C_s)$$

5.2.4 Maintenance related sugar consumption

Part of the sugar produced is aerobically respired to produce energy in the form of adenosine triphosphate (ATP) which supports growth and cellular maintenance. The amount of sugar required for growth is described by the biomass yield on sugar ($Y_{x/s}$ in Equation 5.2). Additional sugar is continuously respired to support cellular maintenance. This is described by the maintenance related sugar consumption rate (m_s) in Equation 5.3. It was ascertained in this study that the maintenance related sugar consumption decreases with diminishing sugar availability, in line with observations for microalgae (Ruiz-Martinez et al. 2016), plants (Gary et al. 2003) and bacteria (Hoehler and Jorgensen 2013; Riedel et al. 2013). Based on our observations (Chapter 5.5.1), we also included a term for the consumption of functional biomass (m_x) in Equation 5.2 to ensure a base level of maintenance even if all internal sugar is consumed.

The decrease in the maintenance related sugar consumption rate as a function of the internal sugar concentration was abrupt. For this reason, we describe the relation between maintenance related sugar consumption and internal sugar fraction with the Richards Equation (Richards 1959), resulting in four new parameters: the maximal maintenance related sugar consumption rate ($m_{s,m}$), which is obtained from literature (Blanken et al. 2016) and three empirical parameters that were determined through parameter fitting on experimental data.

Equation 5.11 $$m_s(C_s) = m_{s,m} \cdot \left(1 + e^{(d - a \cdot b \cdot f_{s/b})}\right)^{-1/b}$$

5.2.5 Biofilm growth

Microalgal growth in a biofilm is not in steady state. This means that the system variables depend on time and place resulting in a system description by partial differential equations. In order to avoid the use of this type of equation, a microalgal biofilm can also be represented by a large, but finite, number of layers with depth Δz resulting in a set of ordinary differential equations. For this reason, Equation 5.2 and 5.3 were rewritten into Equation 5.12 and 5.13 as they depend on the thickness of a biofilm layer Δz. The increase of the depth Δz of each layer represents biofilm

growth. It is presupposed that the total biomass concentration (C_b) in a biofilm layer remains constant (Equation 5.14). Employing Equation 5.14 and the product rule, Equation 5.15 and 5.16 were formulated to predict the functional biomass concentration change and the sugar concentration in a biofilm layer, Equation 5.17 is formulated to predict the change in biofilm layer thickness. Note that the specific sugar production rate is multiplied with the fraction of the biofilm disk exposed to light ($f_{I/disk}$).

Equation 5.12 $$\frac{d}{dt}(C_x \cdot \Delta z) = \left(Y_{x/s} \cdot q_{s,c}(C_s, t) - m_x\right) \cdot C_X \cdot \Delta z$$

Equation 5.13 $$\frac{d}{dt}(C_s \cdot \Delta z) = \left(q_{s,p}(C_x, z) \cdot f_{I/disk} - q_{s,c}(C_s, t) - m_s(C_s)\right) \cdot C_X \cdot \Delta z$$

Equation 5.14 $$\frac{d}{dt}(C_x + C_s) = 0$$

Equation 5.15 $$\frac{d}{dt}(C_x) = \left\{\left(Y_{x/s} \cdot q_{s,c}(C_s, t) - m_x\right) - \left[\left(Y_{x/s} \cdot q_{s,c}(C_s, t) - m_x\right) + q_{s,p}(C_x, z) \cdot f_{I/disk} - q_{s,c}(C_s, t) - m_s(C_s)\right] \cdot \frac{C_X}{C_X + C_s}\right\} \cdot C_X$$

Equation 5.16 $$\frac{d}{dt}(C_s) = \left(q_{s,p}(C_x, z) \cdot f_{I/disk} - q_{s,c}(C_s, t) - m_s(C_s)\right) \cdot C_X - \left[\left(Y_{x/s} \cdot q_{s,c}(C_s, t) - m_x\right) + q_{s,p}(C_x, z) \cdot f_{I/disk} - q_{s,c}(C_s, t) - m_s(C_s)\right] \cdot \frac{C_X \cdot C_s}{C_X + C_s}$$

Equation 5.17 $$\frac{d}{dt}(\Delta z) = \left[\left(Y_{x/s} \cdot q_{s,c}(C_s, t) - m_x\right) + q_{s,p}(C_x, z) \cdot f_{I/disk} - q_{s,c}(C_s, t) - m_s(C_s)\right] \cdot \frac{C_X}{C_X + C_s} \cdot \Delta z$$

5.3 Computational methods

Most parameters describing microalgal biofilm growth under day/night conditions were estimated from information obtained from literature (Blanken et al. 2016). The remaining model parameters were obtained by fitting the model equations to dedicated experiments in this study. All model parameters are depicted in the results section of Table 5.2 except for the microalgal specific light absorption coefficient ($a_{x,\lambda}$) which is listed in Appendix 5.A. Additionally, the microalgal biofilm growth

model requires the following input values: the incoming light intensity, the light spectrum (Appendix 5.A) and, in the event of suspension cultivation, the photobioreactor thickness. These input values are provided in the Materials and Methods; the spectral distribution of the incoming light is listed in Appendix 5.A.

5.3.1 Calibration of the maintenance rate

A microalgal respiration rate experiment was used to calibrate the maintenance rate (Equation 5.11) in order to predict the shift in maintenance rate between starvation and growth. Dark respiration was measured as specific oxygen consumption rates and includes the maintenance related sugar consumption rate (in cmol-s (cmol-x s)$^{-1}$ described by Equation 5.11) and the maintenance related biomass consumption rate (in cmol-x (cmol-x s)$^{-1}$). To fit the measured maintenance related oxygen consumption, Equation 5.11 was rewritten to Equation 5.18 (with $Y_{s/O2}$=1). Parameter *a*, *b*, and *d* of Equation 5.18 were fitted employing the MATLAB 2012a robust fit function while the maximal maintenance related sugar consumption rate ($m_{s,m}$) was obtained from literature. The maintenance related biomass consumption rate (m_x) was obtained by taking the minimal measured oxygen consumption rate and multiplying it by the biomass yield on oxygen ($Y_{x/O2}$=1.11).

Equation 5.18 $$m_{O2}(C_s) = \frac{m_{s,m}}{Y_{s/O2}} \cdot \left(1 + e^{\left(d - a \cdot b \cdot \frac{f_s}{b} \cdot 100\right)}\right)^{-1/b} + \frac{m_x}{Y_{x/O2}}$$

5.3.2 Calibration of diurnal carbon-partitioning

A suspended batch culture with a day/night cycle was used to calibrate the diurnal carbon-partitioning (Equations 5.1 to 5.3). With this experiment, the model parameters of the maximal specific sugar consumption rate ($q_{s,m,c}$) and minimal internal sugar fraction ($f_{s/b,min}$) were calibrated. The calibration was performed with the literature based parameter estimation and employed the results from the maintenance rate calibration. The MATLAB R2012a fminsearch function was utilized to minimize the sum of squared errors (Equation 5.19) for internal sugar concentration (C_s), functional biomass concentration (C_x), and total biomass concentration (C_b). The model was discretised for 250 layers and solved employing

the MATLAB R2012a ode15s solver. The experimental observations at time zero were used as the initial conditions. To improve the fit, a light correction factor (c_I) (Blanken et al. 2016) was also included in the parameter calibration.

Equation 5.19 $$SSE = \sum \left(\frac{C_{i,obs} - C_{i,pre}}{C_{i,obs}} \right)^2$$

5.3.3 Biofilm growth predictions

The biofilm growth model was validated with experiments in an Algadisk reactor, a rotating biological contactor based photobioreactor design (Blanken et al. 2014). The biofilm growth model equations (Equation 5.15 to 5.17) were discretised over 250 layers and solved by employing the MATLAB R2012a ode15s solver. The initial functional biomass and sugar concentrations were calculated based on an observed total biomass concentration in a microalgal biofilm of 173 kg m^{-3} (Blanken et al. 2014) and a minimal sugar fraction ($f_{s/b,min}$) which was obtained with the "diurnal carbon-partitioning calibration". The initial thickness of the biofilm was derived from the substratum properties and estimated to be 54 µm which is half of the mesh thickness multiplied with the porosity of the mesh. The initial layer thickness inside the biofilm was selected such that, at the conclusion of the simulation, all 250 layers remained below 16 µm thickness. Finally, the model accuracy was evaluated according to the mean average percentage error (MAPE)(Equation 5.20).

Equation 5.20 $$\text{MAPE} = \frac{100}{n} \sum \left(\frac{\left| \frac{M_X}{A}_{obs} - \frac{M_X}{A}_{pre} \right|}{\left| \frac{M_X}{A}_{obs} \right|} \right)$$

5.3.4 Comparison between microalgal biofilm and suspension growth

To identify the advantages of biofilm cultivation, a microalgal biofilm simulation was compared to a simulation of a suspension cultivation. For both the biofilm and suspension, a seven day batch cultivation was simulated employing 16/8 day/night block light of 400 µmol $(m^2\ s)^{-1}$. The starting biomass concentration in the biofilm was 9.3 g $(m^2\ s)^{-1}$ which was equal to a 0.5 kg m^{-3} starting biomass concentration in a suspension reactor of 18 mm thick. Both the suspension model and the biofilm

model were discretised for 250 layers and feature the same model input parameters. Thus, the biofilm was modelled as if the complete surface was illuminated.

5.4 Materials and Methods

5.4.1 Microalgae and pre-cultivation

The microalgae *Chlorella sorokiniana* (CCAP 211/8k) was maintained and pre-cultivated in shake flasks with M-8a medium (Kliphuis et al. 2010). This algae suspension was utilized to inoculate the experiments. All experiments were performed in M8-a media supplemented with 30 mM Urea and set to a pH of 6.7.

5.4.2 Microalgal respiration rate experiment

To calibrate the change of the maintenance rate, a suspended culture experiment was performed. The experiment consisted of two phases including a growth phase in which light was supplied, and *C. sorokiniana* was grown in batch followed by a dark starvation phase during which the specific oxygen consumption rate was determined and employed to quantify the maintenance related sugar consumption rate.

The biomass was cultivated in a 4 L stirred tank reactor (Applikon, , the Netherlands, Delft), continuously and homogenously illuminated from all sides with red LEDs (YZ-R5N30 Yoldal, Taiwan, Zhonghe City), yielding 380 µmol $(m^2\ s)^{-1}$ on the reactor wall. The tank was stirred at 300 rpm, and pH was controlled at 6.7 by automatic CO_2 addition. Temperature was controlled at 37 ^oC. The reactor was inoculated with 0.01 kg m^{-3} *C. sorokiniana* which grew to 1.16 kg m^{-3} in 2.6 days.

After the growth phase, the culture broth was divided over two darkened 2 L reactors (Applikon, the Netherlands, Delft). During the dark phase, the pH was controlled at 6.7 by HCl addition, and temperature was controlled at 37 ^oC. Oxygen was continuously supplied by aeration such that the dissolved oxygen was maintained between 95% and 100% air saturation. During the dark phase, samples were withdrawn from the microalgal culture to obtain oxygen consumption rate, dry weight, cell volume, cell size and number, and starch. The protocols to obtain dry weight, cell volume, cell size, and cell number are described in Kliphuis et al

(Kliphuis et al. 2010), and the starch analysis is described in de Winter. et al (de Winter et al. 2013).

During the measurement of the oxygen consumption rate, care was taken that the samples were not exposed to light. In the gas tight sample vessel, the change in oxygen concentration in time was measured with a fluorescent based oxygen microsensor (IMP-PSt1-L5-LIC0-BGF3-TF-OIW, Presens, Regensburg, Germany) and processed with a dedicated transmitter (Microx T3, Presens, Regensburg, Germany). During the measurement, the culture was continuously stirred, and the temperature was controlled at 37 ^{o}C by placing the sample in a water bath. From the linear decrease of oxygen concentration in time and the biomass concentration, the specific oxygen consumption rate was calculated and converted into a sugar consumption rate according to the stoichiometry of cellular respiration ($Y_{O2/s}$ = 1 mol-O_2 cmol-s^{-1}).

5.4.3 Diurnal carbon-partitioning calibration experiment

To calibrate the diurnal carbon-partitioning, batch cultivations where performed with microalgal suspension cultures in a newly designed incubator (Algaebator, 'ontwikkel-werkplaats' Wageningen University, the Netherlands, Wageningen). In this incubator, the microalgae were cultivated in 250 mL shake flasks which were illuminated from the bottom by a warm-white LED lamp (BXRA W1200, Bridgelux, USA, Livermore). The average incident light intensity was 427 µmol (m^2 $s)^{-1}$ (measurement scheme in Appendix 5.A). Mixing was provided by an impeller constructed with a magnetic stirring bar hanging above the flask bottom which was propelled by a small magnetic driver placed between the light source and the flask (140 rpm). The air inside the incubator was conditioned so that the air temperature was 37 ^{o}C and gaseous CO_2 was 5 % v/v. Additionally, the headspace of the cultivation was continuously refreshed with air to prevent oxygen accumulation.

The microalgae in the flasks were incubated under a 16/8 hours block shaped day/night cycle in a repeated batch scheme. One hour before sunrise, 3 ml of culture was transferred to a new flask containing 99 ml fresh M8a medium preheated at 37

^{o}C. This was performed for three consecutive days with two independent cultures. The total liquid volume of 102 ml in the 250 ml shake flasks corresponded to a light path of 18 mm.

5.4.4 Biofilm cultivation in the Algadisk

To assess biofilm growth under day/night cycles and validate the biofilm growth model, experiments were performed in a gas-tight rotating biological contactor based photobioreactor (the Algadisk) (Figure 5.1) (Blanken et al. 2014). The Algadisk reactor contains one rotating disk that was vertically placed and partially submerged such that the biofilm cultivated on the disk alternated between a liquid and gas phase at 9 rpm. During the liquid phase (M8a medium with 30 mM urea), the biofilm was kept in the dark so that only the biofilm exposed to the gas receives light (44% of the disk surface). Light was provided by the same LEDs as those employed in the Algaebator. The disk surface was a stainless steel mesh, Twilled Dutch Weave type 80/700 (GKD SolidWeave, Düren, Germany) which was clamped with stainless steel rings (16 mm wide) on a stainless steel disk (diameter of 302 mm). To rotate the disk, gears were used which resulted in an inner circle not available for microalgal growth (diameter of 47.5 mm) (Figure 5.1). The total medium volume was 4.1 L. The temperature of the liquid was controlled at 37 ^{o}C by pumping the medium through a heat exchanger at 540 ml min^{-1} which also provided mixing to homogenously distribute all of the nutrients. The pH of the medium was controlled at 6.7 by automatic addition of 1 M NaOH.

The Algadisk reactor was operated in batch. Every growth-harvest cycle represented exactly one week of batch growth. During harvest, the biomass was removed from the disk surface by scraping the woven structure of the disk in a manner that ensures inoculum remaining for the next growth-harvest cycle (Blanken et al. 2014). The microalgal biomass growing on the clamping rings and inside the liquid medium was harvested separately. The reported disk productivity represents the productivity per m^2 woven disk surface (woven disk area is 0.055 m^2), and the total productivity includes the biomass in the liquid medium and the biomass growing on the clamping

rings (total disk area is 0.069 m^2). Analysis and calculation of productivities are described in Blanken et al. (Blanken et al. 2014).

The gas-tight Algadisk reactor was operated at two CO_2 concentrations and four different light regimes (Table 5.1). Experiments were performed with a 16/8 h block shaped day/night cycle and a 12/12 h block shaped day/night cycle , both at 399 µmol $(m^2\ s)^{-1}$. This incident light intensity was the average over 15 points which are presented in Appendix 5.A. In addition, a 16/8 h sine shaped day/night cycle was applied with a daily light dose equal to that applied for the 16/8 h block shaped cycle, which is equivalent to 23 mol $(m^2\ d)^{-1}$ (Table 5.1) (light regime figure in Appendix 5.A). The various light schemes were compared while employing 5% v/v CO_2 in the air in the headspace. Furthermore, biofilm growth without a day/night cycle, thus featuring a constant light intensity of 399 µmol $(m^2\ s)^{-1}$, is compared between 5% and 10% CO_2 in the incoming gas (200 ml min^{-1}).

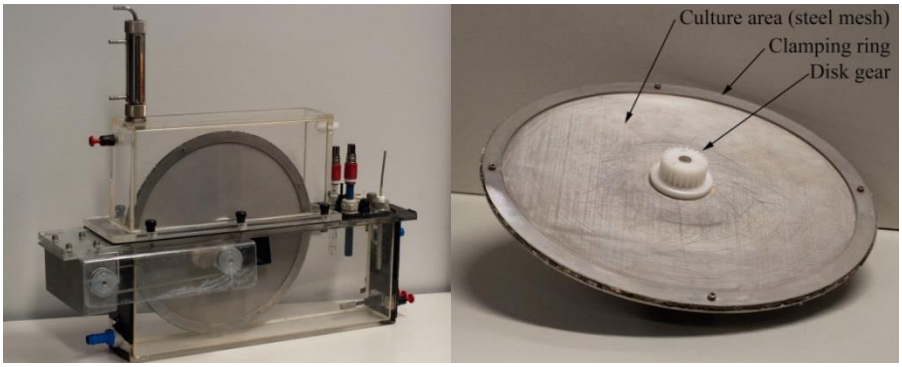

Figure 5.1. Picture of the gas tight Algadisk reactor and the stainless steel disk that holds the biofilm.

Table 5.1. Experimental conditions to evaluate biofilm cultivation in the Algadisk and validate the biofilm growth model.

CO_2 in	**Light regime**	**Incident light**	**Daily light sum**
	h-day/h-night	µmol $(m^2\ s)^{-1}$	mol $(m^2\ d)^{-1}$
5%	Block 16/8	399	23,0
5%	Sine 16/8	12-635	23,3
5%	Block 12/12	399	17,2
5%	Constant	399	34,4
10%	Constant	399	34,4

5.4.5 Off gas analysis Algadisk biofilm reactor

The carbon dioxide and oxygen produced or consumed in the Algadisk system was measured continuously and converted to biomass production based on stoichiometry (Kliphuis et al. 2010). The oxygen concentration in the incoming pressurized air was measured online (Servomex 4100, the Netherlands, Zoetermeer). The ingoing gas mixture was obtained by mixing pure CO_2 with pressurized dry air by mass flow controllers (GF40 Brooks, the Netherlands, Ede). The outgoing gas from the reactor was analyzed for both the carbon dioxide concentration (Servomex 1400 with an infrared sensor) and the oxygen concentration (Servomex 4100 with a paramagnetic sensor). The off-gas was first cooled to 4 ^{o}C by utilizing a condenser integrated in the Algadisk system in order to minimize evaporation. The gas volume entering the reactor was converted to total mol m^{-3} with the ideal gas law, and the outgoing gas stream was corrected for composition changes and water vapor accumulation (Equation 5.21) (Wagner and Pruss 1993).

Equation 5.21 $$F_{g,out} = \frac{F_{g,in} + r_{O2}(t) \cdot V - r_{CO2}(t) \cdot V}{1 - f_w}$$

The mass balance, Equation 5.22, is rewritten to Equation 5.23 as the oxygen exchange rate (r_{O2}*V) and the carbon dioxide exchange rate (r_{CO2}*V) can be calculated in (c)mol-i s^{-1} by neglecting accumulation. From r_i * V, the productivity can be calculated according to Equation 5.24 employing the stoichiometry of

microalgae growth. By means of Equation 5.25, the cumulative biomass in g m^{-2} can then then calculated with time increments of one minute. Where $M_x(0)$ equals the starting condition for the biofilm growth model prediction (9.3 g m^{-2}).

Equation 5.22 $$\frac{dM_i}{dt} = F_{g,in} \cdot f_{i,in} - F_{g,out} \cdot f_{i,out} - r_i(t) \cdot V$$

Equation 5.23 $$r_i(t) \cdot V = F_{out} \cdot f_{i,out} - F_{in} \cdot f_{i,in}$$

Equation 5.24 $$P_x(t) = \frac{r_i(t) \cdot V}{A_{disk}} \cdot MW_x \cdot Y_{x/i}$$

Equation 5.25 $$\frac{M_x(t)}{A_{disk}} = \frac{M_x(0)}{A_{disk}} + \sum_0^t P_x(t) \cdot \Delta t$$

5.5 Results and discussion

5.5.1 Maintenance rate calibration

In order to calibrate the biofilm growth model, the decrease in the maintenance related sugar consumption rate was assessed under prolonged dark incubation following a phototrophic growth phase in a culture with suspended cells. During 12 days of darkness, the dry weight, the maintenance rate, and the starch fraction decreased while the cell number remained constant (Figure 5.2).The maintenance rate was calculated based on the respiratory oxygen consumption rate. These observations accord with results of starvation experiments for microalgae (Ruiz-Martinez et al. 2016), plants (Gary et al. 2003) and bacteria (Hoehler and Jorgensen 2013; Riedel et al. 2013).

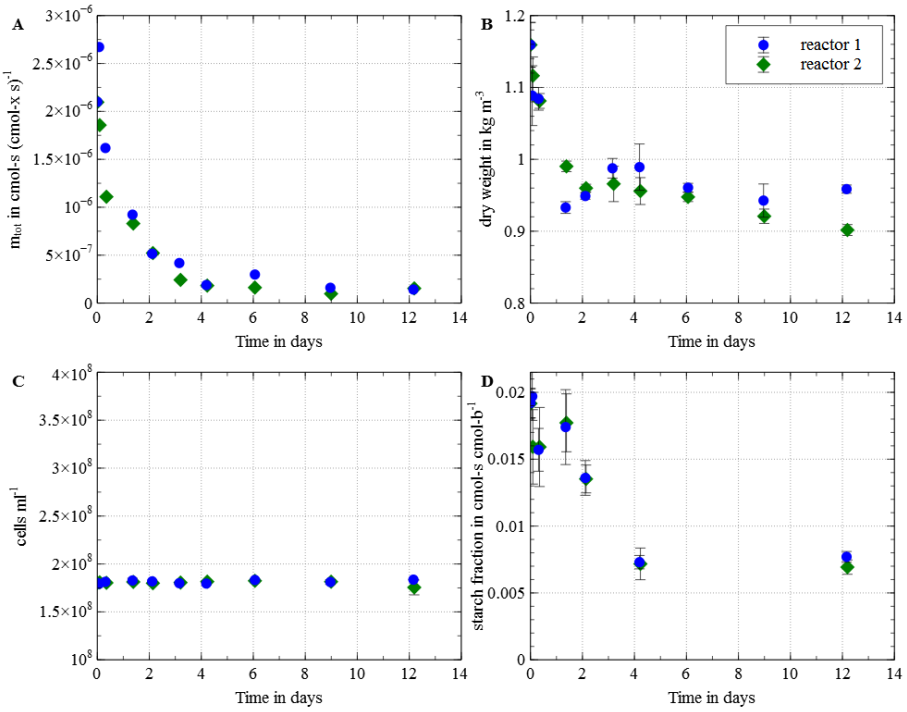

Figure 5.2. Microalgal activity during 12 days of darkness after a photosynthetic growth phase. Total maintenance rate (m_{tot}) (A), dry weight (B), cell number (C), and starch fraction in the biomass (D). Error bars indicate the standard deviation of triplicate measurements. The total maintenance (A) rate was obtained by a linear fit of the measured decrease of oxygen concentration over time; all linear fits had a r^2 above 0.90.

In order to obtain a model description for the maintenance related sugar consumption, the experimental data were used to calibrate the model. In Figure 5.3, the maintenance rate is plotted against the starch fraction in the microalgae. These data demonstrate a precipitous decrease in the maintenance rate from 2% starch to 1.5% starch. Because there is no data with starch above 2%, it was assumed that, from 2% starch upward, the maintenance related sugar consumption remains constant at $2.54E^{-6}$ cmol-s (cmol-x s)$^{-1}$. This value was obtained from literature and is based on 18 measurements from four independent studies (Blanken et al. 2016). In Figure 5.3, one point is above the predicted maximal maintenance rate which is a

measurement just before the switch from light to dark, therefore, it includes respiratory sugar consumption that is required to instigate biomass growth.

At a starch fraction of approximately 0.73 %, the maintenance rate stabilized (Figures 5.2 and 5.3) while the starch fraction did not change. This indicated that the remaining 0.73% starch was not available for consumption by the microalgae. Because it was uncertain what the microalgae consume instead of the starch, a second maintenance consumption term was included, i.e., the maintenance related biomass consumption rate (m_x). Thereby, it was assumed that the complete functional biomass decomposed evenly to supply the energy necessary for maintenance.

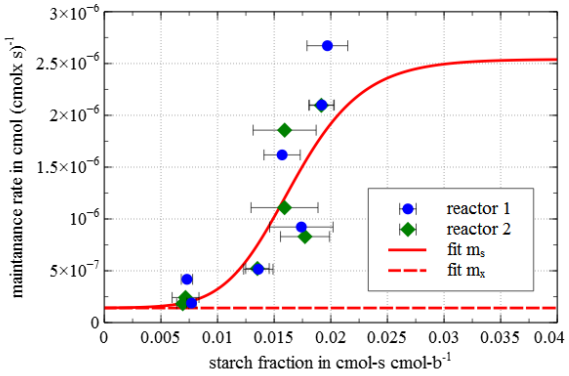

Figure 5.3. The calibration of the maintenance rate on the respiration rate measurements. The model fit parameters are depicted in Table 5.2. The error bars indicate the standard deviation of triplicate measurements.

5.5.2 Diurnal carbon-partition calibration

The diurnal carbon-partitioning in the biofilm growth model was calibrated for the maximal sugar consumption rate and the minimal starch fraction in the cell. These parameters could not be obtained from literature, therefore, were fitted on the data of a repeated-batch experiment on a microalgal suspension culture grown under a day/night cycle. During the day, the microalgae grew rapidly with 5.2 biomass doublings in 16 hours and an increase of internal sugar over the day followed by a

decrease overnight. The night time decrease in total biomass was mainly internal sugar that was consumed while the functional biomass concentration only slightly decreased (Figure 5.4).

To obtain the maximal sugar consumption rate and the minimal starch fraction in the cell, the diurnal carbon-partitioning was calibrated to experimental data (Figure 5.4); resulting model parameters are listed in Table 5.2. The obtained minimal starch fraction in the cell was 2%, which is in accordance with the observations from the respiration rate experiment and observations in literature (Tuantet 2015). The fitted maximal sugar consumption rate ($q_{s,c,max}$) was 80% of the maximal sugar production rate ($q_{s,p,max}$) which resulted in a model formulation where *C. sorokiniana* can produce sugar faster than it can consume it during the daytime. The question remains whether this is a physical limitation or that the maximal sugar consumption rate can be regulated by *C. sorokiniana*. The latter seems to be more likely based on observations in *Arabidopsis* (Stitt and Zeeman 2012). However, to model the starch accumulation, it is common to assume that it functions as a carbon overflow mechanism (Ross and Geider 2009).

After fitting the relevant model parameters, the growth model including the diurnal carbon-partitioning can describe the accumulation of sugar during the day and decrease during the night. Because the sugar consumption during the night was accurately described, the total and functional biomass decrease overnight was also indirectly predicted accurately. However, the accumulation of total and functional biomass over the day was underestimated. The sugar concentration peaked during the light hours and decreases during the dark hours. This model trend is the result of increasing biomass density which causes less light per cell, a subsequent lower photosynthetic sugar production and, therefore, less sugar overflow towards the storage. The highest predicted sugar fraction was 0.30 cmol-s cmol-b^{-1} which accorded with the 0.27 cmol-s cmol-b^{-1} observed for *C. sorokiniana* cultivated in chemostat under high growth rate diurnal light conditions (Tuantet 2015).

To describe the diurnal carbon-partitioning, it was decided to maintain the maximal sugar production rate constant. Therefore, the sugar consumption rate was lowered to create a carbon overflow into sugar storage by fitting the model to experimental data (Figure 5.4). An alternative approach would be to determine the consumption rate based on the maximal growth rate, and increase the sugar production rate to create a carbon overflow into storage (Ross and Geider 2009). Likely, the second strategy would better fit the measured data, however, with this strategy, the predicted maximal specific growth rate would increase above real measured values. Therefore, it was decided to employ the strategy of lowering the sugar consumption rate.

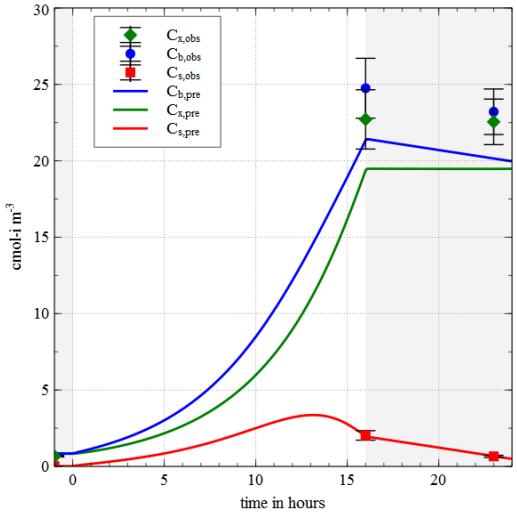

Figure 5.4. Calibration of the diurnal carbon-partitioning on experimental data of the growth of a microalgal suspension culture under day/night cycles. The model calibration was performed to obtain the maximal specific sugar consumption rate and the minimal starch fraction in the cell (Table 5.2). The grey area indicates the night, and the error bars indicate the standard deviation (n=6, three sample days form two reactors).

Table 5.2. All parameter values employed in the microalgal biofilm growth model.

Name	Symbol	Value	Unit	Reference
literature based parameter estimates				
maximal specific sugar production rate	$q_{s,p,max}$	1.296E^{-4}	cmol-s (cmol-x s)$^{-1}$	(Blanken et al. 2016)
biomass yield on sugar	$Y_{x/s}$	0.59	cmol-x cmol-s^{-1}	(Blanken et al. 2016)
sugar yield on light	$Y_{s/ph}$	0.1	cmol-s mol-ph^{-1}	(Blanken et al. 2016)
specific absorption coefficient	$\alpha_{x,average}$	7.1	m^2 cmol-x^{-1}	(Blanken et al. 2016)
molar weight per carbon mol biomass	M_x	24	g cmol-x^{-1}	(Blanken et al. 2016)
total biomass concentration in biofilm	$C_{b,biofilm}$	173	kg m^{-3}	(Blanken et al. 2014)
system specific parameters				
fraction disk illuminated	$f_{I/disk}$	0.443		this study
fitted parameters				
maximal specific sugar consumption rate	$q_{s,c,max}$	1.0265E^{-4}	cmol-s (cmol-x s)$^{-1}$	this study
minimal sugar fraction in the total biomass	$f_{s/b,min}$	0.0198	cmol-s cmol-b^{-1}	this study
light correction factor suspension experiment	$c_{I,susp}$	1.8429		this study
maximum maintenance related sugar consumption rate	$m_{s,max}$	2.54E^{-6}	cmol-s (cmol-x s)$^{-1}$	(Blanken et al. 2016)
maintenance related biomass consumption rate	m_x	1.56E^{-7}	cmol-x (cmol-x s)$^{-1}$	this study
empirical value for m_s (C_s)	a	557.3		this study
empirical value for m_s (C_s)	b	0.5003		this study
empirical value for m_s (C_s)	d	3.755		this study

5.5.3 Biofilm cultivation in the Algadisk

To validate the biofilm growth model for diurnal conditions, five experimental conditions were evaluated in the Algadisk reactor. These conditions included four light regimes and two incoming CO_2 concentrations (Table 5.1). It was validated that only light was limiting by comparing the productivity of 5% (C24 5%CO_2) and 10% CO_2 (C24 10%CO_2) in the incoming gas under continuous light intensity (illuminated 24 hours per day) (Figure 5.5). Therefore, the remaining light regimes were compared employing 5% CO_2 in the incoming gas.

Comparing the block light with a 16/8 day/night cycle (B16) to the sine light with a 16/8 day/night cycle (S16), the observed productivities were the same. This indicated that the light fluctuations and the peak light intensity of 635 μmol $(m^2\ s)^{-1}$ in S16 experiment did not inhibit the biofilm growth, which was also reflected in a similar biomass yield on light (Figure 5.5B). Compared to the 16/8 day/night cycle, the block light with a 12/12 day/night cycle (B12) resulted in lower productivity. The lower productivities of the day/night regimes compared to continuous light were solely due to the lower total light per day supplied as no statistical difference was ascertained for the biomass yield on light (Anova $p=0.715>0.05$ for total biomass and $p=0.317>0.05$ for disk biomass). These results confirm that the overnight decrease in total biomass did not influence the biomass yield on light integrated over 24 hours (de Winter 2015). This indirectly confirms the model assumption that the majority of the total biomass lost overnight represented sugar consumption for synthesis of new functional biomass and maintenance related respiration. However, the inherent mechanisms regulating diurnal carbon partitioning in microalgae remain unknown (Baroukh et al. 2014; Post et al. 1986) but may possibly be similar to those observed in higher plants (Scialdone et al. 2013; Stitt and Zeeman 2012).

The obtained biomass yields on light in the gas tight Algadisk were similar to previously obtained productivities with an open Algadisk system (Blanken et al. 2014) and comparable with those observed in suspension cultures (Cuaresma Franco et al. 2012). Disk productivities, however, were lower in the current work compared to the open Algadisk system (Blanken et al. 2014); this is the result of a smaller illuminated disk fraction in the gas tight Algadisk compared to the open system. Therefore, the productivity of the Algadisk systems can be easily increased by enlarging the illuminated fraction of the disk in future designs. Furthermore, the obtained productivities in this study are in the high range of those reported in literature (Berner et al. 2014), although it should be taken into account that there is a large variation in lighting and CO_2 conditions between different studies.

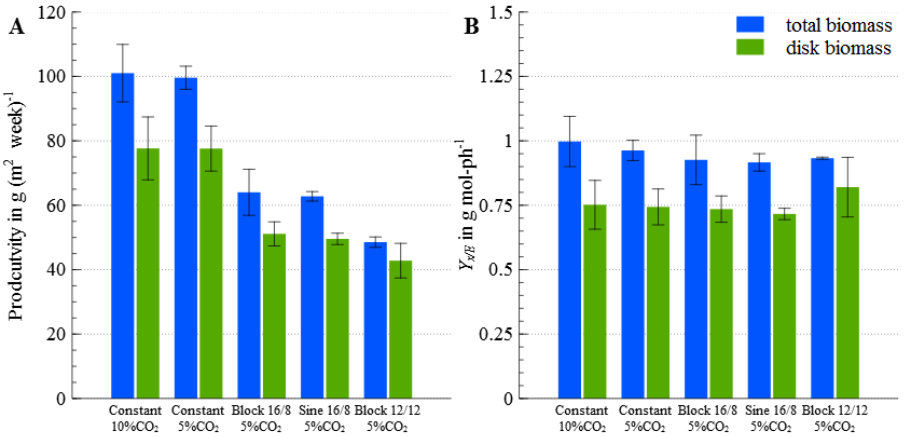

Figure 5.5. Measured productivity of microalgal biofilm cultures repetitively grown for seven days under three different day/night regimes and under two constant light regimes while comparing 5% CO_2 and 10% CO_2 (Table 5.1). Graph A shows the productivity, and Graph B shows the biomass yield on light. Values calculated based on the total biomass include microalgal growth on the clamping rings and the biomass collected from the liquid. Values calculated based on the disk biomass only contain the biomass scraped from the woven metal mesh. Error bars indicate the standard deviation of minimally four 7-day experiments.

5.5.4 Predicting microalgal biofilm growth

The measured productivity under the four different light regimes was used to validate the microalgal biofilm growth model. The model predictions were compared with the observed total biomass harvested and the calculated cumulative biomass based on the off gas analysis (Figure 5.6). Employing the biofilm growth model, the measured productivities of the four light regimes were predicted with a MAPE of 5.2% (Figure 5.6). The calculated biofilm growth based on the off gas analysis showed a considerable variation with a small number of cases of significant overestimation of the final harvest. However, the same experiments also demonstrated overnight biomass increase which most likely must have been caused by ambient air leaking into the system. This will consequently lead to increasing O_2 levels and decreasing CO_2 levels and thus an overestimating of microalgal growth. Clearly, a gas-tight Algadisk system represents a technological challenge. Despite

this measurement variation, the gas-analysis based calculation of biofilm growth was still employed as a gross model validation and to validate the shape of the model predictions. Both the predicted and measured biofilm growth exhibited changes in growth that were more gradual during the day for the sine light regime compared to the sharper transitions for the block light regime.

To visualize the starch fluctuation inside the biofilm, the sugar fraction was added to the biofilm growth predictions (Figure 5.7). In Figure 5.7, the light is entering the biofilm from the x-axis. It can be also observed in this figure that, during the day, the sugar fraction increases followed by a decrease during the night. Furthermore, deeper into the biofilm, the sugar fractions become lower. At a depth of approximately 180 μm, the sugar fraction begins to decrease below the minimal sugar fraction of 2% which is insufficient to support growth. Therefore, all of the cells that are deeper than 180 μm in the biofilm will experience starvation.

Comparing the sine light to the block light (Figure 5.7), the block light demonstrated rapid starch accumulation at sunrise which then remained stable during the day and decreased slowly overnight. For the sine light, the sugar fraction increased more slowly but featured a higher peak. In addition, the sugar fraction already began decreasing during the day, and there was less sugar available during the night. Consequently, the sugar fraction dropped further in comparison to the block light.

By separating the functional biomass from the sugar storage, a limited degree of photoacclimation was also added to the model. The specific absorption coefficient was normalized to functional biomass and, as such, cells with a high internal sugar fraction had a lower specific absorption coefficient per carbon mol total biomass. Cells exposed to relatively high light intensities accumulated sugar up to 30% of total biomass which thus resulted in a reduction of the specific light absorption coefficient by 30%. On the one hand, this trend is according to the finding of dedicated photoacclimation studies where high light grown cells accumulate more carbohydrates and express a lower absorption cross section (Ross and Geider 2009). On the other hand, the current model will be unable to completely describe the

factor two change in absorption coefficient observed for green microalgae such as *Chlorella sorokiniana (Blanken et al. 2016)*.

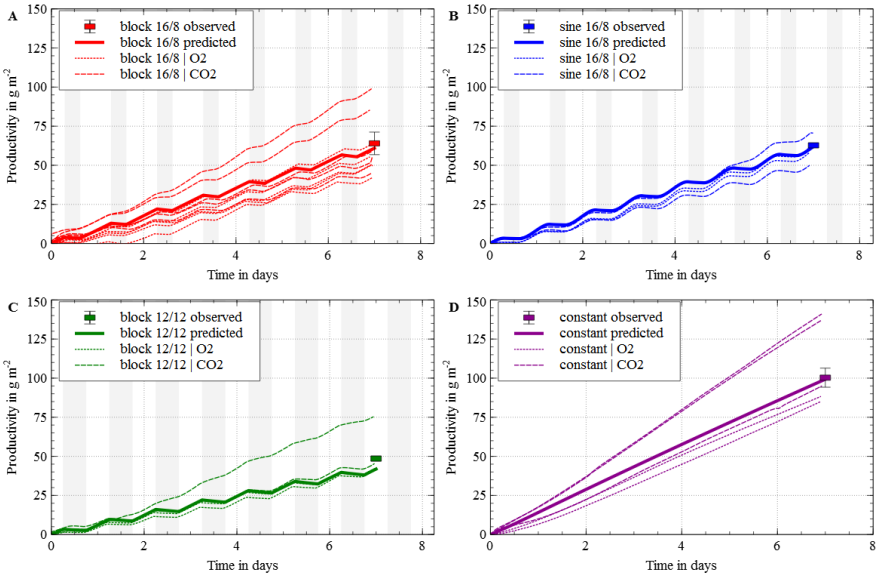

Figure 5.6. Measured and predicted productivity of microalgal biofilm cultures repetitively grown for seven days under three different day/night cycle regimes and one constant light regime (Table 5.1). The predictions were compared to the total biomass harvested after seven days and the cumulative biomass calculated based on the off gas analysis for O_2 and CO_2. The error bars on the total biomass harvested indicate the standard deviation. The data for constant light are composed of the results derived for both 5% and 10% v/v incoming CO_2.

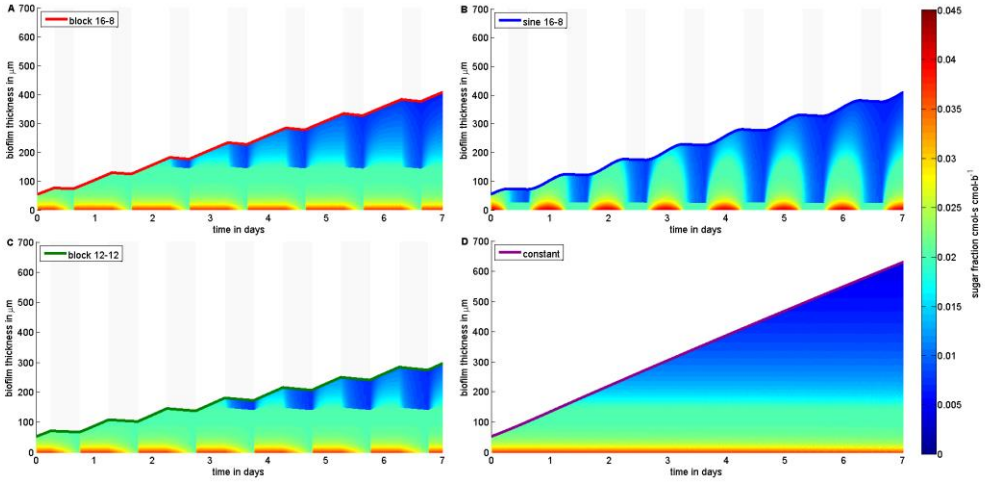

Figure 5.7. The predicted microalgal biofilm thickness combined with the predicted local starch fractions in the form of a heat map. Light is entering the biofilm from the x-axis, thus the light travels from the bottom to the top of the image. All predictions are for seven days of biofilm growth and include three different day/night cycle regimes and one constant light regime (Table 5.1).

5.5.5 Biofilm vs suspension cultures

With the validated biofilm growth model, a comparison can be made between microalgal biofilm growth and an equivalent suspension cultivation. Both culture strategies are compared with a model simulation of a seven-day batch cultivation (Figure 5.8) featuring 16/8 day/night block light with 400 μmol $(m^2\ s)^{-1}$, full culture illumination, and the same starting biomass concentration. With this approach, it can be evaluated why biofilm cultures can feature similar productivities as suspension cultures (Cuaresma Franco et al. 2012). However, it should be noted that, for suspension cultivation, optimal yields are typically obtained by preventing dark zones in the reactor (de Mooij et al. 2014; Takache et al. 2012). Therefore, a 7-day batch cultivation is not the most optimal cultivation strategy for suspension cultivation. However, in this study, it provides a tool in order to compare biofilm to suspension cultivation.

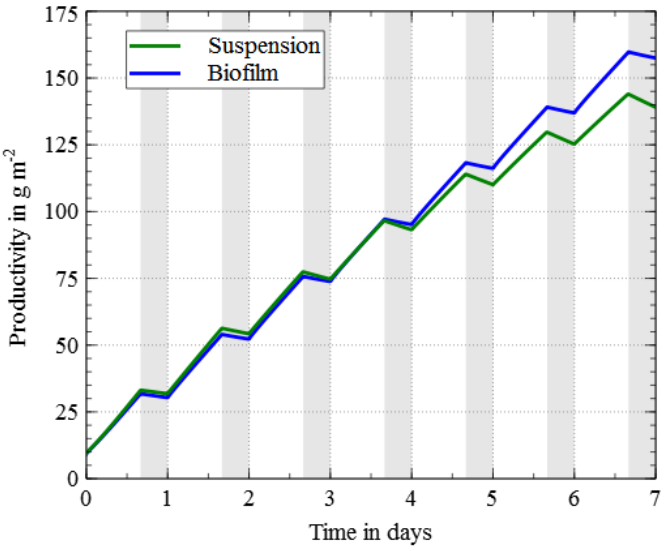

Figure 5.8. Comparison between a simulated seven-day batch cultivation of a suspension and biofilm culture. The simulation features 16/8 day/night block light with 400 µmol $(m^2\ s)^{-1}$, full culture illumination, and the same starting biomass concentration.

The difference between the biofilm simulation and the suspended batch simulation was primarily caused by the difference in total maintenance related sugar consumption in the culture. For the first two days, light still penetrated to the back of the culture while, after day two, a dark zone developed. In the biofilm, microalgae located in the dark zone lowered their maintenance rate and subsequently decreased the biomass losses in the dark zone. In a suspension culture, however, the microalgae cells move between the dark zone and light zone. This continuous movement prevents the cells from decreasing their maintenance related sugar consumption. Therefore, the productivity of the simulated suspension diminished while the biofilm productivity appeared to be unaffected by the dark zone. This simulation thus confirmed previous conclusions that dark zones should be prevented in microalgal suspension cultures (de Mooij et al. 2014; Takache et al. 2012).

Another advantage of the biofilm is that the microalgae featured local photoacclimation. The spatial position of cells in a biofilm is fixed; therefore, cells

located at the front of the simulated biofilm accumulated high sugar fractions during the day. With high sugar fractions, the absorption coefficient dropped, and the light penetrated deeper into the biofilm. In contrast, suspended microalgae acclimated to the average light intensity resulting in an overall higher absorption coefficient compared to the biofilm. This higher absorption coefficient is the reason that the simulated suspension grew faster in the first two days as there was less light exiting the back of the culture. However, in the later growth stages when all of the light was absorbed in the culture, the biofilm featured a deeper light penetration and thus greater productivity.

5.6 Conclusions

Growth of light-limited microalgal biofilm could be accurately predicted for both diurnal and continuous illumination schemes. It was ascertained that the tested illumination schemes did not influence the light utilization efficiency. This confirms that the biomass that was lost overnight represented synthesis of new functional biomass and sugar consumption for maintenance related respiration.

The light limited biofilm growth model was obtained by calibrating the diurnal carbon-partitioning with suspension batch data and calibrating the maintenance rate in a light starvation experiment. From the model analysis, it was determined that the photosynthetic efficiency of biofilm growth was as efficient, or even more so, than suspension growth because the maintenance rate of the biofilm in dark zones was lower compared to that of suspension cultures with a dark zone.

5.7 Nomenclature

Parameters	
a	specific (light) absorption coefficient in m^2 $cmol^{-1}$
A	area in m^2
C	concentration in mol m^{-3}
c_I	light correction factor
cmol	mol-i normalized to carbon
f	fraction
I	light in mol-ph $(m^2\ s)^{-1}$
M	Mass in carbon mol
MW	molar mass in g mol^{-1}
m	cell maintenance in mol $(cmol\text{-}s)^{-1}$
MAPE	mean absolute percent error
n	number of experimental points
t	time in hours
q	rate in mol $(cmol\text{-}x\ s)^{-1}$
r	rate in mol $(m^3\ s)^{-1}$
SSE	squared sum of errors
z	distance in m
Y	yield in (mol/mol)
V	volume in m^3

Subscripts	
b	total biomass in cmol-b
d	day
x	functional biomass in cmol-x
s	internal sugar in cmol-s
c	consumption
p	production
m	maximal
min	minimal
obs	observed
ph	photons in mol-ph
pre	predicted
λ	wavelength
I	light
light	during daytime
dark	during night time
disk	total disk area
O2	oxygen in mol-O_2
w	water vapour

5.8 Appendices

Appendix 5.A

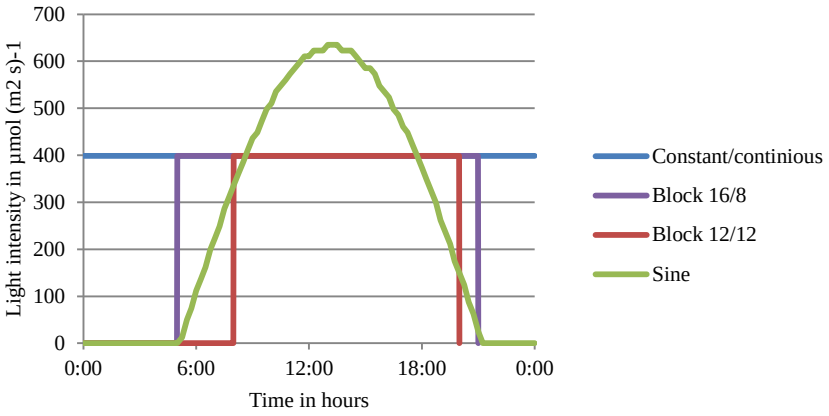

Figure 5.A.1. Light regimes employed to evaluate biofilm cultivation in the Algadisk and validate the biofilm growth model.

Table 5.A.1. Light intensity per position in % of the average light intensity over all points. +- column shows the standard deviation of 5 measurements.

position	% of mean	+-
1	89	3,6
2	94	1,7
3	93	2,9
4	85	4,3
5	104	3,0
6	113	1,8
7	115	3,2
8	111	3,5
9	99	5,4
10	93	7,4
11	106	5,0
12	105	10,4
13	107	4,3
14	103	8,4
15	84	6,8

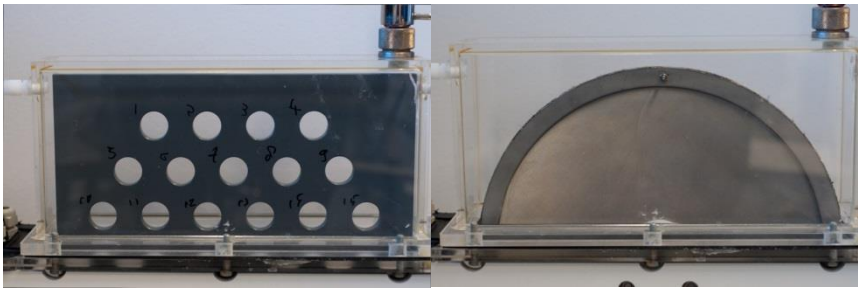

Figure 5.A.2. Picture of the measurement light measurement grid, the numbers of the measurement grid correspond to the numbers in table 1, and below a picture of the reactor with the disk.

Table 5.A.2. Calibration line light measurements for a range of set points. See Figure 5.A.3 for the calibration line.

Set point %	**light intensity** µmol (m^2 s)$^{-1}$	**standard deviation** µmol (m^2 s)$^{-1}$	**Calculated light intensity** µmol (m^2 s)$^{-1}$
0	0	0	0
25	319	15	311
50	639	21	623
75	956	35	934
100	1219	28	1245

Figure 5.A.3. Light calibration line and formula. Diamonds indicate the light measurements and standard deviation of 5 measurements.

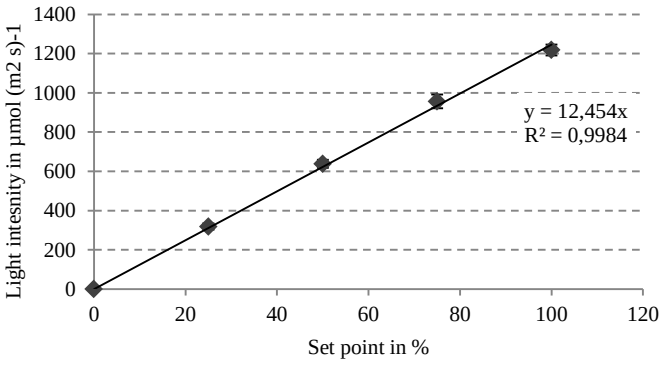

Chapter 6 Optimizing carbon dioxide utilization for microalgae biofilm cultivation

This chapter is prepared manuscript for submission as:
Blanken, W.; Schaap, S..; Theobald, S.; P.; Rinzema, A.; Wijffels, R.H.; Janssen, M. "Optimizing carbon dioxide utilization for microalgae biofilm cultivation"

Abstract

The loss of carbon dioxide (CO_2) to the environment during microalgae cultivation is undesirable for both environmental and economic reasons. In this study, a phototrophic biofilm growth model was developed and validated with the objective to maximize both CO_2 utilization efficiency and production of microalgae in biofilms. The model was validated in growth experiments with CO_2 as the limiting substrate. The CO_2 utilization and biomass productivity were maximized by changing the gas flow rate, the number of biofilm reactors in series, and gas composition. Based on simulations, the maximum CO_2 utilization efficiency that was reached was 96% based on a process employing flue gas. The corresponding drop in productivity was only 2% in comparison to the non-CO_2 limited reference situation. In order to achieve this, 25 biofilm reactors units, or more, must be operated in series. Based on these results, it was concluded that concentrated CO_2 streams and plug flow behaviour of the gaseous phase over the biofilm surface are essential for high productivity and CO_2 utilization efficiency.

6.1 Introduction

Microalgae produce valuable products from CO_2 and sunlight. The photosynthetic efficiency of microalgae is higher than that of terrestrial crops because process conditions can be better controlled (Wijffels and Barbosa 2010). An important factor in obtaining optimal growth conditions is an adequate CO_2 supply which is commonly obtained employing concentrated CO_2 streams. Common CO_2 streams include flue gas (Yen et al. 2015) or mixtures of pure CO_2 with air. Pure CO_2 can possibly be obtained by carbon capture from flue gas or even captured from air (Brilman et al. 2013; Keith 2009). However, incoming CO_2 streams are often not completely utilized by the microalgae and, consequently, part of the CO_2 is lost to the environment. This is undesirable as carbon capture requires energy (Lackner 2013), therefore, CO_2 discharge to the atmosphere should be minimized.

For microalgae grown in suspended cultures, processes with minimal CO_2 loss have been developed by employing experimentally validated models (Doucha and Lívanský 2006; Rubio et al. 1999; Valiorgue et al. 2014; Yang 2011). Their primary conclusion is that CO_2 utilization can be improved by increasing the mass transfer from the gas to the liquid (Doucha and Lívanský 2006; Rubio et al. 1999; Valiorgue et al. 2014; Yang 2011). For microalgal biofilm cultivation, however, processes with minimal CO_2 loss have not been developed, though it has been demonstrated that elevated CO_2 levels are required for maximal productivity (Blanken et al. 2014; Ji et al. 2013a; Schultze et al. 2015). Models are available that can mathematically predict CO_2 limited biofilm growth (Li et al. 2016; Murphy and Berberoglu 2014; Wolf et al. 2007). By including additional mass balances, these biofilm models can be utilized to maximize CO_2 utilization and biomass productivity. Based on these principles, the phototrophic biofilm growth model presented in Chapter 5 was extended to include carbon dioxide limited growth. The model was validated in an Algadisk (a rotating biological contactor based reactor design (Chapter 5)) for *Chlorella sorokiniana*. The validated model was then used to find the process conditions where the CO_2 loss is minimized and biofilm productivity maximized.

6.2 Theory

Microalgal biofilm growth is mostly limited by either carbon dioxide (CO_2) supply, oxygen (O_2) removal, or light supply. Transport and growth kinetics for CO_2 and O_2 were included in the light-limited biofilm growth model (Chapter 5) developed before (Figure 6.1).

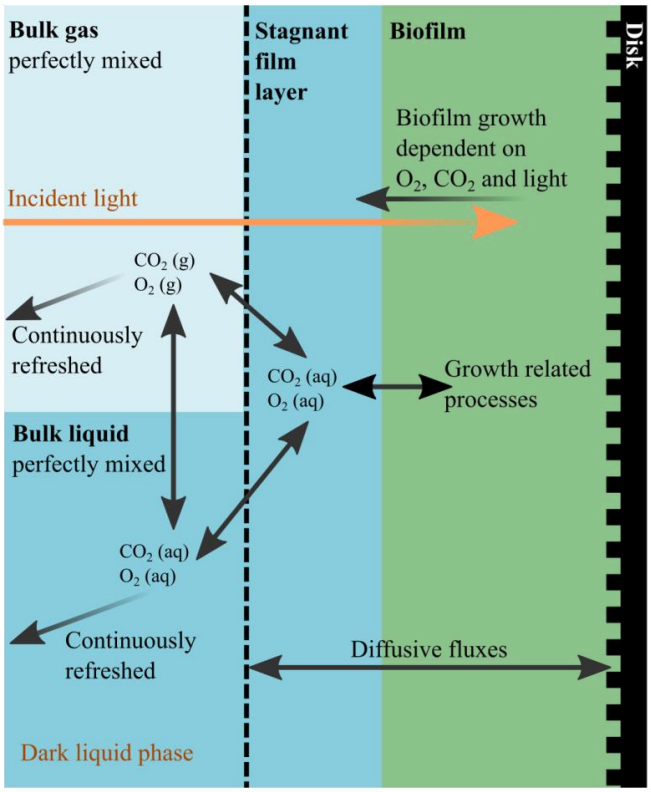

Figure 6.1. A schematic display of the four compartments employed in the biofilm growth model of a biofilm. Both bulk liquid and gas are assumed to be perfectly mixed and are refreshed continuously by a constant feed. Only the gas-exposed part of the disk is illuminated thus the bulk liquid and submerged part of the disk are dark. In the biofilm growth model, CO_2(aq) is modelled as total dissolved inorganic carbon (DIC). In both the biofilm and stagnant film layer, mass transfer is only possible by diffusion.

Gaseous CO_2 dissolves in water and reacts by forming a chemical equilibrium with carbonic acid (H_2CO_3) and bicarbonate (HCO_3^{-1}). However, in practice, H_2CO_3 concentrations are very low compared to CO_2(aq) and HCO_3^{-1} at neutral pH and is usually included in the CO_2(aq) term. In addition, *C. sorokiniana* can use both CO_2(aq) and HCO_3^{-1} (Nielsen and Jensen 1958). For this reason, CO_2 and HCO_3^{-1} were combined in a dissolved inorganic carbon (DIC). The CO_2(aq) concentration at gas-liquid equilibrium can be calculated with Henry's Law (Sander 2015), and the corresponding HCO_3^{-1} can be calculated employing the dissociation constant of CO_2/ H_2CO_3 and the pH. The dissociation constant is calculated (Harned and Davis 1943) and corrected for the ion concentration ($K_{a,DIC,ion}$) (Stumm and Morgan 1995). Consumption of DIC represents consumption of CO_2 and will lead to a shift in the equilibrium between the DIC species CO_2 and HCO_3^{-1}. This results in the accumulation of hydroxide (OH^-) and an increase of the pH inside the biofilm (Li et al. 2015a; Li et al. 2016). Using DIC, however, the shifts in the chemical equilibrium of DIC species can be ignored, significantly decreasing the number of balances. In the event of oxygen, only Henry's Law is employed to calculate the equilibrium concentration between gas and liquid (Sander 2015).

6.2.1 Light limited biofilm growth

The model description of light limited biofilm growth is based on previous work (Chapter 5) and (Blanken et al. 2016). This work includes: light dependent sugar production, partitioning of produced sugar between sugar storage (starch) and functional biomass, and cellular maintenance. This model will be summarized in Appendix 6.A, however, the model details and its validation were previously presented Chapter 5.

6.2.2 CO_2 and O_2 limited biofilm growth

Dissolved inorganic carbon (DIC) is the substrate for photosynthetic sugar production. Therefore, photosynthetic sugar production ($q_{s,p,ph}$) is not only dependent on light but also on the DIC concentration. This dependency is described with the Monod Equation (Equation 6.1) (Li et al. 2016; Murphy and Berberoglu 2014; Wolf et al. 2007) for which a half saturation constant ($K_{s,DIC}$) measured under conditions

with only HCO_3^{-1} (Lin et al. 2003) was employed which is most representative for DIC limitation in the deeper biofilm layers.

Equation 6.1 $$q_{s,p,DIC} = q_{s,p,m} \cdot \frac{C_{DIC}}{C_{DIC}+K_{s,DIC}}$$

Additionally, at low CO_2 and high O_2 ratios, photorespiration can occur which decreases photosynthetic sugar production. Photorespiration is described according to Li et al (Li et al. 2016) by Equation 6.2 and 6.3 where the CO_2/O_2 ratio is included in parameter $R_{CO2/O2}$.

Equation 6.2 $$q_{s,p,O2} = q_{s,p,m} \cdot \frac{C_{O2}}{C_{O2}+{C_{O2}}^2/K_{O2,in}}$$

Equation 6.3 $$K_{O2,in} = K_{O2,in,m} \cdot \frac{R_{CO2/O2}}{R_{CO2/O2}+K_{R_{CO2/O2}}}$$

Because multiplication of limiting factors can underestimate the productivity, the lowest sugar production rate ($q_{s,p}$) is selected by Equation 6.4 (Wolf et al. 2007).

Equation 6.4 $$q_{s,p} = \min\left[q_{s,p,ph}, q_{s,p,DIC}, q_{s,p,O2}\right]$$

Oxygen is required as an electron acceptor for the oxidation of sugars for respiration. This dependency can be described similar to that for DIC by Monod kinetics (Li et al. 2016; Wolf et al. 2007).

In contrast to CO_2 limitation, the microalgae metabolism under anaerobic conditions is not comprehensively studied. Due to this knowledge gap in combination with the fact that, in practice, oxygen limitation is easily prevented, oxygen limited growth was not included in the model.

6.2.3 Diffusion of CO_2 and O_2

Within the biofilm, there is no spatial mixing, therefore, transfer of CO_2 and O_2 is solely dependent on diffusion. Diffusion is only considered in one dimension by Equation 6.5 whereby the consumption or production rate is equal to the specific rate (q_i) times the functional biomass concentration (C_x). The diffusion coefficient

for DIC is calculated by weighing the diffusion coefficient of CO_2(aq) and HCO_3^{-1} according to their equilibrium concentration ratio at pH 6.7 which is the pH of the growth medium employed in the validation study (D_{DIC}=0.24*D_{CO2} (Morales-Rodriguez et al. 2011)+0.76*D_{HCO3} (Morales-Rodriguez et al. 2011)).

Equation 6.5 $$\frac{dC_i}{dt} = D_{i,bio} \cdot \frac{d^2C_i}{dz^2} + q_i \cdot C_x$$

In order to integrate the diffusion into the light limited biofilm growth model, the method of lines was used to discretize Equation 6.5 and obtain Equation 6.6. Fick's Law is used to describe the molar fluxes (J) (molar fluxes are listed in Appendix 6.B).

Equation 6.6 $$\frac{dC_{i,bio}^j}{dt} = \frac{A_d}{V^j} \cdot J_{i,in}^j - \frac{A_d}{V^j} \cdot J_{i,out}^j - q_i^j \cdot C_x^j - \frac{C_{i,bio}^j}{\Delta z^j} \cdot \frac{d\Delta z^j}{dt}$$

In Equation 6.6, the superscript 'j' indicates the layer inside the biofilm grid, and the subscript 'i' defines the diffusing species. The first term describes the molar flux into the biofilm layer ($J_{i,in}$). The second term depicts the molar flux out of the biofilm layer ($J_{i,out}$). The molar flux is dependent on the concentration gradient, the diffusion coefficient, and the diffusion path. The third term describes the biological conversion rate of the dissolved species ($C_{i,bio}$). The fourth term corrects the concentration of the dissolved species for the change in the biofilm layer thickness (Δz) due to growth.

The conversion rate of CO_2 and O_2 (the considered dissolved species) is calculated from sugar production, or consumption, by employing the relevant CO_2 or O_2 yield on sugar (Table 6.1). All yields are derived from when the stoichiometry of the conversions is taken into account: photosynthetic sugar production (produces O_2 and consumes CO_2); sugar consumption for biomass formation (consumes O_2 and produces CO_2); maintenance related sugar consumption (consumes O_2 and produces CO_2); and maintenance related biomass degradation (consumes O_2 and produces CO_2) are included. Thereby, primary processes related to microalgal growth are addressed.

By simplifying the problem to one dimension, only two boundary conditions are obtained. At the back of the biofilm on the biofilm-disk interphase, there is no diffusion possible. Therefore, the last layer can be described by excluding the second term from Equation 6.6. At the front of the biofilm at the interphase with the stagnant film layer, the dissolved species only need to be transported from the interphase into the first biofilm layer. Therefore, for the first biofilm layer, the diffusion distance is only half of the biofilm layer thickness.

The diffusion coefficient inside the biofilm ($D_{i,bio}$) is calculated by multiplying the diffusion coefficient in water ($D_{i,w}$) with the porosity of the biofilm (ε_{bio}) (Equation 6.7). The biofilm porosity is calculated based on the biomass volume per unit of dry biomass which is 2.5 ml g^{-1} (derived from data in Chapter 5). This results in a biofilm porosity of 0.57 ml liquid per ml total biofilm, assuming a constant total biomass concentration ($C_{x,tot}$) in the biofilm of 173 kg m^{-3} (Blanken et al. 2014).

Equation 6.7 $$D_{i,bio} = D_{i,w} \cdot \varepsilon_{bio}$$

6.2.4 Stagnant film layer

In between the biofilm and the bulk liquid or gas, there is a stagnant film layer of water. Therefore, the DIC and O_2 must first diffuse through this layer before entering the biofilm (Equation 6.8). The mass transfer coefficient is estimated by dividing the diffusion coefficient with the calculated stagnant film layer thickness (d_{film}) (Dutta 2007). It is assumed that there was no biological activity in the film layer.

Equation 6.8 $$\frac{dC_{i,film}}{dt} \cdot V_{film} = A_{exp} \cdot J_{i,exp} + A_{sub} \cdot J_{i,sub} - A_d \cdot J_{i,film,out}$$

In Equation 6.8, three terms describe the change in concentration of the dissolved species in the stagnant film layer. The first term describes the molar flux of gaseous components between the bulk gas and the gas-exposed part of the film layer by diffusion (J_{exp}). The second term depicts the diffusion of dissolved components between the bulk liquid and the submerged part of the film layer (J_{sub}). The third term represents the diffusion of species through the interphase between the stagnant

water film and the biofilm ($J_{film,out}$). The thickness of the stagnant film layer (d_{film}) of the gas-exposed part of the disk is calculated according to a validated empirical relation (Dutta 2007; Zhevalkink et al. 1978). To keep the model simple, the same thickness is employed for the submerged part of the disk.

6.2.5 Mass balances for the bulk liquid and gas

The change of the CO_2 and O_2 concentrations in the bulk liquid ($C_{i,l,bulk}$) and gas ($C_{i,g,bulk}$) are described with additional mass balances (Equation 6.9 and Equation 6.10); both include four terms. In Equations 9 and 10, the first term describes the incoming mass flow rate. The incoming concentrations O_2(g) and CO_2(g) are established values while the incoming liquid is assumed to be in equilibrium with atmospheric gas 20.9 % v/v O_2 and 0.04 % v/v CO_2). The second term describes the outgoing mass flow rate for which it is assumed that the bulk is perfectly mixed. The outgoing gas flow rate is corrected for changes in the gas mass flow rate and its composition according to Equation 6.11. The third term describes the molar flux between bulk gas or liquid and the stagnant film layer (J_{exp}). The fourth term represents the molar flux between the gas and liquid interphase (J_{liq}) of which the mass transfer coefficient ($K_{l,liq}$) was obtained experimentally.

Equation 6.9 $$\frac{dC_{i,bulk,g}}{dt} \cdot V_g = F_{g,in} \cdot C_{i,g,bulk,in} - F_{g,out} \cdot C_{i,g,bulk} - A_{exp} \cdot J_{i,exp} - A_{liq} \cdot J_{i,liq}$$

Equation 6.10 $$\frac{dC_{i,bulk,l}}{dt} \cdot V_l = F_l \cdot C_{i,l,bulk,in} - F_L \cdot C_{i,l,bulk} - A_{sub} \cdot J_{i,sub} + A_{liq} \cdot J_{i,liq}$$

Equation 6.11 $$F_{g,out} = F_{g,in} + \frac{(-J_{CO2,exp} - J_{CO2,liq} - J_{O2,exp} - J_{O2,liq})}{C_T}$$

6.3 Computational methods

Model parameters were all obtained from literature and are listed in Table 6.1 except for the mass transfer coefficient between the bulk gas to the bulk liquid (K_{liq}) which was obtained experimentally.

6.3.1 Model validation

The initial biofilm thickness was set to 54 μm (Chapter 5) and was divided in a grid of 200 layers and spaced such that, after one week of simulated biofilm growth, all layers were below 35 μm. For every biofilm layer, five differential equations were solved including: functional biomass, sugar biomass, biofilm layer thickness, CO_2 concentration, and O_2 concentration. Additionally, differential equations for CO_2 and O_2 concentrations were solved for the stagnant film layer, bulk liquid, and bulk gas. This system of ordinary differential equations was solved with the ode15s solver in MATLAB R2012a. Model accuracy was evaluated with the mean average percent error (MAPE) (Equation 6.12).

Equation 6.12 $$\text{MAPE} = \frac{100}{n}\sum\left(\frac{|P_{obs}-P_{pre}|}{|P_{obs}|}\right)$$

6.3.2 Minimizing CO_2 loss

To maximize CO_2 utilization in a single Algadisk (biofilm reactor), three conditions were evaluated including: pure CO_2, flue gas (12% CO_2 and 9% O_2) and air (0.04% CO_2 and 21% O_2). In order to decrease modelling time, this analysis was performed with only 50 biofilm layers. All simulations performed to optimize CO_2 utilization did not feature a liquid flow rate because, in practice, O_2 and CO_2 transfer occurs predominately via the gas phase. For pure CO_2 and flue gas 150 gas flow rates were evaluated to identify the optimal conditions. These rates were linearly spaced between 0.014 to 18 gas volume replacements per day (with 34 m^2 disk surface per m^3 of enclosed gas volume for the Algadisk system). Optimal conditions were selected by maximizing the sum of the percentage of maximal productivity achieved and the percentage of CO_2 consumed. In the event of cultivation in air, a very substantial air refreshment rate of 10^4 dilutions per day was used to represent a constant atmospheric CO_2 concentration in the headspace.

To optimize CO_2 utilization in a system with multiple Algadisk units in series, only flue gas (12% CO_2 and 9% oxygen) was evaluated. Thereby it is assumed that the gas is perfectly mixed in each single biofilm unit. Therefore, when considering an extensive number of units in series, a plug-flow behavior of the gas phase was

simulated. First, biomass production of a single biofilm reactor was simulated for 200 different CO_2 concentrations and corresponding O_2 concentrations ranging from 0 % CO_2 to 12% CO_2 and 22% O2 to 9% O_2, respectively (calculated based on stoichiometry). With these data, the biomass production rate in the Algadisk was expressed as a function of a CO_2 fraction in the gas phase ($r_b(C_{CO2,g,bulk})$ in cmol-b $(m^2\ s)^{-1}$) employing the interp1 function in MATLAB R2012a (results are presented in Appendix 6.C). With the relation between biomass production rate and CO_2 and O_2 gas concentration being known, the productivity for any series of Algadisk units could be calculated with a mass balance over the gas phase (Equation 6.13).

Equation 6.13 $$\frac{dC_{CO2,g}}{dt} \cdot V_g = F_{g,in} \cdot C_{CO2,g,in} - F_{g,out} \cdot C_{i,g,bulk} - r_b\left(C_{CO2,g,bulk}\right) \cdot Y_{CO2/b} \cdot A_d$$

To simulate multiple reactors in series, it was assumed that the first reactor features a maximal biomass production rate, which proved to be valid. For all following reactors, the incoming CO_2 concentration equals the bulk concentration of the previous reactor. Conditions were optimized by averaging the productivity over all algadisk units expressed as a percentage of maximal productivity. The percentage productivity was added to the percentage of CO_2 consumed in the reactor series and maximized by multiplication minus one and employing the fminsearch function in MATLAB R2012a.

Table 6.1. Input parameters required for the biofilm growth model.

Symbol	Description	Value	Units	Reference
		Process related		
T	Temperature	37	^{o}C	
P	Pressure	101325	Pa	
V_g	Volume gas phase	4	L	
A_d	Disk area in algadisk	0,138	m^2	
A_{liq}	Area of the liquid gas interphase	0,032	m^2	
f_{sub}	Disk fraction submerged	0,386	-	
-	Disk rotation speed	9	Rpm	
d_{disk}	Diameter disk	0,3	M	
d_{gear}	Diameter gear area	0,048	M	
H_l	Distance between shaft and liquid	0,024	M	
F_g	Gas flow rate	200	ml min^{-1}	
F_l	Liquid renewal rate	17	ml min^{-1}	
	pH	6,7	-	
I_{in}	Incident light intensity	389	µmol $(m^2\ s)^{-1}$	
$f_{O2,air}$	fraction O_2 in air	0,209	mol-O_2 mol-t^{-1}	
$f_{CO2,air}$	fraction CO_2 in air	0,0004	mol-CO_2 mol-t^{-1}	
$K_{DIC,l}A$	Mass transfer coefficient of DIC between gas and liquid	1,9E-05	s^{-1}	this study
$K_{O2,l}A$	Mass transfer coefficient of O_2 between gas and liquid	2,3E-05	s^{-1}	this study
$f_{l/disk}$	fraction disk illuminated	0.443		
$L_{bio,0}$	Initial biofilm thickness	54E-6	m	blanken et al 2016b
		General inputs		
$H_{T,CO2}$	Henry coefficient for CO_2	0,255	mmol $(m^3\ Pa)^{-1}$	(Sander 2015)
$H_{T,O2}$	Henry coefficient for O_2	0,0104	mmol $(m^3\ Pa)^{-1}$	(Paradiso et al. 2011)
$K_{a,DIC,ion}$	Dissociation constant CO_2 <> HCO_3^{-1}	6,3E-07	-	(Harned and Davis 1943; Stumm and Morgan 1995)
$D_{DIC,w}$	Diffusion coefficient DIC in water	1,16E-09	$m^2\ s^{-1}$	see text (Morales-Rodriguez et al. 2011)]
$D_{O2,w}$	Diffusion coefficient O_2 in water	2,99E-09	$m^2\ s^{-1}$	(Wilke and Chang 1955)
m_{DIC}	Partitioning coefficient gas-liquid for CO2	0,37	mol-CO_2 mol-DIC^{-1}	calculated
m_{O2}	Partitioning coefficient gas-liquid for O2	36,97	mol-O_2 mol-O_2^{-1}	calculated
d_{film}	Stagnant film layer thickness	8,75E-05	m	calculated (Zhevalkink et al. 1978)

Table continuous on next page

Table 6.1 continued

Symbol	Description	Value	Units	Reference
	Biological parameters			
$q_{s,p,max}$	maximal specific sugar production rate	$1.296E^{-4}$	cmol-s (cmol-x s)$^{-1}$	(Blanken et al. 2016)
$q_{s,c,max}$	maximal specific sugar consumption rate	$1.0265E^{-4}$	cmol-s (cmol-x s)$^{-1}$	Blanken et al 2016b
$Y_{x/s}$	biomass yield on sugar	0.59	cmol-x cmol-s^{-1}	(Blanken et al. 2016)
$Y_{s/ph}$	sugar yield on light	0.1	cmol-s mol-ph^{-1}	(Blanken et al. 2016)
$\alpha_{x,average}$	specific absorption coefficient	7.1	m^2 cmol-x^{-1}	(Blanken et al. 2016)
M_x	molar weight per carbon mol biomass	24	g cmol-x^{-1}	(Blanken et al. 2016)
$C_{b,biofilm}$	total biomass concentration in biofilm	173	kg m^{-3}	(Blanken et al. 2014)
$f_{s/b,min}$	minimal sugar fraction in the total biomass	0.0198	cmol-s cmol-b^{-1}	blanken et al 2016b
$m_{s,max}$	maximum maintenance related sugar consumption rate	$2.54E^{-6}$	cmol-s (cmol-x s)$^{-1}$	blanken et al 2016b
$m_{x,max}$	maximum maintenance related biomass consumption rate	$1.41E^{-7}$	cmol-x (cmol-x s)$^{-1}$	blanken et al 2016b
ε_{bio}	Porosity of the biofilm	0,57	m^3-w m^{-3}-biofilm	see text
$f_{b\text{-}wet/b\text{-}dry}$	Volume-dry mass ratio biomass	2.5	ml-b-wet g-b-dry^{-1}	see text
$Y_{DIC/s,p}$	Yield DIC during photosynthetic sugar production	1	mol-DIC mol-s^{-1}	calculated
$Y_{DIC/s,c}$	Yield DIC during biomass formation	0,41	mol-DIC mol-s^{-1}	calculated
$Y_{DIC/s,m}$	Yield DIC during maintenance	1	mol-DIC mol-s^{-1}	calculated
$Y_{DIC/s,mx}$	Yield DIC during endogenous maintenance	1	mol-DIC mol-x^{-1}	calculated
$Y_{O2/s,p}$	Yield O_2 during photosynthetic sugar production	1	mol-O_2 mol-s^{-1}	calculated
$Y_{O2/s,c}$	Yield O_2 during biomass formation	0,35	mol-O_2 mol-s^{-1}	calculated
$Y_{O2/s,m}$	Yield O_2 during sugar-based maintenance	1	mol-O_2 mol-s^{-1}	calculated
$Y_{O2/s,mx}$	Yield O_2 during endogenous maintenance	1,11	mol-O_2 mol-x^{-1}	calculated
$Y_{CO2/b}$	Yield CO_2 per total biomass produced	1	mol-CO_2 mol-b^{-1}	calculated
$Y_{O2/b}$	Yield O_2 per total biomass produced	1,11	mol-O_2 mol-b^{-1}	calculated
$K_{s,DIC}$	Half saturation coefficient DIC	9,84E-04	mol m^{-3}	(Lin et al. 2003)*
$K_{r,DIC/O2}$	Ratio saturation coefficient for photosynthesis	0,35	mol-DIC mol-O_2^{-1}	(Li et al. 2016)
$K_{O2in,m}$	Maximal inhibition coefficient of O_2	1	mol m^{-3}	(Li et al. 2015b)

* This value is obtained for HCO_3^{-1}, thereby we assume worst-case scenario

6.4 Materials and methods

6.4.1 Microalgae and pre-cultivation

The microalgae *Chlorella sorokiniana* (CCAP 211/8k) was maintained and pre-cultivated in shake flasks with M-8a medium (Kliphuis et al. 2010) supplemented with 30 mM Urea. This algae suspension was utilized to inoculate experiments.

6.4.2 CO_2-limited biofilm growth validation experiment

To assess biofilm growth under CO_2 limiting conditions and validate the biofilm growth model, experiments were performed in a gas-tight Algadisk photobioreactor which was previously described in detail in Chapter 5. Briefly, the Algadisk contained one rotating disk that was vertically placed and partially submerged such that the biofilm cultivated on the disk alternated between liquid and gas phase at 9 rpm. The liquid phase (M8a medium with 30 mM NH_4Cl, (Kliphuis et al. 2010)) was kept dark such that only the biofilm exposed to the gas received light (44% of the disk surface). The liquid was mixed homogeneously and temperature and pH controlled. The Algadisk operating conditions are listed in Table 6.1.

The liquid phase of the Algadisk reactor was continuously diluted with a flow rate of 17 ml min^{-1}. Every growth-harvest cycle represents exactly one week of biofilm growth. During harvest, the biomass was removed from the stainless steel disk surface by scraping while the woven structure of the mesh ensured inoculum remaining for the next growth-harvest cycle (Blanken et al. 2014). The productivity of the Algadisk represented the productivity per m^2 woven disk surface. Analysis and calculation of productivities are described in Blanken et al. 2014.

The Algadisk was operated at five incoming CO_2 concentrations (10%, 5%, 4% 1.25% and 0.625% CO_2 v/v) and continuous illumination at 389 μmol $(m^2\ s)^{-1}$. The average incident light intensity was the average over 15 points (Chapter 5). The incoming CO_2 concentrations were set by mixing pure CO_2 with dry pressurized air. The incoming gas flow rate was 200 ml min^{-1}.

6.4.3 Mass transfer coefficient between bulk gas and bulk liquid

The mass transfer coefficient between bulk gas and bulk liquid was measured according to the dynamic method (Tribe et al. 1995; van 't Riet and Tramper 1991) under Algadisk operating conditions (Table 6.1). The medium in the algadisk was first deaerated by sparging with nitrogen. Next, pressurized air was blown into the headspace at 200 ml min^{-1} while measuring the oxygen concentration in the medium with a clark-type dissolved oxygen sensor (InPro6050, Mettler Toledo, USA, Columbus) and in the outgoing gas with a paramagnetic oxygen sensor (Servomex 4100, the Netherlands, Zoetermeer). The change in oxygen concentration in time can be described by Equation 6.14 from which the mass transfer coefficient for oxygen ($K_{O2,l}A$) was derived. The mass transfer coefficient for DIC ($K_{DIC,l}A$) was calculated from the $K_{O2,l}A$ by multiplying with 0.53 (Royce and Thornhill 1991). Note that the results of this experiment are only listed in Table 6.1.

Equation 6.14 $$\frac{dC_{o2,l}}{dt} = K_{O2,l}A \cdot \left(\frac{C_{o2,g}}{m} - C_{o2,l}\right)$$

6.5 Results and discussion

6.5.1 Biofilm growth model validation

The biofilm growth model was validated on CO_2-limited biofilm growth experiments in the Algadisk in which five CO_2 levels in the incoming gas stream were compared (Figure 6.2). Based on a Dunnett's T3 test on the measured productivity data, 10%, 5%, and 4% w/w CO_2 were not significantly different from each other ($p>0.05$) and thus not limiting microalgae growth while 1.25% and 0.625% w/w CO_2 were significantly different from all other conditions ($p<0.05$) and thus limiting microalgal growth in the Algadisk (Figure 6.2). The average productivity under non-limiting conditions was 100 g $(m^2\ week)^{-1}$ with a biomass yield on light of 1.0 g mol-ph^{-1}. These observations accord with previous results obtained with the Algadisk (Chapter 5) and (Blanken et al. 2014) and in the high range of phototrophic biofilm productivities reported in literature (Berner et al. 2014).

The measured conditions were predicted with the biofilm growth model with a MAPE of 10.9% (Figure 6.2). The non-limiting conditions were predicted with a high accuracy while at low CO_2 concentrations, the model underestimated the observed productivity. Likely this deviation is caused by simplifications in the model. To further improve the model, it could be considered to: improve the estimation/measurement of the stagnant film layer (Dutta 2007); improve the estimation/measurement of biofilm porosity (Dutta 2007); include charge balances in the description of the transport of chemical species within the biofilm (Wesselingh and Krishna 2006); include possible convective transport within the biofilm (Li et al. 2016; Murphy and Berberoglu 2014); and include the effect of carbon concentrating mechanisms on the rate of photosynthesis (Giordano et al. 2005). Despite the more modest model accuracy at low DIC, the model underestimation ensures that, during the optimization of CO_2 utilization inside the Algadisk, a worst case scenario is depicted. Consequently, optimized conditions represent situations which are practically feasible and not a consequence of model inaccuracy. Furthermore, it should be noted that the model is only based on measured or calculated parameters and did not require any fitting to experimental data. The predicted gradients of CO_2 and O_2 inside the biofilm are discussed and displayed in Appendix 6.D.

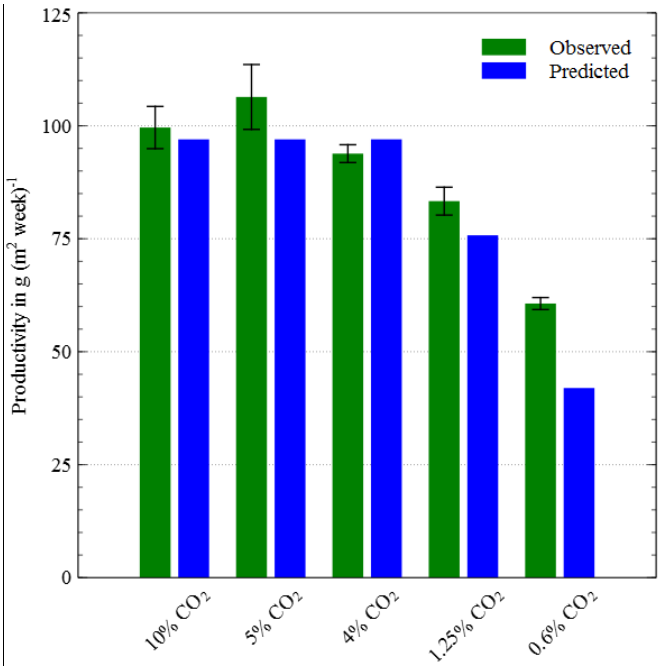

Figure 6.2. Validation of the biofilm growth model on CO_2-limited biofilm growth experiments in the Algadisk. Observed disk productivity error bars indicate the standard deviation of four measurements. Predicted disk productivities are obtained with the biofilm growth model. Experimental results were analyzed for homogeneity of variance by a Levene's test ($p=0.001<0.05$) and, therefore, the post hoc multiple comparison test Dunnett's T3 was performed. Based on the Dunnett's T3 test: 10%, 5%, and 4% w/w CO_2 were not significantly different from each other ($p>0.05$) while 1.25% and 0.625% w/w CO_2 were significantly different from all other conditions ($p<0.05$).

6.5.2 Maximization of CO_2 utilization and biomass productivity by design

In order to maximize the CO_2 utilization efficiency inside the Algadisk, three CO_2 sources were compared: flue gas, pure CO_2, and air. Algadisk performance (CO_2-uptake and biomass productivity) was optimized for both flue gas and pure CO_2 by varying the gas flow rate (figure 6.3). From the simulations presented in Figure 6.3, it can be observed that it is very difficult to obtain a high CO_2 utilization in combination with a high productivity with pure CO_2. With flue gas, however, it is possible to obtain a high CO_2 utilization efficiency combined with a high

productivity. It is not surprising that flue gas performs better compared to pure CO_2 considering that at all CO_2 is converted to O_2 which exposes the microalgae to almost pure O_2 at maximal CO_2 uptake efficiency. High O_2/CO_2 ratios cause photorespiration and, therefore, decrease productivity (Kliphuis et al. 2011c; Li et al. 2016; Pope). Cultivation in air is not depicted in Figure 6.3 because, when doing so, CO_2 utilization efficiency is irrelevant. Therefore, to simulate the biofilm growth in air, an infinite large gas flow rate was employed to represent a constant CO_2 concentration. However, due to the low concentration of CO_2 in air, only a productivity of 11 g $(m^2\ week)^{-1}$ was predicted which is only 12% of the non-limited biofilm productivity of 97.3 g $(m^2\ week)^{-1}$.

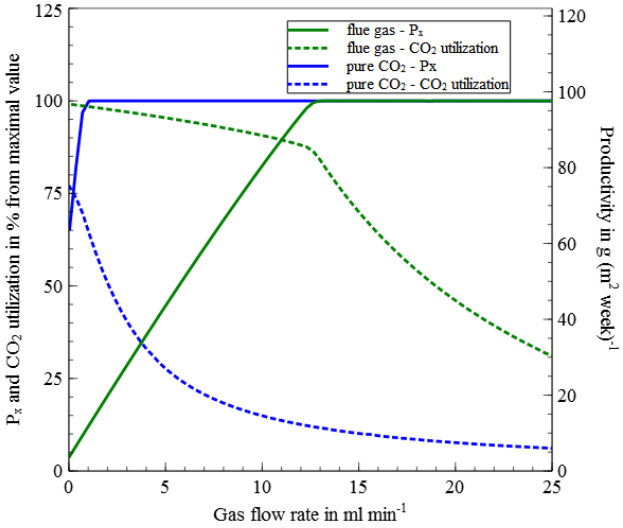

Figure 6.3. Optimization of biomass productivity and CO_2-utilization efficiency in a single Algadisk biofilm reactor by varying the incoming gas flow rate for both pure CO_2 and flue gas. Air is not depicted as an infinite large gas flow rate is assumed to represent exposure to atmosphere CO_2. Optimization is performed employing the validated biofilm growth model. The predicted maximal productivity of 97.3 g $(m^2\ week)^{-1}$ equals 100%.

A disadvantage of the Algadisk is that the gas phase is perfectly mixed because, higher CO_2 utilization efficiencies are theoretically obtained with gas moving in plug flow over the biofilm surface. In traditional gas-liquid contactors, plug flow of one or both phases ensures a higher driving force (i.e., concentration gradient) integrated over the transfer area. Plug-flow behavior can be simulated by placing multiple ideally mixed units in series. Therefore, to increase the CO_2 utilization, a system of multiple Algadisk units was investigated whereby the gas was coupled in series such that the outgoing gas from reactor one is the incoming gas for reactor two, and so forth. From Table 6.2, it can be concluded that, with multiple Algadisks in series, the CO_2 utilization efficiency can be increased without a significant decrease in productivity. Optimal conditions were obtained with 25 Algadisk units, or more, in series utilizing 96% of the incoming CO_2 instead of the 86% in a single reactor. It should be noted that, in the last Algadisk units, microalgae grow CO_2 limited and, therefore, the complete system is 2% less productive (Table 6.2) than in a situation without CO_2 limitation. This is the result of the choice to maximize CO_2 utilization and productivity equally. This could be easily adapted by including different weighing factors to CO_2 utilization and biomass productivity (e.g., favoring biomass productivity).

Table 6.2. Optimization of the CO_2 utilization in the Algadisk for three different CO_2 sources. Because flue gas performed best, flue gas was selected to be further optimized by placing multiple Algadisk units in series and simulating plug-flow behavior of the gas phase. The predicted maximal productivity $P_{x,pre,max}$ equals 97.3 g $(m^2\ week)^{-1}$.

		Series of reactors with flue gas				**Flue gas**	**Pure CO_2**	**Air**
Reactors	N	50	25	10	5	1	1	1
Productivity	% of $P_{x,pre,max}$	98%	98%	99%	99%	99%	97%	12%
CO_2 efficiency	% CO_2 consumed	97%	96%	94%	93%	86%	70%	*
Dilution rate	day^{-1}	215	109	45	23	4,6	0,3	2E+04

*not relevant when cultivating microalgae on atmospheric CO_2

The modelling approach presented in this study enabled greatly increasing CO_2 utilization efficiency in a simulated Algadisk cultivation. From these results, it can be observed that obtaining plug flow over the biofilm surface is essential for high CO_2 utilization efficiencies. Although this study was the first to optimize CO_2 utilization for biofilm cultivations, the results are in the high range of results with suspension cultivations. Two studies demonstrated CO_2 utilization efficiencies around 70% without significant productivity penalties (Valiorgue et al. 2014; Yang 2011). Other studies report CO_2 utilization efficiencies up to 95%, however, the implications for biomass productivity were not quantified (Doucha and Lívanský 2006; Rubio et al. 1999). To perform these optimizations, a mathematical model specific for the cultivation system is required, therefore, this model is specific for the Algadisk reactor. The model can be adapted for other biofilm photobioreactors by changing the mass balances for the bulk and stagnant layer. Nevertheless, based on the results of this study case, it can be concluded for other biofilm photobioreactors as well that obtaining plug flow over the biofilm surface is essential for maximal CO_2 utilization efficiency. Gas supply and gas mixing should, therefore, be considered during the design stage of biofilm photobioreactors. This will both reduce the impact on the environment and the operating costs of the microalgae cultivation.

6.6 Conclusions

A microalgal biofilm growth model was developed which predicted biofilm productivity exposed to a range of CO_2 concentrations with a MAPE of 10.9%. The biofilm growth model was consequently employed to increase CO_2 utilization efficiency of a biofilm photobioreactor. By operating 25 reactors units in series, the CO_2 utilization efficiency increased such that 96% of the flue gas CO_2 was exploited with only a 2% productivity drop. Based on these results, it was identified that both concentrated CO_2 streams and plug flow behavior over the biofilm surface were essential for high CO_2 utilization efficiencies, improving both environmental impact and the economics of the microalgae cultivation.

6.7 Appendices

Appendix 6.A

In this appendix the model description of light limited biofilm growth is based on previous work (Chapter 5) and (Blanken et al. 2016) is summarized. The carbon partitioning between sugar-storage biomass and functional biomass is modelled based on two mass balances: Equation 6.A.1 for sugar-storage biomass (C_s) and Equation 6.A.2 for functional biomass (C_x). The model is solved using the methods of lines and thus considering a substantial number of biofilm layers. The total biomass concentration in the biofilm layers is constant. The thickness of the biofilm layers (Δz), however, will increase during growth (Equation 6.A.3).

Equation 6.A.1 $$\frac{d(C_S \cdot \Delta z)}{dt} = \left(q_{s,p}(I_{ph}, C_{DIC}, C_{O2}, z) \cdot f_{\frac{I}{disk}} - q_{s,c}(C_s, C_{O2}, t) - m_s(C_s)\right) \cdot C_X \cdot \Delta z$$

Equation 6.A.2 $$\frac{d(C_X \Delta z)}{dt} = \left(Y_{x/s} \cdot q_{s,c}(C_s, C_{O2}, t) - m_x\right) \cdot C_X \cdot \Delta z$$

Equation 6.A.3 $$\frac{d(\Delta z)}{dt} = \frac{d\left((c_X + c_S) \cdot \Delta z\right)}{dt} \cdot \frac{1}{(c_X + c_S)}$$

The sugar-storage biomass balance (Equation 6.A.1) includes: production of sugar from photosynthesis ($q_{s,p}$) on the illuminated disk fraction ($f_{I/disk}$); sugar consumption related to biomass growth ($q_{s,c}$) which includes consumption of sugar for respiration to support this growth; and consumption of sugar for maintenance (m_s). The functional biomass balance (Equation 6.A.2) includes: biomass production from sugar ($Y_{x/s} \cdot q_{s,c}$); and endogenous respiration (m_x). Finally, light starvation is modelled such that the maintenance related sugar consumption will decrease when microalgae are exposed to long periods of darkness. Light traveling through the biofilm compartment is calculated based on Lambert-Beer and includes the wavelengths in the range of 400 to 700 nm (Blanken et al. 2016).

Appendix 6.B

Below the Fick's law equations are listed that describe the discretized molar flux (*J*) per compartment. Inside the biofilm:

Equation 6.B.1 $$J_{i,bio}^{j} = D_{i,bio} \cdot \left(\frac{c_{i,bio}^{j-1} - c_{i,bio}^{j}}{0.5\Delta z^{j-1} + 0.5\Delta z^{j}} \right)$$

From the biofilm/film-layer interphase into the biofilm:

Equation 6.B.2 $$J_{i,film} = D_{i,bio} \cdot \left(\frac{C_{i,film} - C_{i,bio}^{1}}{0.5 \cdot \Delta z_{i,bio}^{1}} \right)$$

From the bulk gas to the biofilm/film-layer interphase:

Equation 6.B.3 $$J_{i,exp} = \frac{D_{i,w}}{d_{film}} \cdot \left(\frac{C_{i,bulk,g}}{m_i} - C_{i,film} \right)$$

From the liquid gas to the biofilm/film-layer interphase:

Equation 6.B.4 $$J_{i,sub} = \frac{D_{i,w}}{d_{film}} \cdot \left(C_{i,bulk,l} - C_{i,film} \right)$$

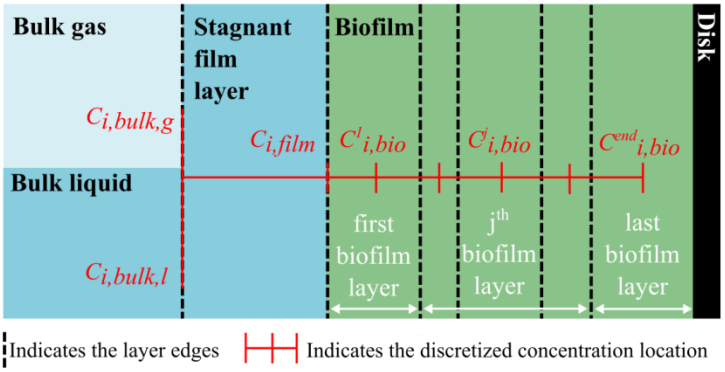

Figure 6.B.1. Schematic depiction of how the biofilm is discretized.

Appendix 6.C

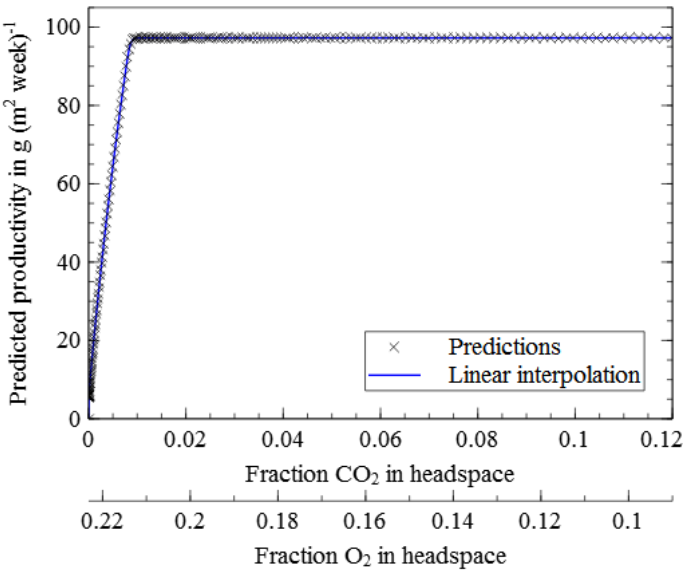

Figure 6.C.1. Simulation results that were employed to perform the optimization of multiple Algadisk units in series. The predictions are model simulations with a fixed CO_2 and O_2 fraction which were linear interpolated and employed in the optimization simulation.

Appendix 6.D

With the biofilm growth model, concentration profiles for DIC and O_2 inside the biofilm are predicted (Figure 6.D.1). In this model, the DIC profiles accord closely with the bulk gas concentration. Inside the biofilm, the CO_2 concentrations drop sharply while they increase in the dark part of the biofilm. As expected, the O_2 profiles exhibit the exact opposite with an increase in O_2 concentration in the illuminated zone and a decrease in the dark zones. Note that, for all conditions, oxygen concentration are well above air saturation and, therefore, not limiting microalgal growth. In contrast for both 4% and 5% CO_2, oxygen concentrations are 6 times higher than air saturation; these O_2 concentration are very high but in line with observations in photosynthetic active biofilms (Li et al. 2015a). Furthermore,

by comparing the observed productivities of 4%, 5%, and 10% CO_2, it appears that the microalgae are not inhibited by the high oxygen concentrations.

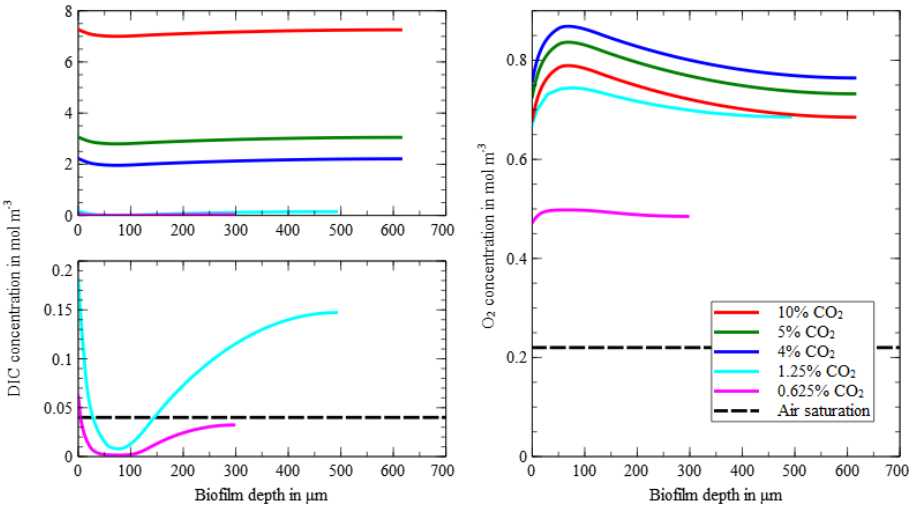

Figure 6.D.1. Concentration profiles of (A) dissolved inorganic carbon (DIC) and (B) dissolved oxygen (O_2) over the biofilm depth for five different CO_2 concentrations in the incoming gas phase. The profiles reflect the situation at the end of a seven-day growth cycle. Note that, in Graph A, the low range is plotted with a higher resolution below the main graph.

Chapter 7 General discussion

7.1 Advantages of biofilm photobioreactors

Biofilm photobioreactors for the production of microalgal biomass can solve a number of bottlenecks associated with suspended microalgae cultivation. Advantages of biofilm cultivation are:

- Direct harvest of concentrated microalgal biomass
- The uncoupling of the hydraulic retention time from the microalgal retention time (Gross et al. 2015)
- Local photoacclimation within the biofilm
- Reduced cellular maintenance in dark zone

First, the advantages of a biofilm photobioreactor will be discussed followed by the state-of-the-art of this technology and ending with guidelines for improved design and operation of biofilm photobioreactors.

7.1.1 Harvesting concentrated microalgal biomass

Phototrophic biofilms that are harvested by scraping the biofilms yield an average dry solid concentration of 160 kg m^{-3} (Table 7.1). These results are in the same range as biomass concentrations obtained after centrifugation of a suspended culture (Pahl et al. 2013). Therefore, biofilm cultivation can save on downstream processing and capital costs compared to suspended cultivation (Pahl et al. 2013). Based on current research, it appears that the dry solid content of a biofilm is influenced by the harvesting strategy (Boelee et al. 2013) and hydrodynamic forces; it is also species dependent (Naumann et al. 2012).

7.1.2 Uncoupling the hydraulic retention time

In a biofilm photobioreactor, the microalgal biomass is attached to a solid surface. Therefore, it is possible to uncouple the hydraulic retention time (HRT) from the microalgal retention time (SRT) which subsequently affords employing both dilute nutrient streams (e.g., most types of wastewater) as well as concentrated nutrient streams. Because of this feature, most phototrophic biofilm research initially aimed at treating wastewater (Adey et al. 2011; Wilkie and Mulbry 2002) and this application are still current subjects of research (Boelee et al. 2014; Christenson and

Sims 2012). A possible disadvantage of utilizing dilute nutrient streams is that biofilm productivity is lower than theoretically possible because of nutrient limitation. Cultivation on concentrated streams is more favorable as it allows for light limited growth and reduced liquid handling. Decreasing the liquid volume to be processed is very beneficial as most microalgae cultivation costs are related to liquid handling (Norsker et al. 2011) [introduction]. In conclusion, the flexible HRT is advantageous as it allows for increased freedom in photobioreactor operation.

7.1.3 Local photoacclimation in photic zone

Phototrophic biofilm productivity is driven by light energy and, in order to fully understand this relation, light gradients inside the biofilm will be discussed in detail. At the front of the photic zone, microalgae will be exposed to oversaturating light intensities while the light intensity will rapidly decrease when moving deeper into the biofilm (Li et al. 2015a). Because of light absorption by the microalgae, a fully grown biofilm can be divided into a photic zone and a dark zone.

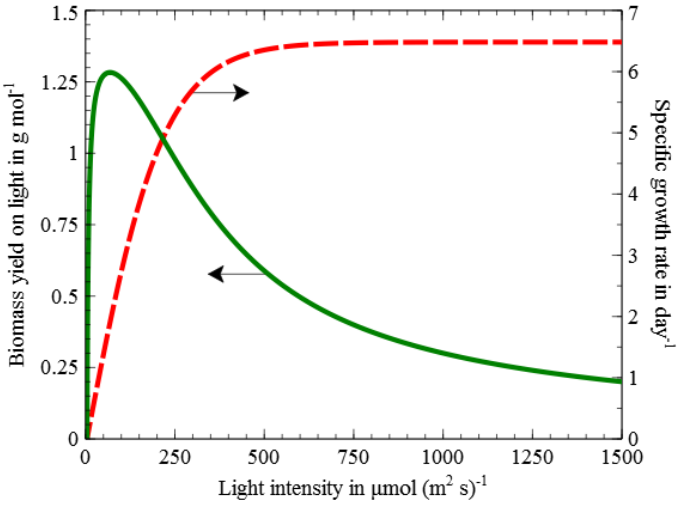

Figure 7.1. Estimation of the biomass specific growth rate (dashed line) and biomass yield on light (solid line) as a function of the light intensity for a single cell. Calculated according values and formulas presented in Blanken et al (Blanken et al. 2016) for a monolayer of microalgae cells.

In the photic zone, light levels are above the light compensation point with the maximal value at the light exposed side of the biofilm. In the dark zone, light levels are below the light compensation point. This is very similar to suspended cultivation, however, microalgae are fixed within the biofilm and do not move through the light gradient. This is an advantage because it allows individual microalgal cells acclimate to their local light regime (Blanken et al. 2016; Li et al. 2016; Ross and Geider 2009) and (Chapter 5).

To prevent damage to photosystems and light dissipation in the oversaturating top layer of the photic zone, microalgae will acclimate and reduce their specific photon absorption capacity which can result in a two-fold decrease in the specific light absorption coefficient (Dubinsky and Stambler 2009; Takache et al. 2012; Vejrazka et al. 2011; Zijffers et al. 2010). This is an advantage for the microalgae cells further inside the biofilm as light will penetrate deeper where the light is converted more efficiently (Figure 7.1) (Grobbelaar and Kurano 2003; Vejrazka et al. 2013). It should be noted, however, that the oversaturating photons will be dissipated as heat and can, at high intensities, result in damage of the photosystems (Deblois et al. 2013; García-Camacho et al. 2012; Vejrazka et al. 2013). Nevertheless, in practice, microalgae have been cultivated at high productivities with continuous illumination of 1000 µmol $(m^2\ s)^{-1}$ (Li et al. 2015a; Schultze et al. 2015) in multiple pilot studies employing sunlight (Table 7.1) (Adey et al. 2011; Christenson and Sims 2012; Gross and Wen 2014). In conclusion, local photoacclimation results in a deeper light penetration and, therefore, overall more efficient light utilization (Li et al. 2016).

7.1.4 Reduced cellular maintenance in dark zone

The dark zone inside the biofilm begins where the light intensity decreases below the light compensation point of microalgae (approximately 10 µmol $(m^2\ s)^{-1}$ (Takache et al. 2010; Vejrazka et al. 2013)). The light compensation point is defined such that the input of energy from photons equals the maintenance energy requirement of the microalgae, resulting in zero net growth. Microalgae that are in the dark zone will need to consume their energy reserves (e.g., starch) to support their maintenance energy requirement which will ultimately result in biomass loss.

Based on experimental results, it was ascertained that the maintenance energy requirement of microalgae exposed to prolonged periods of darkness decreases as their energy reserves decline (Chapter 5). The decreased maintenance energy requirement is an advantage as it leads to reduced biomass loss in the dark zone of the biofilm.

The disadvantage of a biofilm with a dark zone is that the reduced metabolic activity potentially decreases the product productivity. Most interesting, intercellular products produced by microalgae contain chemical energy and will, therefore, be consumed in the dark zones to satisfy maintenance energy requirements. Biofilms cultivated with the goal to produce intercellular microalgal products should, therefore, aim to minimize the development of a dark zone by keeping the biofilm thin and fully illuminated.

7.2 State-of-the-art biofilm photobioreactors

A wide range of different biofilm photobioreactors has been described. The most imported designs are listed in Table 7.1 and schematically depicted in Figure 7.2. Basic features present in a biofilm photobioreactor design are: 1) the biofilm is in contact with the liquid; 2) the biofilm is in contact with the gas phase; and 3) the biofilm is exposed to light. Despite the fact that all designs meet these basic requirements, reported productivities differ over a wide range (Table 7.1). Differences in productivity plausibly originate from different growth characteristics of the microalgal species employed and/or suboptimal cultivation conditions (e.g., carbon dioxide supply, pH, and/or temperature control). Additional deviations in productivities between designs can originate from biomass loss to the liquid due to hydrodynamic shear stress and/or light/dark cycles introduced by designs with rotating biofilms. However, for an adequate comparison, all designs should be evaluated by cultivating robust alga specie with intrinsic high specific growth (e.g., *Chlorella sorokiniana*) under optimal lab conditions. The schematic overview in Figure 7.2 illustrates the extensive number of mechanical designs of biofilm photobioreactors. In general, the mechanical designs can be divided into two

categories of periodically submerged biofilms and biofilms that are continuously in contact with liquid by utilizing perfusion systems (perfused).

7.2.1 Microalgal products produced in biofilms

Currently, most studies on microalgal biofilm cultivation focus on the production of biomass while fewer studies have evaluated the production of specific microalgal products such as pigments or fatty acids. Studies that have evaluated product productivity in microalgal biofilms are listed in Table 7.2. The primary focus of most studies was the production of lipids through nitrogen limitation or starvation, however, the success significantly varied between studies. To meticulously evaluate the results, the best triacylglycerol (TAG, i.e., neutral lipids) productivity from Table 7.2 was compared to a suspension experiment under similar light conditions (Breuer et al. 2012). Based on this comparison, the suspension performed twofold better than the biofilm. Nevertheless, the current number of studies is limited, and it is likely that lipid productivity in biofilms can be further increased in the future by optimizing the accumulation strategies towards biofilm cultivation, for example, by solving the problem of biofilm detachment initiated by the nitrogen starvation phase (Schnurr et al. 2013).

Table 7.1. Overview of the state of the art biofilm photobioreactor designs. Each design is schematically described in Figure 7.2.

		Reactor type	Productivity Lab	Productivity Pilot	Dry solid content	Substratum material	Reference
			g (m^2-growth d)$^{-1}$	g (m^2-ground d)$^{-1}$	kg m^{-3}		
A	**Vertical fixed biofilm**	(Intermittently) submerged	9	NA	60-100	Geotextile (polyethylene)	(Boelee et al. 2014; Boelee et al. 2013)
B	**Twin layer system**	Perfused	1,8	NA	160-280	Spacer - printing paper	(Naumann et al. 2012)
		Perfused	31	Calculated[*1]	-	Capillary mat - printing paper	(Schultze et al. 2015)
C	**Attached cultivation**	Perfused	16	Calculated[*1]	200-300	Cellulose acetate/nitrate filter	(Liu et al. 2012)
D	**Rotating fabric sheets**	Intermittently submerged	3,5	21,5	-	Cotton duct	(Gross and Wen 2014)
E	**Algal turf scrubber**	Intermittently submerged	5,5	39	-	Polyethylene screen	(Adey et al. 1993; Adey et al. 2011; Wilkie and Mulbry 2002)
		Intermittently submerged	9,9	NA	37-215	PVC	(Boelee et al. 2013)
F	**Porous substrate bioreactor**	Perfused	3,1	NA	-	Porous medium	(Murphy and Berberoglu 2014)
G	**Algadisk**	Intermittently submerged	20,1	10	143-192	Stainless steel / PVC	(Blanken et al. 2014) and unpublished pilot data
H	**Rotating rope drums**	Intermittently submerged	NA	31[*2]	120-160	Cotton rope	(Christenson and Sims 2012)
I	**Rotating brush reactor**	Intermittently submerged	-	-	-	Confidential	(2016a)

[*1] See the Illumination section for a detailed discussion on these values.

[*2] Cultivated on wastewater containing BOD and TSS, which likely enhanced the productivity

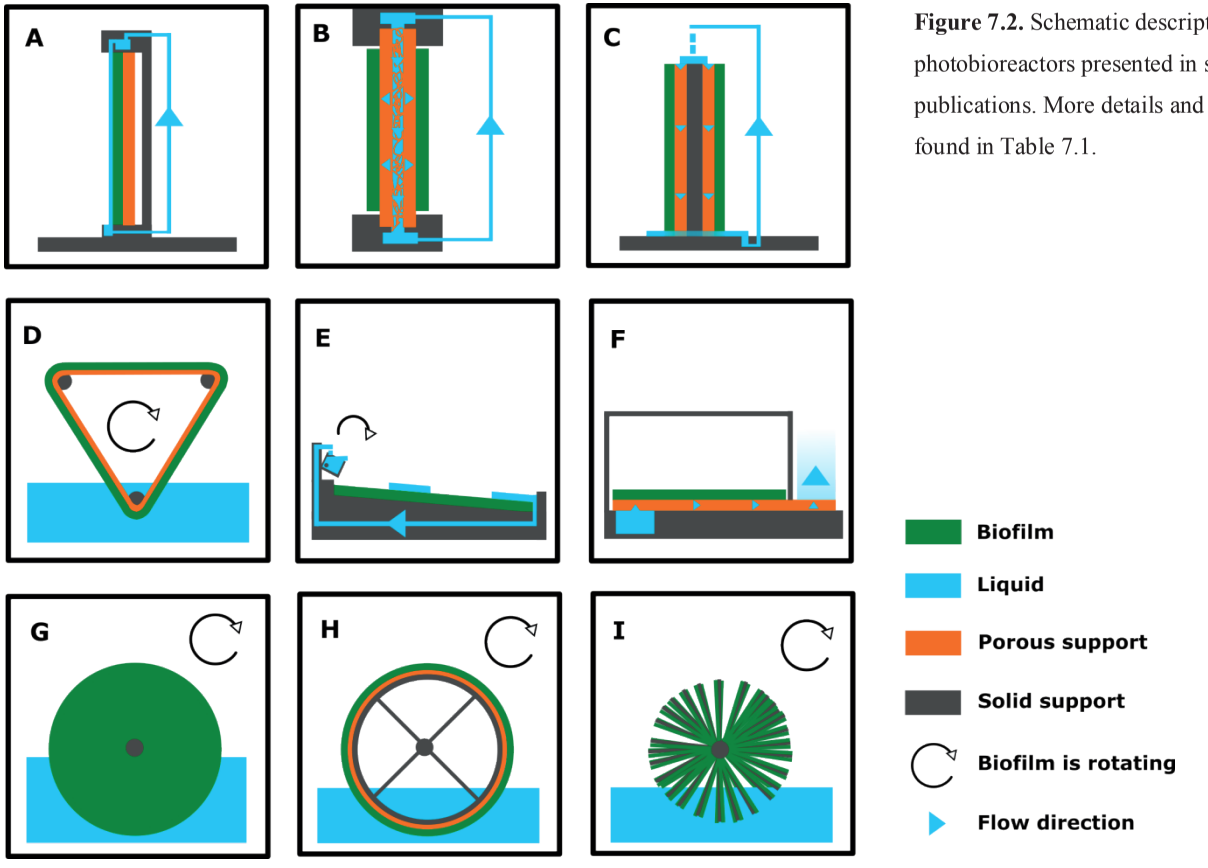

Figure 7.2. Schematic description of biofilm photobioreactors presented in scientific publications. More details and references can be found in Table 7.1.

Table 7.2. Literature overview of products and biomass yields obtained with phototrophic biofilms.

Strain	Productivity Biomass g $(m^2\ d)^{-1}$	Product g $(m^2\ d)^{-1}$	Product	Product $\%_{lipid/dry\ biomass}$	Strategy	References
			Lipids and hydrocarbons			
Aucutodesmus obliquus	9,0	2,5	TAG	37	Fixed low N concentration	(Ji et al. 2013b)
	9,0	3,6	Lipid	46	Fixed low N concentration	
Botryococcus braunii	6,5	2,3	Lipid	43	N starvation	(Cheng et al. 2013)
	6,5	1,1	Hydrocarbon	20	N starvation	
Botryococcus braunii	6,5	2,8	Hydrocarbon	51	Optimized N concentration	(Cheng et al. 2014)
Mixed	31,0	2,5	Lipid	NR	NA	(Christenson and Sims 2012)
Mixed	5,6	0,7	Fuel	NR	NA	(Adey et al. 2011)
Nannochloropsis oculata	3,87	0,45	Lipid	11,6	NA	(Shen et al. 2014a)
Mixed	2,1	-	Lipid	8	NA	(Genin et al. 2014)
Scenedesmus obliquus	2,1	0,2	Lipid	5	N & silicon starvation	(Schnurr et al. 2013)
Nitzschia palea	2,8	0,5	Lipid	16	N & silicon starvation	
Chlorella sp.	2,6	0,2	Lipid	11	NA	(Johnson and Wen 2010)
Chlorella vulgaris	21,5	-	Lipid	8	NA	(Gross and Wen 2014)
Botryococcus braunii	8,1	-	Lipid	42	N starvation	(Shen et al. 2015)
			Carotenoids			
Haematococcus pluvialis	6,0	0,1	Astaxanthin	2,6	Optimized N concentration	(Yin et al. 2015)
Trentepohlia arborum	-	0,1	Zeaxanthin/β-carotene	0.009	N starvation	(Chen et al. 2014)
			Biomass			
Halochlorella rubescens	6,3	NA	NA	NA	NA	(Shi et al. 2014)
Chlorococcum sp.	4,26	NA	NA	NA	NA	(Shen et al. 2014b)
Anabaena variabilis	3,1	NA	NA	NA	NA	(Murphy and Berberoglu 2014)
Isochrysis sp. T.ISO,	0,6	NA	Aquaculture feed	NA	NA	(Naumann et al. 2012)
Phaeodactylum tricornutum	1,8	NA	Aquaculture feed	NA	NA	
Tetraselmis suecica	1,5	NA	Aquaculture feed	NA	NA	
Nannochloropsis sp.	0,8	NA	Aquaculture feed	NA	NA	

7.3 Discussion of the state-of-the-art

7.3.1 Illumination of the biofilm

Light stimulates the growth of phototrophic biofilms. Sunlight is free but subjected to natural day/night variation combined with additional variation in intensity due to cloud cover and shading (e.g., because of changing sun angle). This highly changeable nature of sunlight makes it challenging to efficiently capture sunlight. Despite these challenges, sunlight is preferred because employing artificial illumination results in substantial production costs and a negative energy balance (Blanken et al. 2013).

It has been proposed that the incident sunlight on ground area can be diluted over a larger photobioreactor surface (Liu et al. 2012; Schultze et al. 2015; Wijffels and Barbosa 2010) which is beneficial because light of low intensity is utilized more efficiently by microalgae (Figure 7.1). On high intensity days with clear skies, the major part of sunlight is beam light. The intensity of these beams can be reduced by optical engineering (Breuer et al. 2015), however, due to the changing solar angles, it is not possible to maximally benefit from this effect during the day and in different seasons. Therefore, in practice, sections of the photobioreactor surface will experience high intensity beam light while the other surfaces will only experience low intensity diffuse and reflected light. Based on the above discussion, extrapolating small-scale studies to large-scale areal biomass productivities could overestimate productivity. Therefore, it was decided not to include such extrapolations in Table 7.1 (relevant for (Liu et al. 2012; Schultze et al. 2015)).

7.3.2 Material requirements

Material requirement is an important parameter for the construction costs of a biofilm photobioreactor and can be derived from the schematics depicted in Figure 7.2. Rotating biofilm designs will require more material and supporting equipment compared to a biofilm design without moving parts simply because a liquid container plus a device to rotate the biofilm must be constructed. In addition, it is

required to cover the reactor such that high CO_2 concentrations can be maintained to allow for maximal light-limited production.

From a design and operating perspective, a robust photobioreactor design contains no or minimal moving components as this saves on engineering costs and energy and also minimizes the chance of technical failure. In regard to rotating biofilms, a large scale reactor will consist of a considerable number of small rotating units. The size of a single rotating unit is limited and the larger it is designed, the larger the forces on axels and engines. Furthermore, it is essential that rotation does not fail because biofilms exposed to the gas phase will dry out quickly which will impact productivity and may possibly require re-inoculation to replace the dried biomass. A biofilm photobioreactor without rotating parts, therefore, will be a safer and more economical choice for large scale implementation.

7.3.3 Harvesting

In practice, almost all systems are harvested by scraping (Table 7.1). In the usually small biofilm reactors tested in scientific studies, harvesting is performed by manually scraping the biofilm. Exceptions are the rotating drum reactor, the algal turf scrubber, and the rotating brush reactor of which the latter two are employed on a commercial scale. The algal turf scrubber uses scraping in combination with a vacuum to transport the algal paste (Adey et al. 2011). The rotating brush reactor utilizes water shear, diluting the concentrated biofilm such that it is able to flow like liquid (this observation is based on a public video) (2016a). It is likely that harvesting of algal biofilm will become more economical with larger scale algae production as machines that are more advanced can be designed. For rotating biofilms, the rotation of the biofilm can be employed to harvest a single rotation unit. However, the harvesting device will need to be diligently aligned with every rotational unit. As a large farm will contain numerous small rotational units, the mechanical design of a harvesting device that harvests large static biofilm units will be easier and more economical to construct.

7.3.4 Nutrient supply

Nutrient supply can be divided into components transferred through a gas phase flow (CO_2 and O_2) and dissolved species transferred via liquid flow. Most biofilm photobioreactor designs have an extensive interfacial area between gas and biofilm and, consequently, none of the current state of the art designs require sparging of the liquid which reduces the energy footprint. Although microalgal biofilms are more productive when cultivated on atmospheric CO_2 compared to open production ponds (Christenson and Sims 2012; Gross and Wen 2014), productivity can be further increased when supplying concentrated CO_2 (Blanken et al. 2014; Schultze et al. 2015). The minimal CO_2 concentrations that can be employed will vary between photobioreactor designs, the CO_2 utilization efficiency required, and the biofilm-gas interfacial area. For instance, the rotating fabric sheet and rotating brush design have a larger biofilm-gas interphase area compared to the other designs (Figure 7.2). Therefore, these designs can feature lower CO_2 concentrations without impacting productivity. Based on Figure 7.2, the Algal turf scrubber and Algadisk have the lowest biofilm-gas interphase. Regardless of this, it was calculated that a 96% CO_2 utilization efficiency could be obtained with only a 2% productivity penalty in the Algadisk system (Chapter 6).

The supply of dissolved nutrients is more rapid for perfused systems in comparison to periodically submerged systems. Perfused systems have a fixed interfacial area with the liquid while periodically submerged biofilms are continuously alternating between submerged and exposed stages. Consumption of the dissolved nutrients will continue during the exposed stages. Therefore, during the submerged stage, mass flux of dissolved nutrients into the biofilm has to be such that sufficient nutrients are stored inside the biofilm to support consumption during the exposed stage. To obtain sufficient nutrient storage, higher bulk dissolved nutrient concentrations are required compared to perfused systems, therefore, periodically submerged systems are limited to nutrient streams that are more concentrated.

7.3.5 Hydrodynamic shear stress

Hydrodynamic shear stress can result in loss of biofilm biomass to the liquid. Technically, this biomass is not lost, but it will require more energy to harvest it from the water stream (Pahl et al. 2013), therefore, it is preferred to minimize biofilm loss due to shear. In the perfused systems, there is no direct contact between the biofilm and the liquid so there is no shear force acting on the biofilm. For the periodically submerged systems, the actual shear loss depends on the design and liquid flow rates over the biofilm surface (Roeselers et al. 2008). In the case of the Algadisk, no direct relation was found between rotation speed and shear loss (Blanken et al. 2014), although 19% of the total produced biomass was harvested from the bulk liquid (Chapter 5). In regard to the rotating drum reactor, the suspended algae concentration was reported to decrease over time (Christenson and Sims 2012).

7.3.6 Species control

Species control is especially challenging when moving to large scale algae production facilities. The primary issue is that the species of choice can be overgrown by other more aggressive algal species and or algae grazers (Mooij et al. 2015). For this reason, algae that tolerate extreme culture conditions such as *Spirulina* (tolerates high pH) and *Duniella salina* (tolerates high salinity) perform well on a large scale (Del Campo et al. 2007). Another approach is to reduce the consequences of invading species by separating the algae biomass from the bulk liquid which is a characteristic of perfused biofilm photobioreactors. By separation, invading species that enter the system through the air are only able to create a local colony and are prevented from spreading rapidly via the liquid, making containment of infection possible. To make this strategy successful, it is required that the membrane is axenically inoculated. The possibility of containing infections in perfused systems can possibly further stabilize large scale cultivations as culture crashes can potentially be prevented.

7.4 Proposed new biofilm photobioreactor design

Based on the evaluation of the state-of-the-art design, elements were combined into a new and improved conceptual biofilm photobioreactor design. This design consists of a liquid body within a spacer with a hydrophilic membrane on top on which the biofilm is cultivated (Figure 7.3). These design guidelines can be employed as the basis for a detailed engineering of a biofilm photobioreactor. The advantages of this system are:

- High dry solid concentration of harvest
- Harvesting by scraping from a flat horizontal surface
- Species control by separating biomass from the liquid
- Flexible HRT with no biomass loss due to shear stress
- Temperature control by evaporation and/or a heat exchanger
- Minimal material requirements
- Minimal mechanical movement
- Utilization of turbid nutrient streams

In this design, the key component is the membrane. Key features for the membrane include: durable, non-biodegradable, less expensive, and structured. The structure should provide for the optimal amount of biomass remaining on the membrane after harvesting to allow for rapid regrowth. When the substratum satisfies these requirements, it is likely that the biofilm photobioreactor can be operated for long periods of time; therefore, the initial attachment of the algae to the substratum is of secondary importance. In addition, the hydrophilic membrane should facilitate the diffusion of dissolved nutrients of both anions and cations and prevent the passage of microalgae and bacteria. Rapid diffusion requires a high porosity and minimal thickness while preventing the passage of biomass will limit the maximal pore size, hence, membrane choice will be a compromise between these two features. Finally, the gas phase above the biofilm should be closed so that concentrated CO_2 can be supplied which must be filtered to remove potential airborne infections.

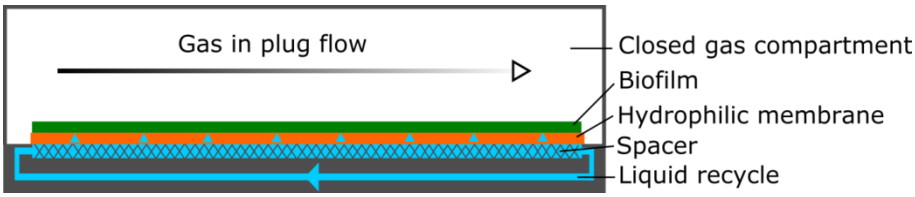

Figure 7.3. Schematic description of an improved conceptual biofilm photobioreactor design.

7.5 Improved process control for phototropic biofilms

Operating a biofilm photobioreactor requires an adequate bioprocess control. Important parameters that influence the productivity are light intensity and temperature which both fluctuate over time. Consequently, the biofilm productivity will vary during the day according to the diel variations and weather conditions. At the same time, the biomass nutrient requirements will differ in accordance with biofilm productivity. For a further improvement of the biofilm photobioreactor productivity, bioprocess control strategies that allow for maximal productivity and maximal nutrient utilization efficiency were suggested and include:

- Management of biofilm thickness by harvesting frequency and substratum choice;
- Temperature control by evaporation and/or by a heat exchanger and an external water source;
- Plug flow movement of nutrients containing water such that nutrient losses are minimized.

7.5.1 Harvesting

By means of frequent and controlled harvesting, the thickness of the biofilm is regulated. The optimal biofilm thickness range depends on the light supply and, after harvesting, biofilm thickness should be such that all microalgae receive light. The exact value of the optimal biofilm thickness after harvesting depends on light intensity. Based on model ((Li et al. 2016) and (Chapter 5)) and experimental observations (Li et al. 2015a), 100 µm will be almost optimal. The harvesting frequency will define how thick the biofilm will grow. Based on starvation

experiments, a harvesting frequency of two weeks will not result in cell death (Chapter 5), although periods up to 30 days are also employed (Naumann et al. 2012). Long periods of darkness, however, could result in undesirable effects such as biomass loss due to maintenance (Chapter 5);(Gary et al. 2003; Hoehler and Jorgensen 2013) and sloughing events (Boelee et al. 2013). In addition, complete biofilm illumination should be ensured when the goal is to accumulate lipids (or other energy-rich compounds) as those would be consumed in a dark zone of the biofilm in order to fuel maintenance processes.

7.5.2 Temperature control

Temperature inside a biofilm photobioreactor is important to control in order to ensure maximal productivity [ref J wolf 2016]. Thin microalgal biofilms have limited heat capacity and will heat up quickly in full sunlight (Béchet et al. 2011; Goetz et al. 2011). For large scale microalgae production, the most effective temperature control options are evaporative cooling (Béchet et al. 2011) or cooling with an external cold water source facilitated by heat exchangers (Goetz et al. 2011). Cooling with a heat exchanger and an external water source is advantageous as there is no net water consumption. This technology, however, is limited to locations where a substantial cold water source is available (e.g., seawater). Evaporation will require a relatively small, fresh water flow. Consequently, this water is lost which can be challenging and costly in dry locations.

To compare the two cooling options, the water requirements to maintain a stable temperature are listed for three locations in Table 7.3 while assuming a culture temperature of 30 ^{o}C. The actual set point for temperature control is strain dependent; strains with a high temperature tolerance will have lower water requirements compared to strains with lower optimal temperatures. In practice, evaporative cooling from the wet biofilm itself will require high flow rates of relatively dry gas. The gas retention time is thus limited, and it will be challenging to prevent CO_2 limitation and/or CO_2 loss via the off-gas. Therefore, the cooling strategy will likely be a combination of a heat exchanger, evaporation from the biofilm surface, and possibly spraying of the outside of the biofilm reactor.

Table 7.3. Water requirements to maintain optimal culture temperature evaluated for the highest irradiance month at three locations. Sunlight power is obtained from PVGIS (2016b) and sea temperatures are based on local measurements. A heat of vaporization of 2249 kJ kg^{-1} was employed. The amount of cooling water required was estimated with a heating capacity of 3993 J $(kg\ K)^{-1}$ and an outflowing water temperature of 28 ^{o}C.

Location		Month	Sea T	Sunlight	Evaporation	Cooling water
	° North		^{o}C	Wh $(m^2\ day)^{-1}$	L $(m^2\ day)^{-1}$	L $(m^2\ day)^{-1}$
Netherlands	52	June	15	5330	8,5	370
South Spain	40	July	22	8070	12,9	1213
Egypt	29	June	22*	8250	13,2	1240

* Deep sea temperature

7.5.3 Nutrient supply

To maximize productivity per ground surface, light should be the limiting substrate. The nutrient penetration depth, therefore, should be equal to or greater than the light penetration depth. Because biofilms consist of densely packed cells, nutrients are transported by diffusion. Consequently, the mass transfer rate and nutrient penetration depth are dependent on the concentration difference between bulk and biofilm. Thus to meet the required penetration depth requirement, elevated nutrient concentrations are required in the bulk liquid that is in contact with the biofilm. These relatively high bulk nutrient concentrations could lead to higher nutrient losses due to wash out of nutrient rich streams. In addition, the incident sunlight intensity is variable during the day, and the light penetration depth will change accordingly. Considering the above, it is clear that obtaining both efficient nutrient utilization and optimal productivity requires a balanced bioprocess control strategy.

To evaluate the best nutrient supply strategy, we first consider the consequences of not meeting the optimal nutrient penetration depth. Carbon dioxide is required to store the photosynthetically produced energy and is essential for optimal productivity. The penetration depth of carbon dioxide, therefore, must match that of the light. Limitations of other nutrients (e.g., nitrogen (Mooij et al. 2014) or phosphate (Ahn et al. 2002)) are more likely to not directly result in productivity

loss but, instead, lead to an accumulation of storage compounds (e.g., starch) which can be converted into functional biomass at a later point in time when light intensities are lower (Chapter 5);(Mooij et al. 2014). Therefore, dissolved nutrient concentrations do not necessarily need to be sufficiently high to match the peak light penetration depth. To summarize, it is beneficial in regard to production-plant design that both the main component required for growth (carbon dioxide) and the main inhibitor of growth (oxygen) are controlled by gas flow as this allows coupling gas flow rate to sunlight intensity while decoupling the supply of dissolved nutrients via the liquid phase (Figure 7.4A).

Preventing carbon dioxide limited microalgae growth is not difficult (Blanken et al. 2014; Gross et al. 2013; Schultze et al. 2015), however, the challenge is to supply sufficient CO_2 such that CO_2 loss to the atmosphere is limited (Chapter 6). Additionally, oxygen accumulation inside the biofilm should be limited as high O_2/CO_2 ratios can inhibit microalgae growth (Pope 1975). Considering both CO_2 and O_2 concentrations, it was identified with a modeling approach that obtaining plug flow movement of gas over the biofilm surface maximizes both biofilm productivity and carbon dioxide utilization efficiency (Figure 7.4B) (Chapter 6). By employing plug flow, the majority of the biofilm is exposed to high CO_2 levels while only a minor part of the biofilm experiences CO_2 limitations. Together, this results in a limited impact on total productivity (Figure 7.4B). This strategy is easily applied when cultivating with a constant light intensity but, in reality, the light intensity will vary during the day. To compensate for the variable light intensity, the inflow of gas must be regulated automatically in accordance with light intensity (Figure 7.4). Because microalgae require lower quantities of dissolved nutrients compared to CO_2, obtaining high utilization efficiency will be easier. It will be less crucial to serve the dissolved nutrients in plug flow, and easier solutions such as feeding concentrated nutrient streams are likely sufficient.

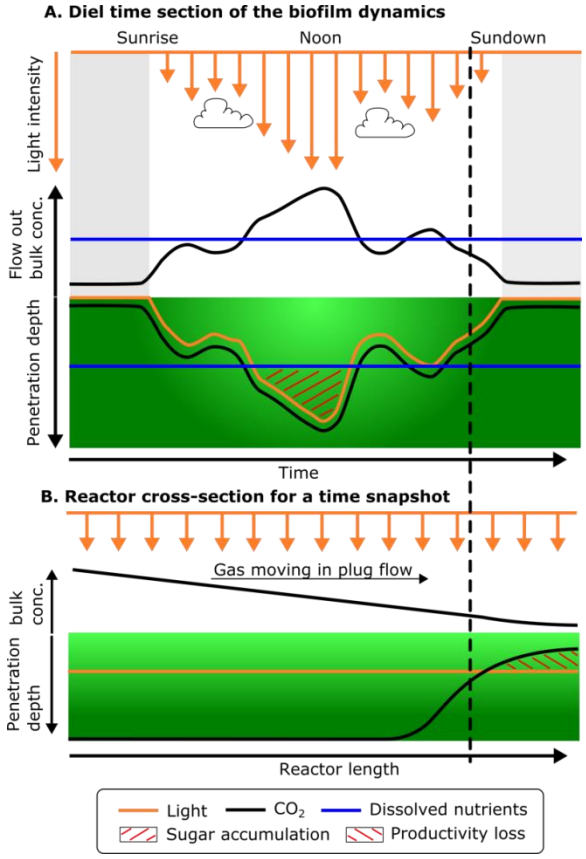

Figure 7.4. Schematic depiction that describes the considerations behind the proposed nutrient supply strategy. **A.** Diel light penetration and the required nutrient concentration fluctuations to prevent productivity loss. Top of the picture describes the incident sunlight intensity during the day. Middle layer describes the bulk concentrations required to obtain sufficient penetration depth into the biofilm. Bottom layer describes the penetration depth (of light, CO_2 and dissolved nutrients) in which the red marked area depicts the carbon that must be stored before it can be utilized for new biomass which require both dissolved nutrients and sugar. **B.** Represents a longitudinal cross-section of a biofilm reactor with gas operated in plug flow. This schematic includes an illustration of how plug flow can be employed to increase the CO_2 utilization efficiency without a significant impact on productivity. The dashed line indicates where A and B match, therefore, when the incident light intensity changes, gas flow must change accordingly.

7.6 Conclusions

State-of-the-art biofilm photobioreactors have demonstrated that phototrophic biofilms can be cultivated resulting in high productivity. With a detailed evaluation, it was identified that current photobioreactor designs and operation strategies could be further improved. Based on this evaluation, design elements from various state-of-the-art reactors were combined into an improved conceptual biofilm photobioreactor design. In addition, bioprocess control strategies were discussed that allow for optimal harvesting frequencies, efficient temperature control, and maximal nutrient utilization efficiency. By employing these guidelines in future research, the full potential of microalgal biofilm photobioreactors can be further evaluated.

References

2016a. BioProcess Algae, LLC. http://www.bioprocessalgae.com.

2016b. Photovoltaic Geographical Information System http://re.jrc.ec.europa.eu/pvgis/index.htm.

Acien FG, Fernandez JM, Magan JJ, Molina E. 2012. Production cost of a real microalgae production plant and strategies to reduce it. Biotechnol Adv 30(6):1344-53.

Adey W, Luckett C, Jensen K. 1993. Phosphorus Removal from Natural Waters Using Controlled Algal Production. Restoration Ecology 1(1):29-39.

Adey WH, Kangas PC, Mulbry W. 2011. Algal Turf Scrubbing: Cleaning Surface Waters with Solar Energy while Producing a Biofuel. BioScience 61(6):434-441.

Ahn C-Y, Chung A-S, Oh H-M. 2002. DIEL RHYTHM OF ALGAL PHOSPHATE UPTAKE RATES IN P-LIMITED CYCLOSTATS AND SIMULATION OF ITS EFFECT ON GROWTH AND COMPETITION1. Journal of Phycology 38(4):695-704.

Allen JF. 2003. Cyclic, pseudocyclic and noncyclic photophosphorylation: new links in the chain. Trends in Plant Science 8(1):15-19.

Amer L, Adhikari B, Pellegrino J. 2011. Technoeconomic analysis of five microalgae-to-biofuels processes of varying complexity. Bioresour Technol 102(20):9350-9.

Arnold W. 1949. A calorimetric determination of the quantum yield in photosynthesis. Photosynthesis in Plants. Ames, Iowa: The Iowa State College Press. p 273-276.

Baroukh C, Munoz-Tamayo R, Steyer JP, Bernard O. 2014. DRUM: a new framework for metabolic modeling under non-balanced growth. Application to the carbon metabolism of unicellular microalgae. PLoS One 9(8):e104499.

Bechet Q, Chambonniere P, Shilton A, Guizard G, Guieysse B. 2014a. Algal productivity modeling: a step toward accurate assessments of full-scale algal cultivation. Biotechnol Bioeng.

Bechet Q, Shilton A, Guieysse B. 2014b. Full-Scale Validation of a Model of Algal Productivity. Environ Sci Technol.

Béchet Q, Shilton A, Park JBK, Craggs RJ, Guieysse B. 2011. Universal Temperature Model for Shallow Algal Ponds Provides Improved Accuracy. Environmental Science & Technology 45(8):3702-3709.

Beeftink HH, van der Heijden RTJM, Heijnen JJ. 1990. Maintenance requirements: energy supply from simultaneous endogenous respiration and substrate consumption. FEMS Microbiology Letters 73(3):203-209.

Ben-Amotz A. 2004. Industrial production of microalgal cell-mass and secondary products — major industrial species — Dunaliella. Handbook of microalgal culture. Richmond,: Blackwell, Oxford. p 8.

Berner F, Heimann K, Sheehan M. 2014. Microalgal biofilms for biomass production. Journal of Applied Phycology 27(5):1793-1804.

Bjorkman O, Demmig B. 1987. Photon yield of O_2 evolution and chlorophyll fluorescence characteristics at 77 K among vascular plants of diverse origins. Planta 170:489-504.

Blanken W, Cuaresma M, Wijffels RH, Janssen M. 2013. Cultivation of microalgae on artificial light comes at a cost. Algal Research 2(4):333-340.

Blanken W, Janssen M, Cuaresma M, Libor Z, Bhaiji T, Wijffels RH. 2014. Biofilm growth of Chlorella sorokiniana in a rotating biological contactor based photobioreactor. Biotechnol Bioeng 111(12):2436-45.

Blanken W, Postma PR, de Winter L, Wijffels RH, Janssen M. 2016. Predicting microalgae growth. Algal Research 14:28-38.

Boelee NA, Temmink H, Janssen M, Buisman CJN, Wijffels RH. 2012. Scenario Analysis of Nutrient Removal from Municipal Wastewater by Microalgal Biofilms. Water 4(2):13.

Boelee NC, Janssen M, Temmink H, Shrestha R, Buisman CJ, Wijffels RH. 2014. Nutrient removal and biomass production in an outdoor pilot-scale phototrophic biofilm reactor for effluent polishing. Appl Biochem Biotechnol 172(1):405-22.

Boelee NC, Janssen M, Temmink H, Taparavičiūtė L, Khiewwijit R, Jánoska Á, Buisman CJN, Wijffels RH. 2013. The effect of harvesting on biomass production and nutrient removal in phototrophic biofilm reactors for effluent polishing. Journal of Applied Phycology.

References

Breuer G, Lamers PP, Janssen M, Wijffels RH, Martens DE. 2015. Opportunities to improve the areal oil productivity of microalgae. Bioresource Technology 186:294-302.

Breuer G, Lamers PP, Martens DE, Draaisma RB, Wijffels RH. 2012. The impact of nitrogen starvation on the dynamics of triacylglycerol accumulation in nine microalgae strains. Bioresour Technol 124:217-26.

Brilman W, Garcia Alba L, Veneman R. 2013. Capturing atmospheric CO2 using supported amine sorbents for microalgae cultivation. Biomass and Bioenergy 53:39-47.

Carvalho AP, Meireles LA, Malcata FX. 2006. Microalgal Reactors: A Review of Enclosed System Designs and Performances. Biotechnology progress 22(6):16.

Chen CY, Yeh KL, Aisyah R, Lee DJ, Chang JS. 2011. Cultivation, photobioreactor design and harvesting of microalgae for biodiesel production: a critical review. Bioresour Technol 102(1):71-81.

Chen F, Johns MR. 1991. Effect of C/N ratio and aeration on the fatty acid composition of heterotrophicChlorella sorokiniana. Journal of Applied Phycology 3(3):6.

Chen F, Johns MR. 1996. Relationship between substrate inhibition and maintenance energy of Chlamydomonas reinhardtii in heterotrophic culture. Journal of Applied Phycology 8(1):4.

Chen H-B, Wu J-Y, Wang C-F, Fu C-C, Shieh C-J, Chen C-I, Wang C-Y, Liu Y-C. 2010. Modeling on chlorophyll a and phycocyanin production by Spirulina platensis under various light-emitting diodes. Biochemical Engineering Journal 53(1):52-56.

Chen L, Zhang L, Zhang W, Liu T. 2014. Comparative analysis of growth and carotenoid accumulation of Trentepohlia arborum in aerial, subaerial, and aquatic cultivation. Journal of Applied Phycology 27(3):1079-1087.

Cheng P, Ji B, Gao L, Zhang W, Wang J, Liu T. 2013. The growth, lipid and hydrocarbon production of Botryococcus braunii with attached cultivation. Bioresour Technol 138:95-100.

Cheng P, Wang J, Liu T. 2014. Effects of nitrogen source and nitrogen supply model on the growth and hydrocarbon accumulation of immobilized biofilm cultivation of B. braunii. Bioresour Technol 166:527-33.

Christenson LB, Sims RC. 2012. Rotating algal biofilm reactor and spool harvester for wastewater treatment with biofuels by-products. Biotechnol Bioeng 109(7):1674-84.

CIE. 2013. http://www.cie.co.at.

Clarens AF, Resurreccion EP, White MA, Colosi LM. 2010. Environmental life cycle comparison of algae to other bioenergy feedstocks. Environmental Science & Technology.

Cole JK, Hutchison JR, Renslow RS, Kim YM, Chrisler WB, Engelmann HE, Dohnalkova AC, Hu D, Metz TO, Fredrickson JK and others. 2014. Phototrophic biofilm assembly in microbial-mat-derived unicyanobacterial consortia: model systems for the study of autotroph-heterotroph interactions. Front Microbiol 5:109.

Cornet J-F, Dussap C-G. 2009. A Simple and reliable formula for assessment of maximum volumetric productivities in photobioreactors. Biotechnology progress 25(2):424-435.

Cornet JF, Dussap CG, Gros JB, Binois C, Lasseur C. 1995. A simplified monodimensional approach for modeling coupling between radiant light transfer and growth kinetics in photobioreactors. Chemical Engineering Science 50(9):1489-1500.

Cuaresma Franco M, Buffing M, Janssen M, Vílchez Lobato C, Wijffels R. 2012. Performance of Chlorella sorokiniana under simulated extreme winter conditions. 24(4):693-699.

Cuaresma M, Janssen M, Vílchez C, Wijffels RH. 2009. Productivity of *Chlorella sorokiniana* in a short light-path (SLP) panel photobioreactor under high irradiance. Biotechnology and Bioengineering 104(2):352-359.

Cuaresma M, Janssen M, Vílchez C, Wijffels RH. 2011. Horizontal or vertical photobioreactors? How to improve microalgae photosynthetic efficiency. Bioresource Technology 102:5129-5137.

Davis R, Aden A, Pienkos PT. 2011. Techno-economic analysis of autotrophic microalgae for fuel production. Applied Energy 88(10):3524-3531.

de Godos I, Gonzalez C, Becares E, Garcia-Encina PA, Munoz R. 2009. Simultaneous nutrients and carbon removal during pretreated swine slurry degradation in a tubular biofilm photobioreactor. Appl Microbiol Biotechnol 82(1):187-94.

de Mooij T, Janssen M, Cerezo-Chinarro O, Mussgnug JH, Kruse O, Ballottari M, Bassi R, Bujaldon S, Wollman F-A, Wijffels RH. 2014. Antenna size reduction as a strategy to increase biomass productivity: a great potential not yet realized. Journal of Applied Phycology.

de Winter L. 2015. Circadian rhythms in microalgae production. Wageningen UR E-depot: Wageningen UR. 166 p.

de Winter L, Klok AJ, Cuaresma Franco M, Barbosa MJ, Wijffels RH. 2013. The synchronized cell cycle of Neochloris oleoabundans and its influence on biomass composition under constant light conditions. Algal Research 2(4):313-320.

Deblois CP, Marchand A, Juneau P. 2013. Comparison of Photoacclimation in Twelve Freshwater Photoautotrophs (Chlorophyte, Bacillaryophyte, Cryptophyte and Cyanophyte) Isolated from a Natural Community. PLoS ONE 8(3):e57139.

Del Campo JA, Garcia-Gonzalez M, Guerrero MG. 2007. Outdoor cultivation of microalgae for carotenoid production: current state and perspectives. Appl Microbiol Biotechnol 74(6):1163-74.

Doucha J, Lívanský K. 2006. Productivity, CO2/O2 exchange and hydraulics in outdoor open high density microalgal (Chlorella sp.) photobioreactors operated in a Middle and Southern European climate. Journal of Applied Phycology 18(6):811-826.

Draaisma RB, Wijffels RH, Ellen Slegers P, Brentner LB, Roy A, Barbosa MJ. 2012. Food commodities from microalgae. Curr Opin Biotechnol.

Droop MR. 1968. Vitamin B12 and Marine Ecology. IV. The Kinetics of Uptake, Growth and Inhibition in Monochrysis Lutheri. Journal of the Marine Biological Association of the United Kingdom 48(03):689-733.

Dubinsky Z, Falkowski PG, Wyman K. 1986. Light harvesting and utilization by phytoplankton. Plant and Cell Physiology 27(7):1335-1349.

Dubinsky Z, Stambler N. 2009. Photoacclimation processes in phytoplankton: mechanisms, consequences, and applications. Aquatic Microbial Ecology 56(2-3):163-176.

Duboc P, Marison I, Von Stockar U. 1999. Quantitative calorimetry and biochemical engineering. In: Kemp RB, editor. Handbook of Thermal Analysis and Calorimetry. Aberystwyth, Wales: Elsevier Science. p 267-365.

Dutta S. 2007. Mathematical Modeling of the Performance of a Rotating Biological Contactor for Process Optimisation in Wastewater Treatment. Karlsruhe: Universität Fridericiana. 224 p.

Emerson R, Lewis CM. 1943. The dependence of the quantum yield of *Chlorella* on wavelength of light. American Journal of Botany 30:165-178.

Energy USDo. 2010. $1/W Photovoltaic Systems. U.S. Department of Energy.

EU. 2012. www.energy.eu.

Evans JR. 1987. The Dependence of Quantum Yield on Wavelength and Growth Irradiance. Australian Journal of Plant Physiology 14:69-79.

Fachet M, Flassig RJ, Rihko-Struckmann L, Sundmacher K. 2014. A dynamic growth model of Dunaliella salina: Parameter identification and profile likelihood analysis. Bioresour Technol 173:21-31.

Fouchard S, Pruvost J, Degrenne B, Titica M, Legrand J. 2009. Kinetic modeling of light limitation and sulfur deprivation effects in the induction of hydrogen production with Chlamydomonas reinhardtii: Part I. Model development and parameter identification. Biotechnol Bioeng 102(1):232-245.

García-Camacho F, Sánchez-Mirón A, Molina-Grima E, Camacho-Rubio F, Merchuck JC. 2012. A mechanistic model of photosynthesis in microalgae including photoacclimation dynamics. Journal of Theoretical Biology 304:1-15.

Gary C, Baldet P, Bertin N, Devaux C, Tchamitchian M, Raymond P. 2003. Time-course of tomato whole-plant respiration and fruit and stem growth during prolonged darkness in relation to carbohydrate reserves. Ann Bot 91(4):429-38.

Geider RJ, Macintyre HL, Kana TM. 1996. A dynamic model of photoadaptation in phytoplankton. Limnology and Oceanography 41(1):1-15.

Geider RJ, MacIntyre HL, Kana TM. 1997. Dynamic model of phytoplankton growth and acclimation: responses of the balanced growth rate and the chlorophyll a:carbon ratio to light, nutrient-limitation and temperature. Marine Ecology Progress Series 148:187-200.

Geider RJ, Osborne BA. 1989. Respiration and microalgal growth - A review of the quantitative relationship between dark respiration and growth. New Phytologist 112(3):327-341.

Genin SN, Stewart Aitchison J, Grant Allen D. 2014. Design of algal film photobioreactors: material surface energy effects on algal film productivity, colonization and lipid content. Bioresour Technol 155:136-43.

Giordano M, Beardall J, Raven JA. 2005. CO2 concentrating mechanisms in algae: mechanisms, environmental modulation, and evolution. Annu Rev Plant Biol 56:99-131.

Goetz V, Le Borgne F, Pruvost J, Plantard G, Legrand J. 2011. A generic temperature model for solar photobioreactors. Chemical Engineering Journal 175:443-449.

Gordon JM, Polle JE. 2007. Ultrahigh bioproductivity from algae. Appl Microbiol Biotechnol 76(5):969-75.

Graus W, Roglieri M, Jawarski P, Alberio L. 2008. Efficiency and capture-readiness of new fossil power plants in the EU. Utrecht: Ecofys Netherlands bv. 70 p.

Grobbelaar JU, Kurano N. 2003. Use of photoacclimation in the design of a novel photobioreactor to achieve high yields in algal mass cultivation. Journal of Applied Phycology 15(2):121-126.

Gross M, Henry W, Michael C, Wen Z. 2013. Development of a rotating algal biofilm growth system for attached microalgae growth with in situ biomass harvest. Bioresour Technol 150C:195-201.

Gross M, Jarboe D, Wen Z. 2015. Biofilm-based algal cultivation systems. Appl Microbiol Biotechnol 99(14):5781-9.

Gross M, Wen Z. 2014. Yearlong evaluation of performance and durability of a pilot-scale Revolving Algal Biofilm (RAB) cultivation system. Bioresour Technol 171:50-8.

Harned HS, Davis R. 1943. The Ionization Constant of Carbonic Acid in Water and the Solubility of Carbon Dioxide in Water and Aqueous Salt Solutions from 0 to 50°. Journal of the American Chemical Society 65(10):2030-2037.

Harris GP, Piccinin BB, van Ryn J. 1983. Physical variability and phytoplankton communities V. Cell size, niche diversification and the role of competition. Arch. Hydrobiol. 98:24.

Heinrich JM, Niizawa I, Botta FA, Trombert AR, Irazoqui HA. 2012. Analysis and design of photobioreactors for microalgae production I: method and parameters for radiation field simulation. Photochem Photobiol 88(4):938-51.

Hoefnagel MHN, Atkin OK, Wiskich JT. 1998. Interdependence between chloroplasts and mitochondria in the light and the dark. Biochimica et Biophysica Acta 1366:235-255.

Hoehler TM, Jorgensen BB. 2013. Microbial life under extreme energy limitation. Nat Rev Microbiol 11(2):83-94.

Hoekema S, Rinzema A, Tramper J, Wijffels RH, Janssen M. 2014. Deceleration-stats save much time during phototrophic culture optimization. Biotechnol Bioeng 111(4):792-802.

Hogewoning SW, Wientjes E, Douwstra P, Trouwborst G, van Ieperen W, Croce R, Harbinson J. 2012. Photosynthetic quantum yield dynamics: from photosystems to leaves. Plant Cell 24(5):1921-35.

Jacobi AJC. 2013. Optimierung der Lichtverteilung in Photobioreaktoren. Deutsche national bibliothek: Karlsruher Institut für Technologie.

Jacobsen A, Grahl-Nielsen O, Magnesen T. 2010. Does a large-scale continuous algal production system provide a stable supply of fatty acids to bivalve hatcheries? Journal of Applied Phycology 22(6):769-777.

Janssen M, de Winter M, Tramper J, Mur LR, Snel JFH, Wijffels RH. 2000. Efficiency of light utilization of *Chlamydomonas reinhardtii* under medium-duration light/dark cycles. Journal of Biotechnology 78:123-137.

Janssen M, Kuijpers TC, Veldhoen B, Ternbach MB, Tramper J, Mur LR, Wijffels RH. 1999. Specific growth rate of Chlamydomonas reinhardtii and Chlorella sorokiniana under medium duration light/dark cycles: 13–87 s. Journal of Biotechnology 70(1–3):323-333.

References

Jassby AD, Platt T. 1976. Mathematical Formulation of the Relationship Between Photosynthesis and Light for Phytoplankton. Limnology and Oceanography 21(4):540-547.

Ji B, Zhang W, Zhang N, Wang J, Lutzu GA, Liu T. 2013a. Biofilm cultivation of the oleaginous microalgae Pseudochlorococcum sp. Bioprocess Biosyst Eng.

Ji C, Wang J, Zhang W, Liu J, Wang H, Gao L, Liu T. 2013b. An applicable nitrogen supply strategy for attached cultivation of Aucutodesmus obliquus. Journal of Applied Phycology.

Johnson MB, Wen Z. 2010. Development of an attached microalgal growth system for biofuel production. Appl Microbiol Biotechnol 85(3):525-34.

Keith DW. 2009. Why Capture CO2 from the Atmosphere? Science 325(5948):1654-1655.

Kliphuis A, Klok A, Martens D, Lamers P, Janssen M, Wijffels R. 2011a. Metabolic modeling of *Chlamydomonas reinhardtii*: energy requirements for photoautotrophic growth and maintenance. Journal of Applied Phycology:1-14.

Kliphuis AJ, Janssen M, van den End E, Martens D, Wijffels R. 2011b. Light respiration in Chlorella sorokiniana. 23(6):935-947.

Kliphuis AMJ, Martens DE, Janssen M, Wijffels RH. 2011c. Effect of O2:CO2 ratio on the primary metabolism of Chlamydomonas reinhardtii. Biotechnology and Bioengineering 108(10):2390-2402.

Kliphuis AMJ, Winter L, vejrazka C, Martens DE, Janssen M, Wijffels RH. 2010. Photosynthetic efficiency of Chlorella sorokiniana in a turbulently mixed short light-path photobioreactor. Biotechnology Progress 26(3):9.

Klok AJ, Verbaanderd JA, Lamers PP, Martens DE, Rinzema A, Wijffels RH. 2013. A model for customising biomass composition in continuous microalgae production. Bioresour Technol 146:89-100.

Kubsad V, Chaudhari S, Gupta SK. 2004. Model for oxygen transfer in rotating biological contactor. Water Res 38(20):4297-304.

Kugaprasatham S, Nagaoka H, Ohgaki S. 1992. Effect of turbulence on nitrifying biofilms at non-limiting substrate conditions. Water Res 26(12):1629-1638.

Lackner KS. 2013. The thermodynamics of direct air capture of carbon dioxide. Energy 50:38-46.

Le Borgne F, Pruvost J. 2013. Investigation and modeling of biomass decay rate in the dark and its potential influence on net productivity of solar photobioreactors for microalga Chlamydomonas reinhardtii and cyanobacterium Arthrospira platensis. Bioresour Technol 138:271-6.

Lee CG, Palsson BØ. 1994. Hig h-Density Algal Photobioreactors Using Light-Emitting Diodes. Biotechnology and bioengineering 44(10):7.

Lee E, Pruvost J, He X, Munipalli R, Pilon L. 2014. Design tool and guidelines for outdoor photobioreactors. Chemical Engineering Science 106:18-29.

Lee Y-K, Ding S-Y, Hoe C-H, Low C-S. 1996. Mixotrophic growth ofChlorella sorokiniana in outdoor enclosed photobioreactor. Journal of Applied Phycology 8(2):6.

Ley AC, Mauzerall DC. 1982. The reversible decline of oxygen flash yields at high flash energies evidence for total annihilation of excitations in photosystem II. Biochimica et Biophysica Acta 680:174-180.

Li T, Piltz B, Podola B, Dron A, de Beer D, Melkonian M. 2015a. Microscale profiling of photosynthesis-related variables in a highly productive biofilm photobioreactor. Biotechnol Bioeng.

Li T, Podola B, de Beer D, Melkonian M. 2015b. A method to determine photosynthetic activity from oxygen microsensor data in biofilms subjected to evaporation. J Microbiol Methods 117:100-7.

Li T, Podola B, Melkonian M. 2016. Investigating dynamic processes in a porous substrate biofilm photobioreactor — A modeling approach. Algal Research 13:30-40.

Li T, Zheng Y, Yu L, Chen S. 2014. Mixotrophic cultivation of a Chlorella sorokiniana strain for enhanced biomass and lipid production. Biomass and Bioenergy 66:204-213.

Lin YH, Leu JY, Lan CR, Lin PHP, Chang FL. 2003. Kinetics of inorganic carbon utilization by microalgal biofilm in a flat plate photoreactor. Chemosphere 53(7):779-787.

Liu T, Wang J, Hu Q, Cheng P, Ji B, Liu J, Chen Y, Zhang W, Chen X, Chen L and others. 2012. Attached cultivation technology of microalgae for efficient biomass feedstock production. Bioresour Technol 127C:216-222.

Liu Z, Liu S, Wang K, Luo X. 2009. Status and prospects for phosphor-based white LED packaging. Frontiers of Optoelectronics in China 2(2):119-140.

Lu C, Li H-C, Lee LY, Lin M-R. 1997. Effects of disc rotational speed and submergence on the performance of an anaerobic rotating biological contactor. Environment International 23(2):253-263.

Lumileds P. 2012. http://www.philipslumileds.com.

Luo HP, Al-Dahhan MH. 2012. Airlift column photobioreactors for Porphyridium sp. culturing: Part II. verification of dynamic growth rate model for reactor performance evaluation. Biotechnol Bioeng 109(4):942-9.

Malkin S, Fork DC. 1996. Bill Arnold and calorimetric measurements of the quantum requirement of photosynthesis - once again ahead of his time. Photosynthesis Research 48:41-46.

Mayer DG, Butler DG. 1993. Statistical validation. Ecological Modelling 68(1–2):21-32.

Milledge JJ. 2010. Commercial application of microalgae other than as biofuels: a brief review. Reviews in Environmental Science and Bio/Technology 10(1):31-41.

Mooij PR, Graaff DR, Loosdrecht MCM, Kleerebezem R. 2014. Starch productivity in cyclically operated photobioreactors with marine microalgae—effect of ammonium addition regime and volume exchange ratio. Journal of Applied Phycology 27(3):1121-1126.

Mooij PR, Stouten GR, van Loosdrecht MCM, Kleerebezem R. 2015. Ecology-based selective environments as solution to contamination in microalgal cultivation. Current Opinion in Biotechnology 33:46-51.

Morales-Rodriguez R, Singh R, Cameron I, Gani R. 2011. Chapter 12 - Modelling for Bio-,Agro- and Pharma-Applications*. Product and Process Modelling. Amsterdam: Elsevier. p 363-432.

Munoz Sierra JD, Picioreanu C, van Loosdrecht MC. 2014. Modeling phototrophic biofilms in a plug-flow reactor. Water Sci Technol 70(7):1261-70.

Murphy TE, Berberoglu H. 2014. Flux balancing of light and nutrients in a biofilm photobioreactor for maximizing photosynthetic productivity. Biotechnol Prog 30(2):348-59.

Myers J, Graham J. 1971. The Photosynthetic Unit in Chlorella Measured by Repetitive Short Flashes. Plant Physiology 48(1):4.

Narukawa Y, Ichikawa M, Sanga D, Sano M, Mukai T. 2010. White light emitting diodes with super-high luminous efficacy. Journal of Physics D: Applied Physics 43(35):354002.

Naumann T, Çebi Z, Podola B, Melkonian M. 2012. Growing microalgae as aquaculture feeds on twin-layers: a novel solid-state photobioreactor. Journal of Applied Phycology 25(5):1413-1420.

Nielsen ES, Jensen PK. 1958. Concentration of Carbon Dioxide and Rate of Photosynthesis in Chlorella pyrenoidosa. Physiologia Plantarum 11(1):170-180.

Norsker NH, Barbosa MJ, Vermue MH, Wijffels RH. 2011. Microalgal production--a close look at the economics. Biotechnol Adv 29(1):24-7.

Nowack EC, Podola B, Melkonian M. 2005. The 96-well twin-layer system: a novel approach in the cultivation of microalgae. Protist 156(2):239-51.

Orandi S, Lewis DM, Moheimani NR. 2012. Biofilm establishment and heavy metal removal capacity of an indigenous mining algal-microbial consortium in a photo-rotating biological contactor. J Ind Microbiol Biotechnol 39(9):1321-31.

Ozkan A, Kinney K, Katz L, Berberoglu H. 2012. Reduction of water and energy requirement of algae cultivation using an algae biofilm photobioreactor. Bioresour Technol 114:542-8.

Pahl SL, Lee AK, Kalaitzidis T, Ashman PJ, Sathe S, Lewis DM. 2013. Harvesting, Thickening and Dewatering Microalgae Biomass.165-185.

Paradiso R, Meinen E, Snel JFH, De Visser P, Van Ieperen W, Hogewoning SW, Marcelis LFM. 2011. Spectral dependence of photosynthesis and light absorptance in single leaves and canopy in rose. Scientia Horticulturae 127(4):548-554.

Patwardhan AW. 2003. Rotating Biological Contactors: A Review. Industrial & Engineering Chemistry Research 42(10):2035-2051.

Philips. 2012a. http://www.lighting.philips.com.

Philips. 2012b. Personal communication.

Picioreanu C, van Loosdrecht MCM, Heijnen JJ. 2000. A theoretical study on the effect of surface roughness on mass transport and transformation in biofilms. Biotechnol Bioeng 68(4):355-369.

Pickett JM. 1975. Growth of Chlorella in a Nitrate-limited Chemostatt. Plant Physiology 55(1):3.

Pilon L, Berberoğlu H, Kandilian R. 2011. Radiation transfer in photobiological carbon dioxide fixation and fuel production by microalgae. Journal of Quantitative Spectroscopy and Radiative Transfer 112(17):2639-2660.

Pimputkar S, Speck JS, den Baars SP, Nakamura S. 2009. Prospects for LED lighting. Nature Photonics 3:3.

Pirt SJ. 1965. The maintenance energy of bacteria in growing cultures. Proceedings of the Royal Society of London, Series B: Biological Sciences 163(991):224-231.

Pope DH. 1975. Effects of light intensity, oxygen concentration, and carbon dioxide concentration on photosynthesis in algae. Microbial Ecology 2(1):1-16.

Post AF, Loogman JG, Mur LR. 1986. Photosynthesis, Carbon Flows and Growth of Oscillatoria agardhii Gomont in Environments with a Periodic Supply of Light. Microbiology 132(8):2129-2136.

Quinn J, de Winter L, Bradley T. 2011. Microalgae bulk growth model with application to industrial scale systems. Bioresource Technology 102.

Richards FJ. 1959. A Flexible Growth Function for Empirical Use. Journal of Experimental Botany 10(2):290-301.

Riedel TE, Berelson WM, Nealson KH, Finkel SE. 2013. Oxygen consumption rates of bacteria under nutrient-limited conditions. Appl Environ Microbiol 79(16):4921-31.

Roeselers G, Loosdrecht MCMv, Muyzer G. 2008. Phototrophic biofilms and their potential applications. Journal of Applied Phycology 20(3):227-235.

Ross ON, Geider RJ. 2009. New cell-based model of photosynthesis and photo-acclimation: accumulation and mobilisation of energy reserves in phytoplankton. Marine Ecology Progress Series 383:53-71.

Royce PNC, Thornhill NF. 1991. Estimation of dissolved carbon dioxide concentrations in aerobic fermentations. AIChE Journal 37(11):1680-1686.

Rubio FC, Fernandez FG, Perez JA, Camacho FG, Grima EM. 1999. Prediction of dissolved oxygen and carbon dioxide concentration profiles in tubular photobioreactors for microalgal culture. Biotechnol Bioeng 62(1):71-86.

Ruijter de JAF, Marcelis LFM, Schreurs M. 2007. Ingrediënten voor een energieneutrale belichte glastuinbouw in 2020. Arnhem: KEMA. 110 p.

Ruiz-Martinez A, Serralta J, Seco A, Ferrer J. 2016. Behavior of mixed Chlorophyceae cultures under prolonged dark exposure. Respiration rate modeling. Ecological Engineering 91:265-269.

Salim S, Gilissen L, Rinzema A, Vermue MH, Wijffels RH. 2013. Modeling microalgal flocculation and sedimentation. Bioresour Technol 144:602-7.

Samejima H, Myers J. 1958. On the Heterotrophic Growth of Chlorella pyrenoidosa. Journal of general microbiology 18(1):10.

Sander R. 2015. Compilation of Henry's law constants (version 4.0) for water as solvent. Atmos. Chem. Phys. 15(8):4399-4981.

Schnurr PJ, Espie GS, Allen DG. 2013. Algae biofilm growth and the potential to stimulate lipid accumulation through nutrient starvation. Bioresour Technol 136:337-44.

Schultze LKP, Simon M-V, Li T, Langenbach D, Podola B, Melkonian M. 2015. High light and carbon dioxide optimize surface productivity in a Twin-Layer biofilm photobioreactor. Algal Research 8:37-44.

Scialdone A, Mugford ST, Feike D, Skeffington A, Borrill P, Graf A, Smith AM, Howard M. 2013. Arabidopsis plants perform arithmetic division to prevent starvation at night. Elife 2:e00669.

Shen Y, Chen C, Chen W, Xu X. 2014a. Attached culture of Nannochloropsis oculata for lipid production. Bioprocess Biosyst Eng 37(9):1743-8.

Shen Y, Xu X, Zhao Y, Lin X. 2014b. Influence of algae species, substrata and culture conditions on attached microalgal culture. Bioprocess Biosyst Eng 37(3):441-50.

Shen Y, Zhang H, Xu X, Lin X. 2015. Biofilm formation and lipid accumulation of attached culture of Botryococcus braunii. Bioprocess Biosyst Eng 38(3):481-8.

Shi J, Podola B, Melkonian M. 2007. Removal of nitrogen and phosphorus from wastewater using microalgae immobilized on twin layers: an experimental study. Journal of Applied Phycology 19(5):417-423.

Shi J, Podola B, Melkonian M. 2014. Application of a prototype-scale Twin-Layer photobioreactor for effective N and P removal from different process stages of municipal wastewater by immobilized microalgae. Bioresour Technol 154:260-6.

Shi X, Chen F, Yuan J, Chen H. 1997. Heterotrophic production of lutein by selected Chlorella strains. Journal of Applied Phycology 9(1):5.

Slegers PM, Wijffels RH, van Straten G, van Boxtel AJB. 2011. Design scenarios for flat panel photobioreactors. Applied Energy 88(10):3342-3353.

Sorokin C, Myers J. 1953. A high-temperature strain of *Chlorella*. Science 117(3039):330-331.

Spolaore P, Joannis-Cassan C, Duran E, Isambert A. 2006. Commercial applications of microalgae. J Biosci Bioeng 101(2):87-96.

Stitt M, Zeeman SC. 2012. Starch turnover: pathways, regulation and role in growth. Curr Opin Plant Biol 15(3):282-92.

Stumm W, Morgan JJ. 1995. Aquatic Chemistry: Chemical Equilibria and Rates in Natural Waters, 3rd Edition. Wiley. p 1040

Takache H, Christophe G, Cornet J-F, Pruvost J. 2010. Experimental and theoretical assessment of maximum productivities for the microalgae *Chlamydomonas reinhardtii* in two different geometries of photobioreactors. Biotechnology Progress 26(2):431-440.

Takache H, Pruvost J, Cornet JF. 2012. Kinetic modeling of the photosynthetic growth of Chlamydomonas reinhardtii in a photobioreactor. Biotechnol Prog 28(3):681-92.

Tanada T. 1951. The photosynthetic efficiency of carotenoid pigments in *Navicula minima*. American Journal of Botany 38:276-283.

Tredici MR. 2010. Photobiology of microalgae mass cultures: understanding the tools for the next green revolution. Biofuels 1(1):19.

Tribe LA, Briens CL, Margaritis A. 1995. Determination of the volumetric mass transfer coefficient (kLa) using the dynamic "gas out–gas in" method: Analysis of errors caused by dissolved oxygen probes. Biotechnology and Bioengineering 46(4):388-392.

Tuantet K. 2015. Microalgae cultivation for nutrient recovery from human urine. Wageningen: Wageningen University. 174 p.

Tuantet K, Temmink H, Zeeman G, Janssen M, Wijffels RH, Buisman CJN. 2014. Nutrient removal and microalgal biomass production on urine in a short light-path photobioreactor. Water Res 55(0):162-174.

Valiorgue P, Ben Hadid H, El Hajem M, Rimbaud L, Muller-Feuga A, Champagne JY. 2014. CO2 mass transfer and conversion to biomass in a horizontal gas–liquid photobioreactor. Chemical Engineering Research and Design 92(10):1891-1897.

van 't Riet k, Tramper J. 1991. Basic bioreactor design. New York: Marcel Dekker, INC. 465 p.

Van Wagenen J, Holdt SL, De Francisci D, Valverde-Perez B, Plosz BG, Angelidaki I. 2014. Microplate-based method for high-throughput screening of microalgae growth potential. Bioresour Technol 169:566-72.

Van Wagenen J, Pape ML, Angelidaki I. 2015. Characterization of nutrient removal and microalgal biomass production on an industrial waste-stream by application of the deceleration-stat technique. Water Res 75:301-11.

Vanthoor-Koopmans M, Wijffels RH, Barbosa MJ, Eppink MHM. 2013. Biorefinery of microalgae for food and fuel. Bioresource Technology 135:142-149.

Vejrazka C, Janssen M, Benvenuti G, Streefland M, Wijffels RH. 2013. Photosynthetic efficiency and oxygen evolution of Chlamydomonas reinhardtii under continuous and flashing light. Appl Microbiol Biotechnol 97(4):1523-32.

Vejrazka C, Janssen M, Streefland M, Wijffels RH. 2011. Photosynthetic efficiency of Chlamydomonas reinhardtii in flashing light. Biotechnol Bioeng 108(12):2905-13.

Vejrazka C, Janssen M, Streefland M, Wijffels RH. 2012. Photosynthetic efficiency of Chlamydomonas reinhardtii in attenuated, flashing light. Biotechnol Bioeng 109(10):2567-2574.

von Stockar U, Gustafsson L, Larsson C, Marison I, Tissot P, Gnaiger E. 1993. Thermodynamic considerations in constructing energy balances for cellular growth. Biochimica et Biophysica Acta 1183:221-240.

von Stockar U, Liu JS. 1999. Does microbial life always feed on negative entropy? Thermodynamic analysis of microbial growth. Biochimica et Biophysica Acta (BBA) - Bioenergetics 1412(3):20.

von Stockar U, Marison I, Janssen M, Patiño R. 2011. Calorimetry and thermodynamic aspects of heterotrophic, mixotrophic, and phototrophic growth. Journal of Thermal Analysis and Calorimetry 104(1):45-52.

Wagner W, Pruss A. 1993. International Equations for the Saturation Properties of Ordinary Water Substance. Revised According to the International Temperature Scale of 1990. Addendum to J. Phys. Chem. Ref. Data 16, 893 (1987). Journal of Physical and Chemical Reference Data 22(3):783-787.

Walls PL, Bird JC, Bourouiba L. 2014. Moving with bubbles: a review of the interactions between bubbles and the microorganisms that surround them. Integr Comp Biol 54(6):1014-25.

Webb W, Newton M, Starr D. 1974. Carbon dioxide exchange of Alnus rubra. Oecologia 17(4):281-291.

Wei Q, Hu Z, Li G, Xiao B, Sun H, Tao M. 2008. Removing nitrogen and phosphorus from simulated wastewater using algal biofilm technique. Frontiers of Environmental Science & Engineering in China 2(4):446-451.

Wesselingh JA, Krishna R. 2006. Mass Transfer in Multicomponent Mixtures Delft, The Netherlands: VSSD. 329 p.

Wijffels RH, Barbosa MJ. 2010. An outlook on microalgal biofuels. Science 329(5993):796-9.

Wijffels RH, Barbosa MJ, Eppink MHM. 2010. Microalgae for the production of bulk chemicals and biofuels. Biofuels, Bioproducts and Biorefining 4(3):8.

Wilke CR, Chang P. 1955. Correlation of diffusion coefficients in dilute solutions. AIChE Journal 1(2):264-270.

Wilkie AC, Mulbry W. 2002. Recovery of dairy manure nutrients by benthic freshwater algae. Bioresour Technol 84(1):10.

Wolf G, Picioreanu C, van Loosdrecht MC. 2007. Kinetic modeling of phototrophic biofilms: the PHOBIA model. Biotechnol Bioeng 97(5):1064-79.

Yang A. 2011. Modeling and Evaluation of CO2Supply and Utilization in Algal Ponds. Industrial & Engineering Chemistry Research 50(19):11181-11192.

Yen H-W, Ho S-H, Chen C-Y, Chang J-S. 2015. CO2, NOx and SOx removal from flue gas via microalgae cultivation: A critical review. Biotechnology Journal 10(6):829-839.

Yin S, Wang J, Chen L, Liu T. 2015. The water footprint of biofilm cultivation of Haematococcus pluvialis is greatly decreased by using sealed narrow chambers combined with slow aeration rate. Biotechnol Lett 37(9):1819-27.

Zhang D, Dechatiwongse P, Hellgardt K. 2015. Modelling light transmission, cyanobacterial growth kinetics and fluid dynamics in a laboratory scale multiphase photo-bioreactor for biological hydrogen production. Algal Research 8:99-107.

Zhevalkink JA, Kelderman P, Boelhouwer C. 1978. Liquid film thickness in a rotating disc gas-liquid contactor. Water Research 12(8):577-581.

References

Zijffers JW, Schippers KJ, Zheng K, Janssen M, Tramper J, Wijffels RH. 2010. Maximum photosynthetic yield of green microalgae in photobioreactors. Marine biotechnology 12.

Zittelli GC, Rodolfi L, Biondi N, Tredici MR. 2006. Productivity and photosynthetic efficiency of outdoor cultures of Tetraselmis suecica in annular columns. Aquaculture 261:932-943.

Summary

Microalgae can be used to produce high-value compounds, such as pigments or high value fatty acids, or as a feedstock for lower value products such as food and feed compounds, biochemicals, and biofuels. In order to produce these bulk products competitively, it is required to lower microalgae production cost. Production costs could be reduced by employing microalgae biofilms as a production platform. The main advantages of microalgae biofilms are a direct harvest of concentrated microalgae paste, and the uncoupling of the hydraulic retention time from the microalgal retention time. The latter allows to decrease the liquid volume or to employ dilute waste streams. To successfully employ biofilms, however, it is required that microalgal biofilms can be cultivated at high productivity and high photosynthetic efficiency. The aim of this thesis was to optimize the productivity of microalgal biofilms.

Light energy drives microalgal growth. Sunlight is free and abundant, but sunlight intensity varies over the day and the seasons. This makes it impossible to maintain optimal production conditions throughout the day. These fluctuations in irradiance can be prevented by applying artificial lighting. Although, artificial lighting will supply a constant light intensity and thus increase productivity and simplify process control, it will also increase microalgae production cost. A quantitative evaluation of lighting costs and energy requirement was still missing and this was the topic of **Chapter 2**. The costs related to artificial lighting were identified as 25.3 $ per kilogram of dry-weight biomass, with only 4% to 6% of the electrical energy required to power the lamps eventually stored as chemical energy in microalgal biomass. Energy loss and increased production cost may be acceptable for the production of high value products, but in general they should be avoided.

In **Chapter 3**, a photobioreactor design based on a rotating biological contactor (RBC) was introduced and used as a production platform for microalgal biomass cultivated in a biofilm. In the photobioreactor, referred to as the Algadisk, microalgae grow in biofilm on vertical rotating disks partially submerged in water with dissolved nutrients. The objective was to evaluate the potential of the Algadisk photobioreactor, and identify the window of operation of the process with respect to

the effects of disk roughness, disk rotation speed and CO_2 concentration. These parameters were evaluated in relation to biomass productivity, photosynthetic efficiency, and the long-term cultivation stability of the production process.

The mesophilic green microalga *Chlorella sorokiniana* was used as a model organism. In the lab-scale Algadisk reactor, a productivity of 20.1 ±0.7 gram per m^2 disk surface per day and a biomass yield on light of 0.9 ±0.04 gram dry weight biomass per mol photons were obtained. This productivity could be retained over 21 weeks without re-inoculation. To obtain maximal and stable productivity it was important that the disk surface provides a structure that allows biomass retention on the disk after harvest. The retained biomass acts as inoculum for the new biofilm and is therefore essential for quick biofilm regrowth. Most important process parameters were CO_2 supply, temperature, and pH. Although deviations of these parameters from the optimal conditions resulted in productivity loss, the system quickly recovered when optimal conditions were restored. These results exhibit an apparent opportunity to employ the Algadisk photobioreactor and biofilm systems in general at large scale for microalgae biomass production provided CO_2 supply is adequate.

In order to better understand the process conditions inside the biofilm a model was developed in the further chapters. These mathematical models were calibrated and validated with dedicated experiments. In **Chapter 4** first a general applicable kinetic model was developed able to predict light limited microalgal growth. This model combines a mathematical description for photoautotrophic sugar production with a description for aerobic chemoheterotrophic biomass growth. The model is based on five measurable biological parameters which were obtained from literature for the purpose of this study. The model was validated on experiments described in literature for both *Chlorella sorokiniana* and *Chlamydomonas reinhardtii*. The specific growth rate was initially predicted with a low accuracy, which was most likely caused by simplifications in the light model and inaccurate parameter estimations. When optimizing the light model and input parameters the model accuracy was improved and validated. With this model a reliable engineering tool became available to predict microalgal growth in photobioreactors. This microalgal

growth model was included in the biofilm growth models introduced in Chapters 5 and 6.

In **Chapter 5** microalgal biofilms of *Chlorella sorokiniana* were grown under simulated day-night cycles at high productivity and high photosynthetic efficiency. The experimental data under day/night cycles were used to validate a microalgal biofilm growth model. For this purpose the light limited microalgal growth model from Chapter 4 was extended to include diurnal carbon-partitioning and maintenance under prolonged dark conditions. This new biofilm growth model was then calibrated and validated experimentally. Based on these experiments and model simulations no differences in the light utilization efficiency between diurnal and continuous light conditions were identified. Indirectly this shows that biomass lost overnight represents sugar consumption for synthesis of new functional biomass and maintenance related respiration. This is advantageous, as this result shows that it is possible to cultivate microalgae at high photosynthetic efficiencies on sunlight and that the night does not negatively impact overall daily productivity. Long periods of darkness resulted in reduced maintenance related respiration.

Based on simulations with the validated biofilm growth model it could be determined that the photosynthetic efficiency of biofilm growth is higher than that of suspension growth. This is related to the fact that the maintenance rate in the dark zones of the biofilm is lower compared to that in the dark zones of suspension cultures, which are continuously mixed with the photic zone.

In Chapter 3 it was identified that concentrated CO_2 streams are required to obtain high productivities. However, over-supplying CO_2 results into loss of CO_2 to the environment and is undesirable for both environmental and economic reasons. In **Chapter 6** the phototrophic biofilm growth model from Chapter 5 was extended to include CO_2 and O_2 consumption, production, and diffusion. The extended model was validated in growth experiments with CO_2 as limiting substrate. Based on the validated model the CO_2 utilization and productivity in biofilm photobioreactors were optimized by changing the gas flow rate, the number of biofilm reactors in

series, and the gas composition. This resulted in a maximum CO_2 utilization efficiency of 96% by employing flue gas, while the productivity only dropped 2% compared to non-CO_2 limited growth. In order to achieve this 25 biofilm reactors units, or more, must be operated in series. Based on these results we conclude that concentrated CO_2 streams and plug flow behaviour of the gaseous phase over the biofilm surface are essential for high CO_2 utilization efficiencies and high biofilm productivity.

In **Chapter 7** the implications of these studies for the further development of biofilm photobioreactors was discussed in the light of current biofilm photobioreactor designs. Design elements of state of the art biofilm photobioreactors, were combined into a new conceptual biofilm photobioreactor design. This new design combines all advantages of phototrophic biofilms minimizing the amount of material required. Further improvements by means of process control strategies were suggested that aim for maximal productivity and maximal nutrient utilization efficiency. These strategies include: control of the biofilm thickness, control of the temperature, and optimized nutrient supply strategies.

Dankwoord

Na vier jaar PhD zit het er nu op! Ik heb van mijn PhD-tijd genoten en ik hoop dat jullie dit met mij delen. Natuurlijk heb ik dit project niet alleen gedaan en wil ik iedereen graag bedanken voor deze leerzame maar vooral ook leuke tijd.

René, bedankt voor de mogelijkheid om mijn PhD te doen bij BPE. Ik ben heel blij met het vertrouwen en de vrijheid die jij mij hebt gegeven gedurende mijn PhD.

Marcel, ik ben blij dat jij mij hebt begeleid tijdens mijn PhD. Jij hebt mij veel geleerd over de basis van het groeien van microalgen. Door jouw inbreng is de wetenschappelijke diepgang van mijn thesis vergroot.

Maria, it was fun and fruitful to have you as supervisor during the start of my PhD. Together with the other members of the Algadisk team we set the basis for the Algadisk photobioreactor.

Hierbij wil ik verder graag alle **collega's van BPE** bedanken voor de geweldige tijd. Ik heb mij altijd goed vermaakt gedurende de vele werkdagen, weekenden, koffie pauzes, borrels, labuitjes en kerstdiners. Daarnaast ben ik blij dat ik, naast het deelnemen aan alle BPE evenementen, ook heb bijgedragen aan de organisatie van de diverse BPE evenementen. Alle commissieleden bedankt voor de briljante brainstormsessies en gezelligheid rondom het organiseren van de diverse uitjes van BPE. Naast alle BPE evenementen was het mij een waar genoegen om deel te mogen nemen aan de Dinner and Beers group, het Worms team en de Fiets groep evenementen. Al deze evenementen hebben er voor gezorgd dat mijn tijd bij BPE onvergetelijk was.

Natuurlijk heb ik niet alle experimenten zelf gedaan. Daarom wil ik graag alle studenten bedanken die hebben geholpen met de data verzameling en de data analyse. **Luisaldo, Daphne, Niels, Petra, Stefan, Lucia, Sophie** and **Ana** all many thanks for your help and hard work. Graag wil ik ook alle BPE technicians: **Fred, Sebastiaan, Wendy** en **Snezana** speciaal bedanken voor de ondersteuning. Zonder jullie hulp en kennis had mijn PhD nog wel een jaartje langer geduurd.

Dear **Algadisk project members** I would like to thank you all for the great collaboration. Our meetings were always fruitful and fun. Furthermore I would like to say a special thanks to **Alfredo**, **Petra**, **Tábor** and **István** from the Algadisk pilot team.

Jeroen en **Lenny**, bedankt voor de vele discussies en ideeën om samen een eigen bedrijf te beginnen. Het verheugt mij dat Jeroen en ik samen de stap hebben gezet en Alcuso hebben opgericht. Hopelijk hebben wij samen met Alcuso een mooie toekomst in de algenwereld! Lenny, ik hoop dat jij een rol wilt blijven spelen als adviseur van Alcuso en wie weet in de toekomst het Alcuso team komt versterken.

Naast al mijn collega's wil ik graag mijn **ouders**, **zusje** en **broertjes** bedanken voor de interesse in mijn Biofilm avontuur. In het bijzonder bedankt voor de welkome afleiding en gezelligheid die jullie mij gaven tijdens mijn bezoeken aan het pittoreske Veenwouden. **Lotte**, bedankt voor de steun tijdens mijn PhD en ik hoop dat wij nog heel lang samen van het leven kunnen genieten.

Ward

About the author

Ward Blanken was born on the 5th of July 1988 in Groningen, The Netherlands. He attended the Lauwers college and graduated from high school in 2005. After high school he started a Bachalor degree in Medical Biotechnology at the Hogeschool van Hall Larenstein in Leeuwarden. With internships at the University Medical Centrum Groningen Clinical Pharmacology group, Delft University of Technology Industrial Microbiology Group and Royal Nedalco. After obtaining the Bachalor degree in 2009 he started in 2010 with his Master of Science degree in Biotechnology at the Wageningen University. His Master of Science degree was obtained in 2012 with a major in Process Engineering and a Master thesis on "Modeling microalgal productivity in a flat panel photobioreactor" at the Wageningen University Bioprocess Engineering group. In 2012 he started his PhD project in the Algadisk project at the Bioprocess Engineering group, Wageningen University. During his PhD project he investigated the opportunities of microalgae production in a biofilm photobioreactor. Currently Ward Blanken works together with Jeroen de Vree as founders of Alcuso.

List of publications

Blanken W, Schaap S, Theobald S, Wijffels RH, Janssen M. Optimizing carbon dioxide utilization for microalgae biofilm cultivation *Manuscript submitted.*

Blanken W, Magalhãesa A, Sebestyénb P, Rinzemaa A, Wijffelsa RH, Janssen M, Microalgal biofilm growth under day-night cycles. *Manuscript submitted.*

Sebestyén P, **Blanken W**, Bacsa I, Tóth G, Martin A, Bhaiji T, Dergez Á, Kesserű P, Koós Á, Kiss I. 2016. Upscale of a laboratory rotating disk biofilm reactor and evaluation of its performance over a half-year operation period in outdoor conditions. Algal Research 18 266–272.

Blanken W, Postma PR, de Winter L, Wijffels RH, Janssen M. 2016. Predicting microalgae growth. Algal Research 14:28-38.

Blanken W, Janssen M, Cuaresma M, Libor Z, Bhaiji T, Wijffels RH. 2014. Biofilm growth of Chlorella sorokiniana in a rotating biological contactor based photobioreactor. Biotechnol Bioeng 111(12):2436-45.

Blanken W, Cuaresma M, Wijffels RH, Janssen M. 2013. Cultivation of microalgae on artificial light comes at a cost. Algal Research 2(4):333-340.

Overview of completed training activities

Discipline specific

Algal BBB (San Diego, USA, 2015)[1]

Metabolic Engineering Course (Wageningen, 2015)

Algaeparc bedrijvendag (Wageningen, 2014) [2]

Young Algaeneers Symposium (Narbonne, France, 2014)[1]

Alg'n'Chem (Montpellier, France , 2014)[2]

Numerical Methods for Chemical Engineers Course (Eindhoven, 2013)

Advanced Biofilm Course, (Karlsruhe, Germany, 2012)

Young Algaeneers Symposium (Wageningen, 2012)[2]

1st international symposium about microalgae biotechnology for Young researchers (Almeria, Spain, 2012)[2]

General

Techniques for Writing and Presenting a Scientific Paper (Wageningen, 2013)

Scientific Writing (Wageningen, 2013)

Teaching and supervising Thesis students (Wageningen, 2013)

Opatel wordpress cursus (Utrecht, 2012)

Competence Assessment (Wageningen, 2012)

VLAG Phd week (Baarlo, 2012)

Optionals

BPE brainstorm days (Wageningen, 2012/2016)

PhD excursion Spain (Spain, 2012)

Writing of a Research proposal (Wageningen, 2012)

[1]Oral presentation

[2] Poster presentation

This study was financially supported by the European Union's Seventh Framework Programme (FP7/2007- 2013) - managed by REA Research Executive Agency - under grant agreement no. 286887.